

# Site U1308<sup>1</sup>

Expedition 303 Scientists<sup>2</sup>

## Chapter contents

Background and objectives	1
Operations	2
Lithostratigraphy	4
Biostratigraphy	6
Paleomagnetism	10
Composite section	11
Geochemistry	11
Physical properties	13
References	14
Figures	17
Tables	49

## Background and objectives

Integrated Ocean Drilling Program Site U1308 constitutes a reoccupation of Deep Sea Drilling Project (DSDP) Site 609 (Figs. F1, F2). Two principal holes (Holes 609 and 609B) were drilled with the variable-length hydraulic piston corer and extended core barrel (XCB) during DSDP Leg 94 (June–August 1983). Two cores were collected from Hole 609A to recover the mudline, and seven XCB cores were collected from Hole 609C to recover the 123–190 meters below seafloor (mbsf) interval. The magnetic stratigraphy at Site 609 was resolved down to polarity Chron 3An (~6 Ma) at 350 mbsf using discrete samples collected shipboard (Clement and Robinson, 1987). Mean sedimentation rates at Site 609 are therefore 5–6 cm/k.y. for the last 6 m.y. The marly foraminiferal nannofossil ooze at this site exhibits distinctive varicolored glacial–interglacial cycles above the base of the Matuyama Chronozone, excellent preservation of calcareous and siliceous microfossils, and the necessary attributes for the generation of high-resolution isotopic and paleointensity-based chronostratigraphies.

DSDP Sites 607 and 609 have been very important for generating benthic  $\delta^{18}\text{O}$ ,  $\delta^{13}\text{C}$ , and  $\text{CaCO}_3$  records for the Pleistocene (Ruddiman et al., 1989) and late Pliocene (Ruddiman et al., 1986; Raymo et al., 1989) and interpreting these records in terms of ice-sheet variability and oceanic circulation changes and for generating orbitally tuned timescales. Almost all the  $\delta^{18}\text{O}$  and  $\delta^{13}\text{C}$  data for these studies were derived from Site 607, partly because of enhanced continuity of the recovered section at this site. The  $\text{CaCO}_3$  data at both sites were used to correlate the  $\delta^{18}\text{O}$  and  $\delta^{13}\text{C}$  data to Site 609.

Site 607 (3427 m water depth) remains the only site in the high-latitude North Atlantic that monitors North Atlantic Deep Water (NADW) throughout the Pleistocene. In a recent compilation of North Atlantic  $\delta^{18}\text{O}$  and  $\delta^{13}\text{C}$  vertical gradients during the Pleistocene, Raymo et al. (2004) utilized Site 607 (3427 m water depth), with the next deepest site being Site 552 (2300 m water depth), presently within North Atlantic Intermediate Water (Fig. F1). These authors concluded that the water mass structure at intermediate depths in the North Atlantic during the Quaternary did not change significantly on glacial–interglacial timescales and that the  $\delta^{13}\text{C}$  signal at Site 607 and other deep Atlantic sites may be more influenced by variations in production of deep water

<sup>1</sup>Expedition 303 Scientists, 2006. Site U1308. In Channell, J.E.T., Kanamatsu, T., Sato, T., Stein, R., Alvarez Zarikian, C.A., Malone, M.J., and the Expedition 303/306 Scientists. *Proc. IODP, 303/306*: College Station TX (Integrated Ocean Drilling Program Management International, Inc.). doi:10.2204/iodp.proc.303306.108.2006

<sup>2</sup>Expedition 303 Scientists' addresses.



around Antarctica than changes in NADW production and the strength of the “conveyor belt.” The large volumetric flux of Norwegian Sea Overflow Water observed today may be caused by current open sea-ice conditions in the Norwegian-Greenland Sea and atypical of Pleistocene interglacials. The water depths at Sites U1308 (3900 m) and U1304 (3024 m) and the ability to derive a benthic stable isotope record at both sites will allow ice sheet/ocean interaction to be placed on a benthic isotopic record that mostly reflects changes in global ice volume. Carbon isotope data will allow high-resolution monitoring of NADW. Ocean Drilling Program (ODP) Leg 162 drift sites (Sites 980–984), from south of Iceland, were all at water depths <2000 m and therefore monitored the intermediate water (Fig. F1). At Site 982 (Rockall Plateau, 1145 m), Venz et al. (1999) proposed that Glacial North Atlantic Intermediate Water (GNAIW) production ceased during terminations and lower NADW production increased. There was apparently a time lag between the shutdown of GNAIW and the renewed production of upper NADW. One of the major objectives at Sites U1308 and U1304 is to provide NADW monitoring at high resolution (high sedimentation rates) in the central Atlantic. Together with Leg 162 sites (980–984) (Fig. F1), Sites U1308 and U1304 will provide a detrital record of millennial-scale changes in the vertical  $\delta^{13}\text{C}$  structure of the water column in the North Atlantic.

The importance of Site 609 was accentuated by the early recognition of detrital (Heinrich-type) layers by lithic counts (Broecker et al., 1992; Bond et al., 1992) and by sea-surface temperature (SST) proxies such as grayscale (Broecker et al., 1990) and percent *Neogloboquadrina pachyderma* (sinistral) (Bond et al., 1993, 1999). The proposed match of SST minima at Site 609 to cold stadials in the  $\delta^{18}\text{O}$  Greenland Summit ice core record led to the proposal that Dansgaard-Oeschger (ice core) cycles are grouped into so-called Bond cycles. Each cycle is terminated by the massive iceberg discharges from Hudson Strait that constitute Heinrich events (Bond et al., 1993; see Hemming, 2004, for comprehensive review). Partly from petrologic characteristics observed at Site 609, Bond and Lotti (1995) showed that Heinrich events are superimposed on another, higher-frequency rhythm of ice-rafting events with detrital sources not only in Hudson Strait but also in Greenland, Iceland, and Europe (see Snoeckx et al., 1999; Grousset et al., 2000). Within marine isotope Stages (MIS) 4–5d at Site 609, the ice-rafted debris (IRD) record and the percent *N. pachyderma* (sinistral) SST proxy can be correlated with the record of climate instability in the Greenland Summit  $\delta^{18}\text{O}$  ice core record (McManus et al., 1994). Oxygen isotope data from the North Greenland Ice Core Project (2004) implies that

the climate on Greenland during at least the younger part of MIS 5e was stable, consistent with the marine record (McManus et al., 1994), with temperatures  $\sim 5^\circ\text{C}$  warmer than today. More recently, the 1500 y cycle has been identified at Site 609 and in a number of piston cores from this part of the central Atlantic, using a number of lithologic characteristics including the percent of hematite-stained grains and percent of Icelandic glass (Bond et al., 1997, 1999).

Site 609 is an obvious candidate for redrilling using modern techniques to recover a demonstrably complete record of the sediment sequence. In the 22 y since the site was originally drilled, much has changed in high-resolution magnetic, sedimentologic, and geochemical techniques both for shipboard and postcruise studies. Shipboard composite section construction did not become routine until after ODP Leg 138 in 1991 (Mayer, Pisias, Janecek, et al., 1992). Apart from the gamma ray attenuation (GRA) densitometer, archive multisensor track, and multisensor track (MST), tools for modern composite section construction were not available during Leg 94. For Sites 607–611, Ruddiman et al. (1987) constructed composite sections postcruise using visual color and magnetic polarity reversals. The record from the two holes (Holes 609 and 609B) could be spliced together down to about Core 94-609-8H with a tenuous correlation to 94-609-9H, and then again down to 94-609-14H, below which the record is demonstrably incomplete (Ruddiman et al., 1987). The archive-half cores of Site 609 (stored until recently at Lamont-Doherty Earth Observatory of Columbia University) are now in poor condition caused by desiccation/contraction, mold growth, and prior sampling and are no longer suitable for most types of further study. Samples from Site 609 have played a major role in driving some of the most exciting developments in paleoceanographic research during the last 10–15 y, such as the recognition and understanding of Heinrich layers, the recognition of the 1500 y pacing in hematite-stained grains and Icelandic glass, and the correlation of ice-core  $\delta^{18}\text{O}$  to SST proxies. The majority of the analyses from Site 609 have dealt with the record younger than MIS 6, partly because of the lack of a continuous pristine composite record. A primary objective at Site U1308 was to recover a demonstrably complete composite record and, hence, considerably enhance the potential for Pliocene–Quaternary climatic records from this site.

## Operations

We departed Site U1307 for Site U1308 (proposed Site IRD1A) at 1300 h on 30 October 2004 using an

indirect route to minimize the effects of a passing low-pressure system. After a 103.8 h, 1111 nmi transit, we arrived at Site U1308 at 2230 on 3 November.

### Hole U1308A

Hole U1308A was spudded with the advanced piston corer (APC) at 1005 h on 4 November 2004. Recovery of a 8.62 m mudline core suggested a seafloor depth of 3871 meters below sea level (mbsl) (3882.3 meters below rig floor [mbrf]). Piston coring advanced the hole to 341.1 mbsf with an average recovery of 94.9% (Table T1). Because of difficulties with three of the four Tensor tool battery packs, the last four piston cores were obtained without orientation so repairs could be made in preparation for Hole U1308B coring. Cores 32H and 36H were obtained with partial strokes of the APC. Heave conditions (maximum of ~6 m) resulted in generally poor core quality in Hole U1308A below Core 18H. Coring was terminated at 341.1 mbsf because extending APC coring depth by drillover was not possible with the existing sea state. The drill string was pulled clear of the seafloor at 1825 h on 6 November, concluding operations in Hole U1308A.

### Hole U1308B

The ship was offset 30 m east of Hole U1308A. Because the swell responsible for the large heave was expected to increase during the evening (eventually reaching a maximum of ~7 m), coring operations were suspended to wait until conditions improved. The heave gradually abated to <3 m by 1030 h on 7 November 2004, and coring operations continued when Hole U1308B was spudded at 1320 h on 7 November. Recovery of the first core indicated a seafloor depth of 3871.1 mbsl (3882.4 mbrf). Piston coring advanced the hole to a total depth of 198.3 mbsf, with an average recovery of 93.9%. Four of the top sixteen cores were recovered with crushed core liners, resulting in pervasive drilling-related disturbance and deformation (Table T1). The last three cores (Cores 20H through 22H) returned with an average recovery of only 30%. All three were partial strokes with overpulls of 20,000 to 40,000 lb required to extract the core barrels. Suspecting problems in the base of the hole, we terminated coring, ending Hole U1308B operations when the bit cleared the seafloor at 2315 h on 8 November.

### Hole U1308C

The ship was offset 60 m east of Hole U1308B. Incomplete firing of the APC resulted in two unsuccessful attempts to spud Hole U1308C, which also included offsetting the ship 30 m north of Hole

U1308A in case the problem was anomalous seafloor conditions. The bit was positioned 15 m above the seafloor for a firing test, which resulted in another incomplete stroke, suggesting the bit was plugged with detritus accumulated during coring at the end of Hole U1308B. The core barrel was recovered and a bit deplugger was dropped to clear the blockage at the bit throat and inside the seal bore drill collar. Following the recovery of the deplugger, Hole U1308C was successfully spudded with the APC at 0730 h on 9 November 2004. Piston coring advanced to 279.9 mbsf, with an average recovery of 96.8%. Six of the top nineteen cores were recovered with crushed core liners (Table T1). Six core barrels (Cores 22H through 27H, 29H, and 30H) were obtained by drillover. The final two coring runs resulted in bent core barrels. The last barrel was difficult to retrieve and extract from the drill string. Thus, coring was terminated to avoid a potential reoccurrence or a need to trip the entire drill string back to the rig floor. The bit was pulled clear of the seafloor at 0045 h on 11 November ending Hole U1308C.

### Hole U1308D

The ship was offset 30 m north of Hole U1308C, and Hole U1308D was spudded with the APC at 0230 h on 11 November 2004. The core was recovered with a crushed liner. To ensure that a gap in the splice near the top of the section was filled, we decided to make another attempt at a mudline core.

### Hole U1308E

Without offset from Hole U1308D, Hole U1308E was spudded with the APC at 0340 h on 11 November 2004, recovering a full core. Piston coring and drilling advanced the hole to 200.5 mbsf, with an average recovery for the cored interval of 89.4%. Three intervals were drilled (57.0–60.0, 83.0–84.0, and 93.5–97.0 mbsf) to maintain stratigraphic offset with previous holes. Core 9H was fired after picking up 5.5 m from the base of Core 8H to position Core 9H for optimal stratigraphic overlap. However, the completeness of the composite section (i.e., covering coring gaps from previous holes) was made difficult by poor recovery in Cores 3H through 11H. The last two cores (Cores 20H and 21H) were obtained by partial strokes of the APC, indicating we were approaching the interval requiring drillover in previous holes. Rather than expend coring time on this slower process, we terminated coring in Hole U1308E in favor of ensuring complete stratigraphic coverage for the upper sedimentary succession by coring in Hole U1308F. The bit cleared the seafloor at 0730 h on 12 November, concluding operations in Hole U1308E.

## Hole U1308F

The ship was offset 30 m west of Hole U1308E. Before initiating coring, an XCB fitted with a center bit was dropped to the bit. We suspected that accumulated debris was causing the abnormally high frequency of crushed core liners and affecting core recovery, so we applied high pump rates to clear the bit nozzles and the internal surfaces of the seal bore drill collar. Following recovery of the XCB, Hole U1308F was spudded with the APC at 1055 h on 12 November 2004. Piston coring continued until available time expired, reaching a total depth of 227.0 mbsf, with an average recovery of 100.7% (Table T1). Although crushed liners were still a problem (in 13 of the top 17 cores), improved recovery in Hole U1308F allowed completion of a composite section to ~239 meters composite depth (mcd) (see “[Composite section](#)”). The last three core barrels (Cores 22 through 24H) required drillover. The bit was pulled free of the seafloor at 1545 h, ending operations in Hole U1308F.

### Transit from Site U1308 to Ponta Delgada

After recovering the drill string and preparing the aft coring line for maintenance to be performed during the transit, we departed for Ponta Delgada (Portugal) at 0030 h on 14 November 2004. The 742 nmi transit took 79.3 h at an average speed of 9.4 kt. At 0817 h on 17 November 2004, the first line was ashore, officially concluding Expedition 303.

## Lithostratigraphy

Six holes were drilled at Site U1308 (Table T1). Core recovery at Site U1308 was 95.4%, although numerous cores were adversely affected by crushed core liners. Core disturbance caused by elevated ship heave adversely affected core quality in the lower part of Hole 1308A. All cores were recovered using the APC. The sediments at Site U1308 are composed of varying mixtures of terrigenous and biogenic components (primarily nannofossils, clay minerals, and quartz) (see “[Site U1308 smear slides](#)” in “[Core Descriptions](#),” Fig. F3). The most common lithologies are nannofossil ooze, foraminifer nannofossil ooze, nannofossil ooze with silty clay, silty clay nannofossil ooze, nannofossil silty clay, silty clay with nannofossils, and silty clay. Most contacts between these lithologies are burrowed or gradational. However, thin ( $\leq 10$  cm) silty clay layers commonly display sharp lower contacts. Abundances of terrigenous components as estimated from smear slides are quartz, 0%–55%; detrital carbonate, 0%–39%; feldspars, 0%–10%; clay minerals 0%–70%; heavy minerals (especially hornblende), 0%–10%; and volcanic glass, 0%–

15%. No discrete ash layers were observed. Dropstones are rare throughout the upper 165 m of Site U1308 (~1 per 3 m of core) but are slightly more abundant in the upper 100 m (~1 per 2 m of core) (Fig. F4). The interval below 210 mcd is virtually devoid of dropstones. Dropstones display a wide range of lithologies, including acidic intrusive and metamorphic (granites, gneisses, and granitoids), basic igneous and/or metamorphic (basalts and metabasalts), and sedimentary and metasedimentary (sandstone and limestone/dolostone) rocks. Abundances of biogenic components, as estimated from smear slides, are nannofossils, 0%–95%; foraminifers, 0%–25%; diatoms, 0%–25%; radiolarians, 0%–trace; and sponge spicules, 0%–5%. Total carbonate contents range from 12 to 94 wt% in these cores (see “[Geochemistry](#),” Table T32). Pyrite (usually associated with burrows) and iron oxide coatings on grains are present throughout, constituting the only authigenic sediment components observed.

Between 168 and 191 mcd, portions of the sedimentary succession exhibit inclined bedding. This is most apparent in the greenish gray diagenetic horizons that either gently dip ( $\sim 10^\circ$ – $15^\circ$ ) or are subparallel. However, very sharp inclined lithologic contacts were observed in Holes U1308B, U1308C, and U1308E (Fig. F5). These features were the only observed evidence of sediment disturbance not induced by coring at Site U1308.

The sediments at Site U1308 are divided into two units. Unit I is composed of a Holocene–Upper Pliocene sequence of interbedded biogenic and terrigenous sediments with dropstones. Unit II is composed of Upper Pliocene–upper Miocene sediments, rich in nannofossil ooze and devoid of dropstones. Subunit IIA is an Upper Pliocene nannofossil ooze interbedded with terrigenous sediment-rich layers but at a lower frequency than Unit I. Subunit IIB is entirely composed of lowermost Upper Pliocene–uppermost Miocene nannofossil ooze that exhibits very little color change. The character of sediment physical properties, including natural gamma radiation (NGR), magnetic susceptibility, and density, exhibits significant changes at each lithologic boundary (see “[Physical properties](#)”).

## Description of units

### Unit I

Intervals: Sections 303-U1308A-1H-1, 0 cm, to 20H-6, 95 cm; 303-U1308B-1H-1, 0 cm, to 19H-6, 126 cm; 303-U1308C-1H-1, 0 cm, to 20H-3, 110 cm; 303-U1308D-1H-1, 0 cm, to 1H- CC, 14 cm; 303-U1308E-1H-1, 0 cm, to 19H-6, 145 cm; and 303-U1308F-1H-1, 0 cm, to 19H-6, 93 cm

Depths: Hole U1308A: 0–187.9 mbsf, Hole U1308B: 0–174.3 mbsf, Hole U1308C: 0–179.5 mbsf, Hole U1308D: 0–6.7 mbsf, Hole U1308E: 0–180.95 mbsf, and Hole U1308F: 0–178.43 mbsf (0–201 mcd)

Age: Holocene–Late Pliocene

Primary biogenic lithologies within Unit I are nanofossil ooze, foraminifer nanofossil ooze, and nanofossil ooze with silty clay. Minor biogenic lithologies include nanofossil ooze with diatoms and nanofossil ooze with clay and diatoms. Interbedded with the biogenic lithologies, at decimeter to millimeter scale, are terrigenous lithologies composed of silty clay, silty clay with nanofossils, nanofossil silty clay, and minor nanofossil clay. Sediments from 0 to ~1.75 mcd exhibit a light yellow-brown to olive-brown color and are interpreted from smear slide data as surface-oxidized equivalents of the underlying lithologies.

Bioturbation is present throughout Unit I; the most common indicators are diffuse centimeter-scale mottling and millimeter-scale pyritic burrow fills. Discrete burrows and macroscopic pyritized burrows were also observed. The bioturbation index ranges from rare to abundant, but most lithologies display common bioturbation. Contacts between these lithologies are generally bioturbated to gradational, although centimeter- to decimeter-scale silty clay layers within each hole commonly exhibit bioturbated upper contacts and relative sharp lower contacts.

The color of nanofossil-rich lithologies ranges from white (N/8 and 5Y 8/1) to dark gray (5Y 4/1) and occasionally light olive-gray (5Y 7/2) to olive-gray (5Y 5/2) and light greenish gray (5GY 7/1) to greenish gray (5GY 6/1), with darker colors typically indicating increased terrigenous content. Terrigenous lithologies are darker, typically ranging from gray (5Y 5/1) to dark gray (5Y 4/1), olive-gray (5Y 5/2) to dark olive-gray (5Y 4/2), and, rarely, grayish brown (2.5Y 5/2) to dark grayish brown (2.5Y 4/2). Thin black (5Y 2.5/1) silty clay beds are also present. Calcium carbonate content averages 59 wt% and ranges between 12 and 90 wt% in Unit I (see “[Geochemistry](#),” Table T32).

## Unit II

### Subunit IIA

Intervals: Sections 303-U1308A-20H-6, 95 cm, to 24H-5, 26 cm; 303-U1308B-21H-1, 0 cm, to 22H-CC, 7 cm; 303-U1308C-20H-3, 110 cm, to 26H-4, 113 cm; 303-U1308E-19H-6, 145 cm, to 21H-CC, 24 cm; and 303-U1308F-19H-6, 93 cm, to 24H-CC, 12 cm

Depths: Hole U1308A: 187.9–239.2 mbsf, Hole U1308B: 184.5–198.3 mbsf, Hole U1308C: 176.3–238.0 mbsf, Hole U1308E: 180.95–200.9 mbsf, and Hole U1308F: 178.43–226.8 mbsf (201–254.4 mcd)

Age: Late Pliocene

Subunit IIA is composed of nanofossil ooze, nanofossil ooze with silty clay, and silty clay nanofossil ooze. The contact between Unit I and Unit II is gradational. Except for one dropstone at 239.7 mcd (215.6 mbsf) in Hole U1308C, Subunit IIA lacks dropstones (Fig. F4). Calcium carbonate content averages 75 wt% and ranges between 68 and 80 wt%, which is a higher average and lower variability than that of Unit I (see “[Geochemistry](#),” Table T32). In Subunit IIA, the sediment lightness ( $L^*$ ) variable and physical properties (magnetic susceptibility, NGR, and density) exhibit reduced amplitude fluctuations relative to those of Unit I (Fig. F6). As determined by visual core description, sediment color ranges from gray, olive-gray, and greenish gray (5Y 5/1, 5Y 6/1, 5Y 5/2, and 5GY 5/1) to light gray, light olive-gray, and light greenish gray (5Y 7/1, 5GY 7/1, and 5Y 7/2) within the upper portion of Subunit IIA, becoming predominantly white (5Y 8/1, N/8) to light gray (5Y 7/1) at the base of Subunit IIA. Greenish gray horizons spaced ~5 to ~10 cm apart are common. Alterations in color occur less frequently than in Unit I, and contacts are typically gradational to bioturbated. Bioturbation is present throughout most of Subunit IIA; the most common indicators are diffuse centimeter-scale mottling and millimeter-scale pyritic burrow fills. Discrete burrows were also observed. The bioturbation index ranges from rare to abundant.

### Subunit IIB

Intervals: Sections 303-U1308A-28H-1, 0 cm, to 36H-CC, 22 cm; and 303-U1308C-26H-4, 113 cm, to 30H-CC, 8 cm

Depths: Hole U1308A: 255.6–341.1 mbsf and Hole U1308C: 238.0–279.9 mbsf (262–355.89 mcd)

Age: Late Pliocene–late Miocene

Smear slide analysis indicates that Subunit IIB is composed entirely of nanofossil ooze (Fig. F3) dominated by white (N/8) color. The Subunit IIA/IIB boundary is easily recognized by ~10 cm gradational lightening of sediment color from light gray (5Y 7/1) in Subunit IIA to white (N/8) in Subunit IIB, which is apparent in both the  $L^*$  values and observed Munsell colors. Calcium carbonate content averages 91 wt% and ranges from 85 to 94 wt% in Subunit IIB (see “[Geochemistry](#),” Table T32). Correspondingly, sedi-

ment NGR and magnetic susceptibility values decrease whereas density increases at the Subunit IIA/IIB boundary (see “[Physical properties](#)”). Greenish gray color bands are present but more diffuse and infrequent than in Subunit IIA. Bioturbation is present throughout most of Subunit IIB; the most common indicators are diffuse centimeter-scale mottling and millimeter-scale pyritic burrow fills. Discrete burrows were also observed. The bioturbation index ranges from rare to common, but most lithologies display moderate bioturbation.

## Discussion

The distribution of abundant lithologies at Site U1308 is presented in Figure F7. Of the 1189 m of sediment recovered at this site, 1044 m (88%) is nanofossil ooze and related derivatives. Silty clay and its variations compose 145 m (12%) of the sediments.

The sedimentary succession recovered at Site U1308 was divided into units and subunits based on the relative abundance of terrigenous material within the sediments. Lithological determinations based on smear slide data indicate that terrigenous content of the sediment increases upsection (“[Site U1308 smear slides](#)” in “[Core Descriptions](#),” Fig. F3) and is accompanied by lower CaCO<sub>3</sub> content (see “[Geochemistry](#),” Table T32). In addition to increasing terrigenous input, the amplitude of lithologic variation increases in the upper part of the succession. This variation is well expressed in the NGR, magnetic susceptibility, and density records (see “[Physical properties](#)”).

The terrigenous component imparts a distinct color change to the sediments recovered at Site U1308. As such, L\* provides an accurate proxy of the terrigenous component and easily displays variations downcore. Two distinct units are identified based on the variability of reflectance. Unit I is characterized by high-frequency and high-amplitude variability in lithology shown by L\* values ranging between 25% and 80% (Fig. F6). In contrast, L\* variability in Unit II is lower with values between 40% and 70% in the upper part of this unit. Unit II was divided based on the appearance of terrigenous components as indicated by sedimentary color. The L\* variable records this a stepwise shift in the mean L\* value from ~60% in Subunit IIA to >75% in Subunit IIB.

The timing of lithologic unit and subunit boundaries is constrained by shipboard age determinations. The base of Unit I (201 mcd) is close to the Matuyama/Gauss boundary (2.58 Ma; ~193 mcd). The base of the Mammoth Subchron (3.33 Ma) is located at ~264 mcd, close to the base of Subunit IIA (262 mcd) (see

“[Paleomagnetism](#)”). Nanofossil datum level-derived ages are in agreement with the ages based on magnetostratigraphic reversals (see “[Biostratigraphy](#)”).

The stepwise increase in terrigenous content in Subunit IIA is consistent with the development of significant ice in the northern hemisphere at ~3.3 Ma (Maslin et al., 1995). At this time, benthic foraminifer  $\delta^{18}\text{O}$  records indicate pronounced deepwater cooling and/or ice sheet growth (Tiedemann et al., 1994). Onset of large-scale glaciation could have provided a possible source for this terrigenous sediment through either ice rafting of fine-grained regolith or increased eolian deposition associated with higher regional/hemispheric wind speeds. The stepwise increase in NGR at this depth indicates increased clay mineral content (see “[Physical properties](#)”).

Heinrich events H0–H6 and H11 (Termination II) are recognizable in magnetic susceptibility data (see “[Physical properties](#)”). H1, H2, H4, and H5 are readily identifiable in split core sections because of their lighter color, typically olive-gray (5Y 5/2 and 5Y 4/2), and sharp basal contacts (Figs. F8, F9, F10, F11). The positions and thicknesses roughly correspond to those identified at Site 609 (Bond et al., 1992). Millennial-scale variability in the magnetic susceptibility record reflects the high-frequency climate recorded in fluctuations documented by previous studies from this region (e.g., Bond et al., 1997, 1999, 2001). Furthermore, the variations continue downcore in the magnetic susceptibility records, indicating that millennial-scale variability may be a persistent feature of the climate system.

## Biostratigraphy

Core catcher samples at Site U1308 reveal species-rich assemblages of calcareous, siliceous, and organic-walled microfossils. Preservation of all microfossil groups is very good to moderate throughout the cored interval. Biostratigraphic datum events mainly derive from coccoliths and are consistent with datum events provided by planktonic foraminifers, diatoms, and dinocysts (Fig. F12). According to these datum events, we recovered an upper Miocene–Quaternary sequence at Site U1308.

Floral and faunal assemblages of planktonic organisms reflect changing paleoclimate and paleoceanographic conditions since the late Miocene. Upper Miocene and lower Upper Pliocene sediments (before 2.74 Ma) contain more warm-water nanofossil species than uppermost Pliocene and Pleistocene sediments. The floral changes can be associated with the onset of northern hemisphere glaciation (NHG). Seasonal changes in bioproductivity and the move-

ment of hydrographic fronts are documented by microfossils at this site.

### Calcareous nannofossils

Calcareous nannofossils were examined in all core catcher samples from Holes U1308A–U1308F (Tables T2, T3, T4, T5, T6, T7). Moderate to well-preserved nannofossils are abundant in almost all samples and species diversity is high. Most of the Late Pliocene–Quaternary datum planes described by Sato et al. (1999) and the upper Miocene–Lower Pliocene markers defined by Martini (1971) have been identified in the sedimentary sequence. Correlation of nannofossil datums between the holes and to magnetostratigraphy are shown in Figure F12.

*Emiliania huxleyi* indicates the uppermost Quaternary Zone NN21 (0–0.25 Ma) and is found in Samples 303-U1308A-1H-CC, 303-U1308B-1H-CC and 2H-CC, 303-U1308C-1H-CC, 303-U1308D-1H-CC, 303-U1308E-1H-CC, and 303-U1308F-1H-CC. The last occurrence (LO) of *Pseudoemiliania lacunosa*, which shows the top of Zone NN19 (0.41 Ma), is recognized in Sample 3H-CC in all holes except U1308D. Both the LO of *Reticulofenestra asanoi* (0.85 Ma) and the first occurrence (FO) of *Gephyrocapsa parallela* (0.95 Ma), situated between the base of the Brunhes Chron and the top of the Jaramillo Subchron, are recognized between Samples 303-U1308A-5H-CC and 6H-CC and 6H-CC and 7H-CC, respectively; 303-U1308C-5H-CC and 6H-CC and 6H-CC and 7H-CC, respectively; 303-U1308E-5H-CC and 6H-CC and 6H-CC and 7H-CC, respectively; and 303-U1308F-5H-CC and 6H-CC and 6H-CC and 7H-CC, respectively. In Hole U1308B, both datums are situated in the same interval between Samples 303-U1308B-6H-CC and 7H-CC. The FO of *R. asanoi* (1.16 Ma), which lies just below the Jaramillo Subchron, is found between Samples 8H-CC and 9H-CC in all holes. Large-form *Gephyrocapsa* spp. (>6 µm) appear between 1.45 and 1.21 Ma and occur in Samples 303-U1308A-9H-CC, 303-U1308B-9H-CC and 10H-CC, 303-U1308C-9H-CC, 303-U1308E-9H-CC, and 303-U1308F-9H-CC and 10H-CC. Samples 303-U1308A-10H-CC to 12H-CC, 303-U1308B-11H-CC to 12H-CC, 303-U1308C-10H-CC to 11H-CC, 303-U1308E-10H-CC to 11H-CC, and 303-U1308F-11H-CC to 12H-CC are characterized by the presence of *Gephyrocapsa oceanica*, *Gephyrocapsa caribbeanica*, and *P. lacunosa* and the absence of large forms of *Gephyrocapsa* spp. Accordingly, these intervals are assigned an age between 1.45 and 1.65 Ma. The assemblages below Samples 303-U1308A-12H-CC, 303-U1308B-12H-CC, 303-U1308C-12H-CC, 303-U1308E-11H-CC, and 303-U1308F-12H-CC contain *Reticulofenestra* spp. (small) and *P. lacunosa* and lack *G. oceanica* and *G. caribbeanica*. Therefore, the Pliocene/Pleis-

tocene boundary defined by the FO of *G. caribbeanica* is situated between Samples 303-U1308A-12H-CC and 13H-CC, 303-U1308B-12H-CC and 13H-CC, 303-U1308C-12H-CC and 13H-CC, 303-U1308E-11H-CC and 12H-CC, and 303-U1308F-12H-CC and 13H-CC.

The Pliocene assemblages at Site U1308 are characterized by the presence of discoasters. The LOs of *Discoaster brouweri*, *Discoaster pentaradiatus*, and *Discoaster surculus* at 1.97, 2.38, and 2.54 Ma, respectively, are situated in the intervals between Samples 303-U1308A-15H-CC and 19H-CC, 303-U1308B-15H-CC and 19H-CC, 303-U1308C-15H-CC and 19H-CC, 303-U1308E-15H-CC and 19H-CC, and 303-U1308F-15H-CC and 19H-CC. *Discoaster tamalis* and *Reticulofenestra ampla* disappeared at 2.74 and 2.78 Ma in the upper part of the Gauss Chron, synchronous with drastic growth of the ice sheet in the Arctic Ocean and final closure of the Isthmus of Panama. The LO of these two species lies between Samples 303-U1308A-19H-CC and 21H-CC, 303-U1308B-20H-CC and 21H-CC, 303-U1308C-20H-CC and 21H-CC, 303-U1308E-20H-CC and 21H-CC, and 303-U1308F-19H-CC and 20H-CC. Below, the assemblages are characterized by abundant occurrences of the warm-water *Discoaster* spp. and by high species diversity. *Reticulofenestra pseudoumbilicus* and *Sphenolithus abies* have their LO in the Middle Pliocene (3.85 Ma) and are found in and below Samples 303-U1308A-28H-CC and 303-U1308C-28H-CC. The LO of *Amaurolithus* spp. (4.50 Ma) and FO of *Ceratolithus rugosus* (4.7 Ma), which are Early Pliocene datums recognized in low- to mid-latitude regions, are found in Samples 303-U1308A-29H-CC and 31H-CC, respectively. *Discoaster quinqueramus*, which has its LO at the Miocene/Pliocene boundary (5.6 Ma), is found in Samples 303-U1308A-35H-CC and 36H-CC. This indicates that the Miocene/Pliocene boundary is situated between Samples 303-U1308A-34H-CC and 35H-CC. Therefore, the bottom of Hole U1308A does correlate with the uppermost Miocene.

The assemblages are characterized by the occurrence of warmer water species compared to other sites of Expedition 303. In particular, the assemblages found in samples older than 2.74 Ma are characterized by high species diversity in all holes. The floral change at Site U1308 can be attributed to the influence of drastic ice sheet growth in the Arctic Ocean and final closure of the Isthmus of Panama (Jansen et al., 1988; Whitman and Berger, 1992; Thiede and Myhre, 1996; Kameo and Sato, 2000; Sato et al., 2004).

### Planktonic foraminifers

Planktonic foraminifers were examined in all core catcher samples from Holes U1308A–U1308F (Tables T8, T9, T10, T11, T12). The core catchers from the

upper cores of each hole contain soft sediment that was washed with tap water. Sediments of the middle sections (generally Sections 20H-CC to 25H-CC of all holes) were treated with H<sub>2</sub>O<sub>2</sub> and occasionally with Calgon solution for several minutes before washing. Planktonic foraminifers are abundant from bottom to top in all holes (Table T8). Preservation of tests is very good to moderate throughout the sections.

The FO of encrusted *N. pachyderma* (sinistral), situated at the top of the Oludvai Subchron (Weaver and Clement, 1987), is unequivocal in Samples 303-U1308A-12H-CC, 303-U1308C-12H-CC, 303-U1308E-12H-CC, and 303-U1308F-12H-CC. In addition, *N. pachyderma* (sinistral) is dominant in Sample 303-U1308A-36H-CC, which may therefore be placed in the lower part of the Gilbert Chron (Weaver and Clement, 1987). The FO of *Globorotalia inflata* is observed in Samples 303-U1308A-15H-CC, 303-U1308B-15H-CC, 303-U1308C-15H-CC, 303-U1308E-14H-CC, and 303-U1308F-15H-CC. The LO of *Negloboquadrina atlantica* at the base of Matuyama Chron (Weaver and Clement, 1987) is recognized in Sample 303-U1308A-18H-CC, 303-U1308B-18H-CC, 303-U1308C-19H-CC, 303-U1308E-18H-CC, and 303-U1308F-18H-CC. The FO of *Globorotalia puncticulata*, placed in the Nunivak Subchron (Weaver and Clement, 1987), is found in Samples 303-U1308A-28H-CC and 303-U1308C-29H-CC. According to planktonic foraminifers, we assign a time span from upper Miocene/Lower Pliocene–Quaternary for the recovered sediments (Fig. F12).

At Site U1308, the deep-dwelling species *G. truncatulinoides* occurs close to its northern distribution limit for the North Atlantic (Ericson et al., 1954; Prell et al., 1999) and is a rare component of the studied faunas. The subtropical to temperate globorotalid species *Globorotalia crassaformis*, *Globorotalia margaritae*, and *Globorotalia conomiozea* are rare (Table T8) and were therefore not considered for biostratigraphy.

Sinistrally coiled *N. pachyderma* occurs frequently throughout the upper Samples 303-U1308A-1H-CC to 12H-CC, indicating polar conditions. Along with *N. pachyderma* (sinistral), *Globigerina bulloides* and *Globorotalia inflata* are abundant. The presence of dextrally coiled *Globorotalia truncatulinoides* in Samples 303-U1308A-1H-CC to 3H-CC and sinistrally coiled specimens in Samples 303-U1308A-6H-CC to 8H-CC indicates that mesobathyal water masses of southern origin were also present at Site U1308 during glacial stages.

Core catcher samples of Hole U1308A are characterized by a small-sized planktonic foraminiferal fauna. In contrast, core catcher samples of Holes U1308B, U1308C, U1308E, and U1308F contain more large-sized, subtropical species and less *N. pachyderma* (sin-

istral). The warm-water fauna frequently contains species such as *Globigerinella siphonifera*, *Globigerinella calida*, *Globigerinoides ruber* (white), *Orbulina universa*, and occasionally *Globigerinoides sacculifer*. During the Pliocene and Pleistocene, *G. puncticulata* and *G. inflata* are abundant and may be indicative of hydrographic fronts at Site U1308. Both glacial and interglacial faunas display significant seasonality, with *Globigerina bulloides* as a typical species following spring blooms of phytoplankton, and dextrally coiled *N. pachyderma* dominating the fauna during summer (Schiebel and Hemleben, 2000).

### Benthic foraminifers

Benthic foraminifers were examined in all core catcher samples from Holes U1308A–U1308F (Tables T13, T14, T15, T16, T17). Benthic foraminifers are rare in Sections 1H-CC to 16H-CC and 24H-CC to 29H-CC and more frequent in Sections 17H-CC to 23H-CC (175–240 mcd) of all holes. Benthic foraminifers are most abundant in Samples 303-U1308A-30H-CC to 36H-CC (297–355.6 mcd). Rotaliid species are frequent at Site U1308, whereas miliolid and agglutinated species are rare. *Oridorsalis umbonatus* is the most frequent benthic foraminiferal species at Site U1308. In contrast to Sites U1302–U1307, *Globocassidulina* is frequent at Site U1308. *Cibicidoides wuellerstorfi* is present in all holes of Site U1308.

### Diatoms

Diatom assemblages were investigated in 133 core catcher samples and 107 smear slides from Holes U1308A–U1308F (Tables T18, T19, T20, T21, T22). The only core catcher sample from Hole U1308D was barren of diatoms. Diatoms are generally rare to common within the upper sequence (0–255 mcd) (Fig. F13) during the Late Pliocene and Pleistocene. The lower part of the sequence between 255 and 355 mcd is barren of diatoms. The valves are moderately preserved throughout the sequence above 255 mcd. Five silicoflagellate species and the siliceous dinoflagellate *Actiniscus pentasterias* are present almost throughout the sequence above 255 mcd.

Although datum placements are inadequately defined because of a discontinuity in diatom occurrences, the four diatom zones used here, previously proposed by Baldauf (1987) for Site 609, are implied by two diatom datum events at Site U1308 (Fig. F12; Tables T18, T19, T20, T21, T22). The LO of *Fragilariopsis reinholdii*, which defines the base of the *Fragilariopsis doliolus* Zone and the top of the *F. reinholdii* Zone at 0.48–0.45 Ma (based on Cande and Kent, 1995, and others), is apparent above Samples 303-U1308A-6H-CC, 303-U1308B-4H-CC, 303-U1308C-4H-CC, 303-U1308E-5H-CC, and 303-U1308F-5H-



CC (56–33 mcd). The FO of *F. doliolus* (1.9 Ma), which defines the bottom of the *F. reinholdii* Zone and the top of the *Alveolus marinus* Zone, is unclear in each hole because of poor diatom abundance in the interval. The LO of *Thalassiosira convexa* var. *convexa* (0.84–0.85 Ma) appears to occur above Samples 303-U1308A-17H-CC, 303-U1308C-19H-CC, and 303-U1308F-19H-CC (201–177 mcd) and gives a secondary datum (2.58–2.68 Ma) within the *A. marinus* Zone. The LO of *Fragilariopsis jouseae* (2.66–2.83 Ma), which defines the bottom of the *F. jouseae* Zone and the top of the *T. convexa* Zone, appears to be above Samples 303-U1308A-28H-CC and 22H-CC and 303-U1308B-21H-CC (285–220 mcd). Below Samples 303-U1308A-29H-CC and 303-U1308B-28H-CC (285–290 mcd), the calcareous-rich lithofacies is barren of diatoms.

A very diverse diatom flora is present in the sedimentary section above 255 mcd. Around 110 marine diatom species were identified (Tables T18, T19, T20, T21, T22). As with previous observations at Site 609 (Baldauf, 1987), the dominant diatoms indicate warm temperate, highly saline waters. The main components of the warm-water assemblage are varieties of *Thalassiosira oestrupii*, *Thalassiosira ferelinata*, *Thalassiosira lineata*, *Fragilariopsis fossilis*, *F. reinholdii*, *Azpeitia* spp., *Hemidiscus cuneiformis*, and *A. marinus*. The tropical/subtropical diatom community is accompanied by a rich assemblage of resting spores of *Chaetoceros*, which reflects high productivity of surface waters (Crosta et al., 1997). Minor influence of cold water masses is suggested by the occurrence of *Actinocyclus curvatus* and the needle-shaped diatoms of the *Thalassiothrix/Lioloma* complex (Andersen et al., 2004).

### Radiolarians

Radiolarians were examined in all core catcher samples from Holes U1308A and U1308C (Table T23). Radiolarians are abundant from the middle part of the sequences (154–280 mcd) and are rare or absent in the upper and the lower parts. Species diversity is generally higher than at Sites U1302–U1307. Abundant groups throughout the sequence are spongodiscids, litheliids, and actinommids. *Cycladophora davisiana davisiana* is abundant in the upper part of the sequence (Samples 303-U1308A-6H-CC and 7H-CC) and becomes rare in the middle part. Radiolarian assemblages are characterized by abundant spongodiscids and litheliids with continuous occurrence of *Axoprunum angelinum*(?) between Samples 303-U1308A-15H-CC and 28H-CC and 303-U1308C-14H-CC and 27H-CC. Below the intervals, radiolarians are poorly preserved and occur sporadically.

Two diagnostic datum events useful for biostratigraphy are observed. The FO of *C. davisiana davisiana* (2.7 Ma) (Goll and Bjørklund, 1989) is observed between Samples 303-U1308A-20H-CC and 21H-CC and 303-U1308C-19H-CC and 20H-CC. The FO of *Spongaster ?tetras* (3.0–3.2 Ma) (Goll and Bjørklund, 1989) is located between Samples 303-U1308A-24H-CC and 25H-CC and 303-U1308C-23H-CC and 24H-CC.

### Palynomorphs

Palynological assemblages were examined in core catcher samples from Holes U1308A and U1308B (Tables T24, T25). The concentration of terrestrial palynomorphs is low in most samples (Fig. F13), which is expected because the site location is distant from a land vegetation source. The pollen abundance is usually <100 grains/cm<sup>3</sup>. It is dominated by *Pinus* and can be related to minor input through atmospheric or ocean circulation. Reworked palynomorphs are rare except in a few samples of the upper 200 m of the sequence where they might be associated with IRD. Reworked palynomorphs are absent in the lower part of the sequence (below 200 mcd). Dinocysts are common to abundant (10<sup>2</sup>–10<sup>4</sup> cysts/cm<sup>3</sup>) in most samples of the upper 200 mcd of the sequence, whereas their concentration is usually lower (<10<sup>2</sup> cysts/cm<sup>3</sup>) below 200 mcd. The dinocyst assemblages are largely dominated by Gonyaulacoid taxa, commonly related to autotrophic productivity. Heterotrophic taxa, such as *Brigantedinium*, occur sporadically and mainly in the upper 145 mcd of the sequence. The species diversity of dinocyst assemblages is high throughout. The dominant taxa are *Operculodinium centrocarpum*, *Nematosphaeropsis labyrinthea*, *Impagidinium aculeatum*, and *Spiniferites mirabilis-hyperhacanthus*. Several *Impagidinium* spp. are present. The most common are *Impagidinium paradoxum*, *Impagidinium patulum*, *Impagidinium velorum*, and *Impagidinium? pallidum*. In general, the dinocyst assemblages suggest cool to warm temperate conditions in surface waters, depending upon the proportion of the warm-water components (*I. aculeatum*, *I. patulum*, *I. paradoxum*, and *S. mirabilis-hyperhacanthus*) versus that of more ubiquitous taxa (*O. centrocarpum* and *N. labyrinthea*). Subpolar taxa, such as *I. pallidum* and *Sphenolithus elongates*, are present in many samples.

The sequence contains many extinct dinocyst taxa that might help to establish a biostratigraphic framework. However, many of these taxa were only recently described and their chronostratigraphic correlations are poorly constrained. This is the case for *Operculodinium tegillatum*, *Pyxidiniopsis vesiculata*, and

*Ataxiodinium zevenboomii* (Head, 1997; Head and Norris, 2003). Many observed specimens belong to taxa difficult to identify at a species level without systematic observations, such as cysts provisionally attributed to *Batiacasphaera* spp., *Impagidinium* spp., and *Achomosphaera* spp. Nevertheless, the overall dinocyst assemblage allows tentative biostratigraphic considerations. The occurrence of *I. velorum* in Sample 303-U1308A-3H-CC suggests an age of at least 0.4 Ma at 28 mcd, and the occurrence of *Filifera filifera* in Sample 303-U1308A-6H-CC suggests sediments older than 0.7 Ma at 62 mcd (cf. de Vernal et al., 1992). The overall assemblage below Sample 303-U1308A-13H-CC (133 mcd) has a Pliocene character, notably because of the presence of *A. zevenboomii*, *Batiacasphaera* spp., and other extinct taxa. The co-occurrence of *Invertocysta lacrymosa*, *Nematosphaeropsis* sp. 1, and incertae sedis sp. 1 in Sample 303-U1308A-20H-CC (202 mcd) indicates an age of ~2.7–2.8 Ma (de Vernal and Mudie 1989; Louwye et al., 2004), which is consistent with the occurrence of *Operculodinium ?eirikianum* based on correlation with DSDP Site 611 (cf. Mudie, 1987). Finally, the significant occurrence of *Corrudinium devernaliae* in Sample 303-U1308A-29H-CC at 290 mcd suggests an age of at least 3.7 Ma (Head and Norris, 2003).

### **Bolboforma**

*Bolboforma* occurred in Sections 303-U1308A-35H-CC and 303-U1308A-36H-CC (346.6–355.6 mcd). In Sample 303-U1308A-35H-CC, *Bolboforma* are rare. They are hemispherical with a flat base. The outer wall has a fine hexagonal structure, and there is an opening on a short smooth neck. *Bolboforma* are frequent in Sample 303-U1308A-36H-CC. The most abundant larger species (maximum diameter = 200–400 μm) is conical with a flat base. The outer wall has a coarse reticulate structure, which often forms hexagons or runs as simple costae toward the simple round opening. The species is possibly *Bolboforma reticulata*, which has been reported from Hole 609B as abundant in the upper Zone NN11 of the upper Miocene (Pallant and Kaminski, 1989). Other species of *Bolboforma* in Section 303-U1308A-36H-CC are

- Globular, hispid, with an opening on a short neck;
- Globular with a fine hexagonal outer structure; and
- Onion-shaped with a small flat base, finely striated, with an aperture on a conical elevation.

### **Paleomagnetism**

The natural remanent magnetization (NRM) of all undisturbed archive-half core sections from Site

U1308 was measured before and after alternating-field (AF) demagnetization in peak fields of 10 mT. Sections 303-U1308B-8H-6, 12H-3, 12H-4, 12H-5 and 303-U1308C-19H-2 and 20H-2 were additionally AF demagnetized in peak fields of 15 and 20 mT. Core 303-U1308F-24H was additionally AF demagnetized in peak field of 15 mT.

The NRM intensities, inclinations, and declinations from Site U1308 are shown in Figures F14, F15, and F16, respectively. Data associated with intervals identified as drilling slurry affected by drilling disturbance or exceptionally coarse grained deposits (see “Lithostratigraphy”) were culled. NRM intensities of Cores 303-U1308A-1H through 24H (lithologic Unit I and Subunit IIA; see “Lithostratigraphy”) range between  $10^{-2}$  and  $10^{-1}$  A/m. Below Core 303-U1308A-25H, the white nannofossil ooze of lithologic Subunit IIB has much lower intensities in the  $10^{-4}$  and  $10^{-3}$  A/m range (Fig. F14). After AF demagnetization at 10 mT, intensities are reduced by ~30% (Fig. F14). Further AF demagnetization at peak fields of 15 mT or 20 mT produced only minor intensity changes and was not routinely undertaken.

Steep positive inclinations observed prior to demagnetization and caused by the drill string magnetic overprint are generally removed by peak AF demagnetization of 10 mT, and inclinations at that level vary around the expected values (approximately  $\pm 68^\circ$ ) for a geocentric axial dipole. Tensor tool-corrected declinations are consistent with inclination-defined polarity interpretations. These results suggest that the characteristic remanent magnetization is usually adequately defined after AF demagnetization at 10 mT peak fields.

Holes U1308A–U1308C, U1308E, and U1308F (only one core was recovered from Hole U1308D) document an apparently continuous sequence of polarity transitions allowing correlation to the geomagnetic polarity timescale (Cande and Kent 1995; Channell et al., 2002; 2003) (Figs. F15, F16). Identification of the Brunhes, Matuyama, and Gauss Chronozones are unambiguous. Additionally, the lower part of Hole U1308A appears to extend into the Gilbert Chronozone. Within the Matuyama Chronozone, the Jaramillo, Cobb Mountain, Olduvai, and Reunion Subchronozones are identified, as are the Kaena and Mammoth Subchronozones within the Gauss Chronozone. The top transition of the Olduvai Subchronozone is truncated at the top and base of Cores 303-U1308A-24H and 303-U1308B-24H. A short interval of normal polarity below the Jaramillo Subchronozone is tentatively interpreted as the Punaruu geomagnetic excursion previously found in a volcanic section on Tahiti (Chauvin et al., 1990) and at ODP Leg 162 Sites 983 and 984 (Channell et al., 2002).

The Gauss/Matuyama transition is complicated by an interval of nonhorizontal bedding (see “**Lithostratigraphy**”) common in Cores 17H through 19H of the different holes. Inclinations above the interpreted Gauss/Matuyama boundary are shallower than expected, possibly as a result of structural deformation. In the lower part of Hole U1308A, a mixed polarity interval is tentatively interpreted as the Gilbert Chronozone. Table T26 summarizes the depths (mbsf and mcd) of the polarity transitions and events identified in the different holes at Site U1308 and the correlation to the geomagnetic polarity timescale (Cande and Kent 1995; Channell et al., 2002, 2003). Age interpretations are summarized in Table T27.

## Composite section

Six holes were drilled at Site U1308 to ensure complete recovery of the stratigraphic section to 239 mcd. Many holes were required because of disturbance in cores caused by excessive heave, poor recovery, and problems with damaged core liners (implosion). Several adjustments were made while drilling Holes U1308E and U1308F to correct offsets among holes by either drilling ahead or advancing by <9.5 m. The latter resulted in recorded sections that overlapped the previous cores but was effective at avoiding lost sections that resulted when drilling ahead.

Because of the lower sedimentation rates at Site U1308, MST data were collected for most cores at a higher spatial resolution (every 2.5 cm) than other Expedition 303 sites. This proved to be beneficial especially for NGR because the signal bears a close resemblance to the marine oxygen isotope record (see “**Physical properties**”). Cores were depth-shifted on the basis of magnetic susceptibility data collected with the “Fast Track” magnetic susceptibility core logger soon after recovery. Features are generally well aligned among holes, although some sections are stretched or compressed relative to others (Fig. F17). It is therefore impossible to align every feature in cores across all holes, but we plan to apply corrections for stretching and squeezing postcruise. The offsets and composite depths are listed in Table T28. Because of the highly disturbed nature of Cores 303-U1308A-18H, 20H, and 24H through 26H, it was not possible to correlate these cores to the other holes. Similarly, Cores 303-U1308B-21H and 22H were not correlated because they represent short disturbed sections.

The sections of core used for the splice are identified in Table T29. When constructing the splice, we plotted the occurrence of all disturbed sections and ex-

cluded them from the splice. The cores from Site U1308 provide a continuous stratigraphic sequence to ~239 mcd with a single problematic interval between ~186 and 196 mcd where sediment deformation was apparent, including inclined bedding and sharp contacts (see “**Lithostratigraphy**”). Although it is possible to construct a continuous stratigraphic section through this interval, it may not be continuous in time. Below Core 303-U1308C-24H, cores were appended to the base of the splice.

A growth factor (GF) of 1.07 is calculated by linear regression for all holes at Site U1308, indicating a 7% increase in mcd relative to mbsf (Fig. F18). We used this value of GF to calculate corrected meters composite depth (cmcd) presented in Table T28 to aid in the calculation of mass accumulation rates.

We calculated sedimentation rates using paleomagnetic datums (Table T30). Linear regression provides a mean sedimentation rate of 8.3 cm/k.y. for the composite section down to 262 mcd (Fig. F19). The interval sedimentation rates vary slightly from 5.6 to 11.0 cm/k.y. Sedimentation rates for Subunit IIB (262.14–355.49 mcd) below the spliced sections were lower, averaging ~3 cm/k.y.

## Geochemistry

### Volatile hydrocarbons

Headspace gas analysis was performed as a part of the standard protocol required for shipboard safety and pollution prevention monitoring. A total of 35 headspace samples from Hole U1308A were analyzed at a sampling resolution of one per core (Table T31). Methane ( $C_1$ ) is the only hydrocarbon detected at this site.  $C_1$  concentrations in Hole U1308A are low and constant, ranging from 1.9 to 4.0 ppmv. The maximum  $C_1$  concentration is 4.0 ppmv at 137 mcd (Fig. F20).

### Sedimentary geochemistry

A total of 57 samples were collected for analysis of solid-phase geochemistry (inorganic carbon and elemental C, N, and H) from Site U1308, with a sample spacing of two per core. Figure F21 shows calcium carbonate ( $CaCO_3$ ) concentrations, total organic carbon (TOC) contents, total N concentrations, and organic C/N ratios. Results of coulometric and elemental analyses are reported in Table T32.

$CaCO_3$  contents for Site U1308 samples range from 12.1 to 94.2 wt% (average = 70.4 wt%) (Fig. F21).  $CaCO_3$  contents fluctuate considerably from the shallowest sediment to 165 mcd and are consistently high (>64 wt%) below this depth. Below 272 mcd,  $CaCO_3$  contents are higher than 90 wt%. TOC and

total N contents range from 0 to 1.5 wt% and from 0 to 0.13 wt%, respectively (Fig. F21). The mean TOC and total N contents at Site U1308 are ~0.3 wt% and ~0.04 wt%, respectively. TOC and total N are below detection limit for several samples (Table T32).

Most C/N values range between 1 and 56 (Fig. F21). Average C/N values of 15 indicate contribution of terrigenous organic matter. Low C/N values of <4 are probably an artifact of low TOC concentrations combined with the tendency of clay minerals to adsorb ammonium ions generated during degradation of organic matter (Müller, 1977).

### Interstitial water chemistry

A total of 16 whole-round samples were collected from Hole U1308A for shipboard interstitial water geochemical analyses. In addition to whole-round samples, interstitial waters were collected from small plug (~10 cm<sup>3</sup>) sediment samples for the upper ~100 mcd for shore-based studies. Results of interstitial water analyses for Site U1308 are reported in Table T33 and Figure F22.

### Chloride, sodium, pH, and boron

Chloride (Cl<sup>-</sup>) concentrations increase abruptly from 562 mM at 21 mcd to 568 mM at 33 mcd. Below 33 mcd, Cl<sup>-</sup> concentrations decrease downhole to 563 mM at the base of the cored interval. Pore fluid sodium (Na<sup>+</sup>) concentrations range from 482 to 500 mM (Fig. F22). Unlike Cl<sup>-</sup>, Na<sup>+</sup> concentrations increase downhole to 215 mcd. pH values range from 6.7 to 7.3 at Site U1308 (Fig. F22). Interstitial waters are slightly acidic below 159 mcd.

Interstitial water boron concentrations range from 425 to 549 µM and are near the seawater value of 427 µM or higher (Fig. F22). Slight decreases in boron concentrations are observed in the upper 66 mcd. Below this depth, boron concentrations increase with depth toward the base of the recovered section. Boron concentrations seem to reflect pH variations, as at Sites U1306 and U1307. These increasing boron concentrations are primarily caused by desorption from clay minerals under low pH conditions (Fig. F21; Table T32).

### Alkalinity, sulfate, ammonium, and dissolved silica

Alkalinity increases steadily from 3.0 mM at the surface to 6.1 mM at 66 mcd. Below 66 mcd, alkalinity varies in a narrow range (5.3–6.6 mM) (Fig. F22). Sulfate (SO<sub>4</sub><sup>2-</sup>) concentrations decrease downhole in the upper 33 mcd (Fig. F22) and then more gradually to the base of the recovered section reaching a minimum of 9 mM. Ammonium (NH<sub>4</sub><sup>+</sup>) steadily increases

from 24 µM at the surface to ~1000 µM at 185 mcd (Fig. F22). Dissolved silica (H<sub>4</sub>SiO<sub>4</sub>) concentrations range from 397 to 1215 µM (Fig. F22). The increase in H<sub>4</sub>SiO<sub>4</sub> concentrations downhole reflects varying degrees of dissolution of biogenic silica in the sediments and reaches a maximum concentration of 1215 µM at 272 mcd. The maximum H<sub>4</sub>SiO<sub>4</sub> concentration coincides with poorest preservation and abundance of siliceous microfossils (see “[Biostratigraphy](#)”).

### Calcium, strontium, and lithium

Calcium (Ca<sup>2+</sup>) concentrations decrease downhole from seawater values for the uppermost sediments to a minimum of 6.8 mM at 126 mcd (Fig. F22). Below this depth, Ca<sup>2+</sup> concentrations substantially increase with depth. At the base of the cored interval, Ca<sup>2+</sup> concentrations reach 16.4 mM exceeding the standard seawater concentration (10.5–10.55 mM). The shallow decrease in Ca<sup>2+</sup> at 126 mcd is likely caused by diagenetic carbonate precipitation because alkalinity reaches a maximum at the corresponding depth. However, the elevated Ca values at depth cannot be attributed to calcite dissolution (see Sr discussion) but rather are likely the result of sedimentary silicate mineral or basement alteration below the drilled interval (e.g., Gieskes and Lawrence, 1981) (i.e., recrystallization; see Sr discussion). Hence, the increase in Ca<sup>2+</sup> at depth is not the result of carbonate dissolution.

Strontium (Sr<sup>2+</sup>) concentrations gradually increase with depth from the seafloor to a maximum of 1592 µM at the base of Hole U1308A (Fig. F22). Sr/Ca ratios reach a maximum of 115 at 215 mcd (Fig. F22). Below this maximum, Sr/Ca ratios remain high to the base of the cored interval. The elevated Sr values and Sr/Ca ratios are interpreted to be the result of dissolution and reprecipitation of biogenic carbonates (i.e., recrystallization), during which Sr<sup>2+</sup> is expelled and released to interstitial water. The elevated Sr values cannot be the result of pure dissolution of CaCO<sub>3</sub>. Dissolution of biogenic carbonates would not result in increasing Sr/Ca ratios because Ca is much more abundant than Sr in carbonates (Baker et al., 1982).

Lithium (Li<sup>+</sup>) concentrations vary little in the uppermost 43 mcd (Fig. F22). Both precipitation of calcite and alteration of volcanic material can remove Li<sup>+</sup> from interstitial water. Based on the calculation using a typical Li/Ca molar ratio of 20 × 10<sup>-6</sup> in marine carbonates, interstitial water Li<sup>+</sup> concentrations should only decrease at most by 0.2 µM because of precipitation of calcite. Hence, Li<sup>+</sup> concentrations in the upper 43 mcd imply uptake of Li<sup>+</sup> into silicate alteration products. At greater depth (>185 mcd), dis-

solved  $\text{Li}^+$  concentrations increase sharply downcore. A maximum  $\text{Li}^+$  concentration of 322  $\mu\text{M}$  was observed at the base of the cored sequence at Site U1308. Several explanations for  $\text{Li}^+$  enrichment in deep interstitial water have been proposed. These include hydrothermal alteration of underlying basalt (Martin et al., 1991; Stoffyn-Egli and MacKenzie, 1984), alteration or ion exchange with clays (Kimura et al., 1997), and diagenetic alteration of biogenic opal A (Gieskes, 1981). High  $\text{Li}^+$  concentrations near the base of the hole cannot be explained conclusively with available data. However, the minimal opal A content in the sediment points toward alteration of silicate minerals or basement.

### Magnesium and potassium

Magnesium ( $\text{Mg}^{2+}$ ) concentrations progressively decrease from seawater values of 51.7 to 24.4 mM at the base of the hole (Fig. F22). Potassium ( $\text{K}^+$ ) concentrations also decrease downcore to a minimum of 8.6 mM at the base of the hole (Fig. F22). These decreasing trends are presumably attributed to clay mineral diagenesis during which  $\text{Mg}^{2+}$  and  $\text{K}^+$  are consumed and  $\text{Ca}^{2+}$  is produced (Gieskes, 1973) and/or diffusional communication with basement alteration (Gieskes and Lawrence, 1981).

### Manganese, barium, and iron

Manganese ( $\text{Mn}^{2+}$ ) concentrations decrease sharply to 33 mcd and remain low throughout the cored interval (Fig. F22). Iron ( $\text{Fe}^{2+}$ ) is almost depleted in the uppermost sample (Fig. F22). Below the surface, the  $\text{Fe}^{2+}$  contents fluctuate between values of 12 and 30  $\mu\text{M}$ . Interstitial water barium ( $\text{Ba}^{2+}$ ) concentrations are low ( $\sim 0.6 \mu\text{M}$ ) throughout the section and show a slight increasing trend with depth (Fig. F22). The average  $\text{Ba}^{2+}$  concentration in interstitial water at Site U1308 is 0.3  $\mu\text{M}$ .

## Physical properties

Measurements of physical properties were conducted at Site U1308 following the procedures described in “Physical properties” in the “Site U1302–U1308 methods” chapter. Two measurements of magnetic susceptibility were conducted, along with GRA density, NGR, and *P*-wave velocity. Moisture and density (MAD) properties were also measured on two discrete samples per core in Hole U1308A, usually at the bottom of Section 1 and the top of Section 6.

### Whole-core magnetic susceptibility measurements

Site U1308 has peak magnetic susceptibility values of  $\sim 200 \times 10^{-5}$  SI and minimum values approaching in-

strument noise levels with most values ranging from  $20 \times 10^{-5}$  to  $100 \times 10^{-5}$  SI (Fig. F23). Magnetic susceptibility values from 0 to  $\sim 193$  mcd show high-amplitude, high-variability changes with an average magnetic susceptibility value of  $73 \times 10^{-5}$  SI, whereas magnetic susceptibility values from  $\sim 193$  to 259 mcd show high-variability changes and have an average value of  $54 \times 10^{-5}$  SI. In the 259–355 mcd interval, magnetic susceptibility values generally approach instrument noise levels with an average value of  $6 \times 10^{-5}$  SI.

### Density

Bulk density measurements taken at Site U1308 show a similar trend among holes and are variable, ranging from 1.0 to 2.0  $\text{g}/\text{cm}^3$  (Fig. F24). Generally, the bulk density plots are highly variable and show a peak to peak match with magnetic susceptibility plots. The density values increase downhole from 0 to 193 mcd with an average value of  $\sim 1.6 \text{g}/\text{cm}^3$ . From 193 to 259 mcd, the average density increases from 1.6 to 1.8  $\text{g}/\text{cm}^3$  and the amplitude of the variation decreases. There is an abrupt increase in the rate of change in density in the 255 to 355 mcd interval with an average value of 1.8  $\text{g}/\text{cm}^3$ . The discrete measurements match the trends of the MST values; however, the discrete measurements are generally lower than GRA density values (Fig. F24).

### Natural gamma radiation

NGR counts range from 0 to 41 cps with the majority of the values between 1 and 20 cps (Fig. F25). From 0 to 188 mcd, NGR covaries with magnetic susceptibility, showing highly variable, high amplitude values that average  $\sim 18$  cps. From 193 to 355 mcd, NGR average values are lower ( $\sim 14$  cps) and show low variability. The 193–355 mcd interval also shows a discontinuity at  $\sim 255$  mcd, which is consistent with magnetic susceptibility plots.

### *P*-wave velocity

Both *P*-wave logger (PWL) and discrete *P*-wave sensor number 3 (PWS3) measurements were performed where possible at Site U1308. Values vary between 1500 and 1700 m/s and increase downhole (Fig. F26). We see an offset between PWL and PWS3 measurements. The exact nature of this offset is unknown and is a long-standing problem not unique to Expedition 303 (see “Physical properties” in the “Site U1302–U1308 methods” chapter).

### Porosity

Porosity was calculated using GRA density measurements and spot-checked with the porosity results

generated from the discrete MAD samples. Porosity values are highly variable and range from 40% to 84% (Fig. F27). As expected, porosity shows an inverse relationship to density, decreasing with depth at Site U1308 to an average minimum value of 50%.

## Discussion

The magnetic susceptibility, density, and NGR records show similar patterns of high-amplitude variability that decrease downcore (Fig. F28). Two distinct changes at 193 and 255 mcd are used to define three geophysical units that are closely related to lithologic Units I and Subunits IIA, and IIB (see “**Lithostratigraphy**”). Geophysical Unit 1 (0 to ~193 mcd, corresponding to lithologic Unit I) is characterized by the highest values and greatest variability in magnetic susceptibility, density, and NGR records. Magnetic susceptibility and NGR generally covary within this interval, whereas density appears to be antithetic. Unit 2 (~193–255 mcd, corresponding to lithologic Subunit IIA) is marked by a decrease in amplitude of the high-frequency variability in magnetic susceptibility and NGR that is observed in Unit 1. Unit 3 sediments (255–355 mcd, corresponding to lithologic Subunit IIB) have low NGR and magnetic susceptibility values (approaching instrument noise levels) and have high densities.

High magnetic susceptibility and NGR amplitudes suggest that the delivery of terrigenous material to Site U1308 is highly variable in Unit 1. Decreased magnetic susceptibility and NGR amplitudes in Unit 2 reflect a reduction in terrigenous materials or an increase in the biogenic component of the sediments. In Unit 3, magnetic susceptibility and NGR values approach instrument noise levels, indicating the presence of little to no terrigenous material. This trend of increasing uphole values in magnetic susceptibility and NGR in Unit 2 may be related to the onset of NHG (see “**Lithostratigraphy**”).

Density values gradually increase downcore through geophysical Unit 1 (0 to ~193 mcd) and the upper part of Unit 2 (193–245 mcd). There is an abrupt increase in density from the base of Unit 2 to Unit 3 (245–355 mcd). We interpret the gradual increase in density in Units 1 and the upper part of Unit 2 to reflect sediment compaction. The sharper increase from the base of Unit 2 through Unit 3 reflects the early stages of the transition of nannofossil ooze to nannofossil chalk (see “**Lithostratigraphy**”).

## References

- Andersen, C., Koç, N., and Moros, M., 2004. A highly unstable Holocene climate in the subpolar North Atlantic: evidence from diatoms. *Quat. Sci. Rev.*, 23:2155–2166. doi:10.1016/j.quascirev.2004.08.004
- Baker, P.A., Gieskes, J.M., and Elderfield, H., 1982. Diagenesis of carbonates in deep-sea sediments—evidence from Sr<sup>2+</sup>/Ca<sup>2+</sup> ratios and interstitial dissolved Sr<sup>2+</sup> data. *J. Sediment. Petrol.*, 52:71–82.
- Baldauf, J.G., 1987. Diatom biostratigraphy of the middle- and high-latitude North Atlantic Ocean, Deep Sea Drilling Project Leg 94. In Ruddiman, W.F., Kidd, R.B., Thomas, E., et al., *Init. Repts. DSDP*, 94 (Pt. 2): Washington (U.S. Govt. Printing Office), 729–762.
- Bond, G., Broecker, W., Johnsen, S., McManus, J., Labeyrie, L., Jouzel, J., and Bonani, G., 1993. Correlations between climate records from the North Atlantic sediments and Greenland ice. *Nature (London, U. K.)*, 365:143–147. doi:10.1038/365143a0
- Bond, G., Heinrich, H., Broecker, W., Labeyrie, L.D., McManus, J., Andrews, J., Huon, S., Jantschik, R., Clasen, S., Simet, C., Tedesco, K., Klas, M., Bonani, G., and Ivy, S., 1992. Evidence for massive discharges of icebergs into the North Atlantic Ocean during the last glacial period. *Nature (London, U. K.)*, 360:245–249. doi:10.1038/360245a0
- Bond, G., Showers, W., Cheseby, M., Lotti, R., Almasi, P., deMenocal, P., Priore, P., Cullen, H., Hajdas, I., and Bonani, G., 1997. A pervasive millennial-scale cycle in North Atlantic Holocene and glacial climates. *Science*, 278:1257–1266. doi:10.1126/science.278.5341.1257
- Bond, G.C., and Lotti, R., 1995. Iceberg discharges into the North Atlantic on millennial time scales during the last glaciation. *Science*, 276:1005–1010.
- Bond, G.C., Kromer, B., Beer, J., Muscheler, R., Evans, M., Showers, W., Hoffmann, S., Lotti-Bond, R., Hajdas, I., and Bonani, G., 2001. Persistent solar influence on North Atlantic climate during the Holocene. *Science*, 2130–2136. doi:10.1126/science.1065680
- Bond, G.C., Showers, W., Elliot, M., Evans, M., Lotti, R., Hajdas, I., Bonani, G., and Johnson, S., 1999. The North Atlantic's 1–2 kyr climate rhythm: relation to Heinrich events, Dansgaard/Oeschger cycles and the Little Ice Age. In Clark, P.U., Webb, R.S., and Keigwin, L.D. (Eds.), *Mechanisms of Global Climate Change at Millennial Time Scales*. Geophys. Monogr., 112:35–58.
- Broecker, W.S., Bond, G., Klas, M., Bonani, G., and Wolfli, W., 1990. A salt oscillator in the glacial Atlantic? 1. The concept. *Paleoceanography*, 5:469–477.
- Broecker, W.S., Bond, G.C., Mieczyslaw, K., Clark, E.A., and McManus, J., 1992. Origin of the northern Atlantic's Heinrich events. In Kelts, K.R. (Ed.), *Past and Present Climate Dynamics: Reconstruction of Rates of Change*. Clim. Dyn. 6(3–4):265–273. doi:10.1007/BF00193540
- Cande, S.C., and Kent, D.V., 1995. Revised calibration of the geomagnetic polarity timescale for the Late Cretaceous and Cenozoic. *J. Geophys. Res.*, 100:6093–6095. doi:10.1029/94JB03098
- Channell, J.E.T., Labs, J., and Raymo, M.E., 2003. The Reunion Subchronzone at ODP Site 981 (Feni Drift, North Atlantic). *Earth Planet. Sci. Lett.*, 215:1–12.

- Channell, J.E.T., Mazaud, A., Sullivan, P., Turner, S., and Raymo, M.E., 2002. Geomagnetic excursions and paleointensities in the Matuyama Chron at ODP Sites 983 and 984 (Iceland Basin). *J. Geophys. Res.*, 107. [doi:10.1029/2001JB000491](https://doi.org/10.1029/2001JB000491)
- Chauvin, A., Roperch, P., and Duncan, R.A., 1990. Records of geomagnetic reversals from volcanic islands of French Polynesia, 2. Paleomagnetic study of a flow sequence (1.2–0.6 Ma) from the island of Tahiti and discussion of reversal models. *J. Geophys. Res.*, 95:2727–2752.
- Clement, B.M., and Robinson, F., 1987. The magnetostratigraphy of Leg 94 sediments. In Ruddiman, W.F., Kidd, R.B., Thomas, E., et al., *Init. Repts. DSDP*, 94 (Pt. 2): Washington (U.S. Govt. Printing Office), 635–650.
- Crosta, X., Pichon, J.-J., and Labracherie, M., 1997. Distribution of *Chaetoceros* resting spores in modern peri-Antarctic sediments. *Mar. Micropaleontol.*, 29:283–299. [doi:10.1016/S0377-8398\(96\)00033-3](https://doi.org/10.1016/S0377-8398(96)00033-3)
- de Vernal, A., and Mudie, P.J., 1989. Pliocene and Pleistocene palynostratigraphy at ODP Sites 646 and 647, eastern and southern Labrador Sea. In Srivastava, S.P., Arthur, M.A., Clement, B., et al., *Proc. ODP, Sci. Results*, 105: College Station, TX (Ocean Drilling Program), 401–422. [PDF]
- de Vernal, A., Londeix, L., Mudie, P.J., Harland, R., Morzadec-Kerfourn, M.T., Turon, J.-L., and Wrenn, J.H., 1992. Quaternary organic-walled dinoflagellate cysts of the North Atlantic Ocean and adjacent seas: ecostratigraphy and biostratigraphy. In Head, M.J., and Wrenn, J.H. (Eds.), *Neogene and Quaternary Dinoflagellate Cysts and Atractarchs*: Salt Lake City (Publisher's Press), 289–328.
- Ericson, D.B., Wollin, G., and Wollin, J., 1954. Coiling direction of *Globorotalia truncatulinoides* in deep-sea cores. *Deep-Sea Res., Part II*, 2:152–158.
- Gieskes, J.M., 1981. Deep-sea drilling interstitial water studies: implications for chemical alteration of the oceanic crust, layers I and II. In Warme, J.E., Douglas, R.G., and Winterer, E.L. (Eds.), *The Deep Sea Drilling Project: A Decade of Progress*. Spec. Publ.—Soc. Econ. Paleontol. Mineral., 32:149–167.
- Gieskes, J.M., 1973. Interstitial water studies, Leg 15: alkalinity, pH, Mg, Ca, Si, PO<sub>4</sub>, and NH<sub>4</sub>. In Heezen, B.C., MacGregor, I.D., et al., *Init. Repts. DSDP*, 20: Washington (U.S. Govt. Printing Office), 813–829.
- Gieskes, J.M., and Lawrence, J.R., 1981. Alteration of volcanic matter in deep-sea sediments: evidence from the chemical composition of interstitial waters from deep sea drilling cores. *Geochim. Cosmochim. Acta*, 45:1687–1703.
- Goll, R.M., and Bjørklund, K.R., 1989. A new radiolarian biostratigraphy for the Neogene of the Norwegian Sea: ODP Leg 104. In Eldholm, O., Thiede, J., Taylor, E., et al., *Proc. ODP, Sci. Results*, 104: College Station, TX (Ocean Drilling Program), 697–737. [PDF]
- Grousset, F.E., Pujol, C., Labeyrie, L., Auffret, G., and Boelaert, A., 2000. Were the North Atlantic Heinrich events triggered by the behavior of the European ice sheets? *Geology*, 28:123–126. [doi:10.1130/0091-7613\(2000\)028<0123:WTNAHE>2.3.CO;2](https://doi.org/10.1130/0091-7613(2000)028<0123:WTNAHE>2.3.CO;2)
- Head, M.J., 1997. Thermophilic dinoflagellate assemblages from the mid Pliocene of eastern England *J. Paleontol.*, 71:165–193.
- Head, M.J., and Norris, G., 2003. New species of dinoflagellate cysts and other palynomorphs from the late Neogene of the western North Atlantic, DSDP Hole 603C. *J. Paleontol.*, 77:1–15.
- Hemming, S.R., 2004. Heinrich events: massive late Pleistocene detritus layers of the North Atlantic and their global climate imprint. *Rev. Geophys.*, 42:1–43. [doi:10.1029/2003RG000128](https://doi.org/10.1029/2003RG000128)
- Jansen, E., Bleil, U., Henrich, R., Kringstad, L., and Slettemark, B., 1988. Paleoenvironmental changes in the Norwegian Sea and northeast Atlantic during the last 2.8 m.y.: Deep Sea Drilling Project/Ocean Drilling Program Sites 610, 642, 643, and 644. *Paleoceanography*, 3:563–581.
- Kameo, K., and Sato, T., 2000. Biogeography of Neogene calcareous nannofossils in the Caribbean and the eastern equatorial Pacific—floral response to the emergence of the Isthmus of Panama. *Mar. Micropaleontol.*, 39:201–218. [doi:10.1016/S0377-8398\(00\)00021-9](https://doi.org/10.1016/S0377-8398(00)00021-9)
- Kimura, G., Silver, E.A., Blum, P., et al., 1997. *Proc. ODP, Init. Repts.*, 170: College Station, TX (Ocean Drilling Program). [HTML]
- Louwye, S., Head, M.J., and De Schepper, S., 2004. Dinoflagellate cyst stratigraphy and palaeoecology of the Pliocene in northern Belgium, southern North Sea Basin. *Geol. Mag.*, 141:353–378.
- Martin, J.B., Kastner, M., and Elderfield, H., 1991. Lithium: sources in pore fluids of Peru slope sediments and implications for oceanic fluxes. *Mar. Geol.*, 102:281–292. [doi:10.1016/0025-3227\(91\)90012-S](https://doi.org/10.1016/0025-3227(91)90012-S)
- Martini, E., 1971. Standard Tertiary and Quaternary calcareous nannoplankton zonation. In Farinacci, A. (Ed.), *Proc. 2nd Int. Conf. Planktonic Microfossils Roma*: Rome (Ed. Tecnosci.), 2:739–785.
- Maslin, M.A., Haug, G.H., Sarnthein, M., Tiedemann, R., Erlenkeuser, H., and Stax, R., 1995. Northwest Pacific Site 882: the initiation of Northern Hemisphere glaciation. In Rea, D.K., Basov, I.A., Scholl, D.W., and Allan, J.F. (Eds.), *Proc. ODP, Sci. Results*, 145: College Station, TX (Ocean Drilling Program), 315–329.
- Mayer, L., Pisias, N., Janecek, T., et al., 1992. *Proc. ODP, Init. Repts.*, 138 (Pts. 1 and 2): College Station, TX (Ocean Drilling Program).
- McManus, J., Bond, G., Broecker, W., Johnsen, S., Labeyrie, L., and Higgins, S., 1994. High resolution climate records from the North Atlantic during the last interglacial. *Nature (London, U. K.)*, 371:326–329. [doi:10.1038/371326a0](https://doi.org/10.1038/371326a0)
- Mudie, P.J., 1987. Palynology and dinoflagellate biostratigraphy of Deep Sea Drilling Project Leg 94, Sites 607 and 611, North Atlantic Ocean. In Ruddiman, W.F., Kidd, R.B., Thomas, E., et al., *Init. Repts. DSDP*, 94 (Pt. 2): Washington (U.S. Govt. Printing Office), 785–812.
- Müller, P.J., 1977. C/N ratios in Pacific deep sea sediments: effect of inorganic ammonium and organic nitrogen compounds sorbed by clays. *Geochim. Cosmochim. Acta*, 41:765–776.

- North Greenland Ice Core Project, 2004. High-resolution record of northern hemisphere climate extending into the last interglacial period. *Nature (London, U. K.)*, 431:147–151.
- Pallant, A., and Kaminski, M., 1989. *Bolboforma* from Leg 105, Labrador Sea and Baffin Bay, and the chronostratigraphy of *Bolboforma* in the North Atlantic. In Srivastava, S.P., Arthur, M.A., Clement, B., et al., *Proc. ODP, Sci. Results*, 105: College Station, TX (Ocean Drilling Program), 381–385. [PDF]
- Prell, W., Martin, A., Cullen, J., and Trend, M., 1999. The Brown University Foraminiferal Data Base, IGBP PAGES/World Data Center-A for Paleoclimatology Data Contribution Series No. 1999-2027: Boulder, CO (NOAA/NGDC Paleoclimatology Program).
- Raymo, M.E., Oppo, D.W., Flower, B.P., Hodell, D.A., McManus, J.F., Venz, K.A., Kleiven, K.F., and McIntyre, K., 2004. Stability of North Atlantic water masses in face of pronounced climate variability during the Pleistocene. *Paleoceanography*, 19:10. doi:10.1029/2003PA000921
- Raymo, M.E., Ruddiman, W.F., Backman, J., Clement, B.M., and Martinson, D.G., 1989. Late Pliocene variation in Northern Hemisphere ice sheets and North Atlantic deep water circulation. *Paleoceanography*, 4:413–446.
- Ruddiman, W.F., Cameron, D., and Clement, B.M., 1987. Sediment disturbance and correlation of offset holes drilled with the hydraulic piston corer: Leg 94. In Ruddiman, W.F., Kidd, R.B., Thomas, E., et al., *Init. Repts. DSDP*, 94 (Pt. 2): Washington (U.S. Govt. Printing Office), 615–634.
- Ruddiman, W.F., McIntyre, A., and Raymo, M., 1986. Matuyama 41,000 year cycles: North Atlantic Ocean and Northern Hemisphere ice sheets. *Earth Planet Sci. Lett.*, 80:117–129.
- Ruddiman, W.F., Raymo, M.E., Martinson, D.G., Clement, B.M., and Backman, J., 1989. Pleistocene evolution: Northern Hemisphere ice sheet and North Atlantic Ocean. *Paleoceanography*, 4:353–412.
- Sato, T., Kameo, K., and Mita, I., 1999. Validity of the latest Cenozoic calcareous nannofossil datums and its application to the tephrochronology. *Earth. Sci.*, 53:265–274.
- Sato, T., Yuguchi, S., Takayama, T., and Kameo, K., 2004. Drastic change in the geographical distribution of the cold-water nannofossil *Coccolithus pelagicus* (Wallich) Schiller at 2.74 Ma in the Late Pliocene, with special reference to glaciation in the Arctic Ocean. *Mar. Micropaleontol.*, 52:181–193. doi:10.1016/j.marmicro.2004.05.003
- Schiebel, R., and Hemleben, C., 2000. Interannual variability of planktic foraminiferal populations and test flux in the eastern North Atlantic Ocean (JGOFS). *Deep-Sea Res., Part II*, 47(9–11):1809–1852.
- Smith, W.H.F., and Sandwell, D.T., 1994. Bathymetric prediction from dense satellite altimetry and sparse shipboard bathymetry. *J. Geophys. Res.*, 99:21803–21824. doi:10.1029/94JB00988
- Snoeckx, H., Grousset, F., Revel, M., and Boelaert, A., 1999. European contribution of ice-rafted sand to Heinrich Layers H3 and H4. *Mar. Geol.*, 158(1–4):197–208. doi:10.1016/S0025-3227(98)00168-6
- Stoffyn-Egli, P., and Mackenzie, F.T., 1984. Mass balance of dissolved lithium in the oceans. *Geochim. Cosmochim. Acta*, 48:859–872.
- Thiede, J., and Myhre, A.M., 1996. Introduction to the North Atlantic-Arctic gateways: plate tectonic-paleoceanographic history and significance. In Thiede, J., Myhre, A.M., Firth, J.V., Johnson, G.L., and Ruddiman, W.F. (Eds.), *Proc. ODP, Sci. Results*, 151: College Station, TX (Ocean Drilling Program), 3–23.
- Tiedemann, R., Sarnthein, M., and Shackleton, N.J., 1994. Astronomic timescale for the Pliocene Atlantic  $\delta^{18}\text{O}$  and dust flux records of Ocean Drilling Program Site 659. *Paleoceanography*, 9:619–638.
- Venz, K.A., Hodell, D.A., Stanton, C., and Warnke, D.A., 1999. A 1.0 Myr record of glacial North Atlantic intermediate water variability from ODP Site 982 in the Northeast Atlantic. *Paleoceanography*, 14:42–52.
- Weaver, P.P.E., and Clement, B.M., 1987. Magnetobiostratigraphy of planktonic foraminiferal datums, DSDP Leg 94, North Atlantic. In Ruddiman, W.F., Kidd, R.B., Thomas, E., et al., *Init. Repts. DSDP*, 94: Washington (U.S. Govt. Printing Office), 815–829.
- Whitman, J.M., and Berger, W.H., 1992. Pliocene–Pleistocene oxygen isotope record, Site 586, Ontong Java Plateau. *Mar. Micropaleontol.*, 18:171–198. doi:10.1016/0377-8398(92)90012-9

**Publication:** 9 September 2006  
**MS 303306ER-108**



**Figure F1.** Location of Expedition 303 sites (red) and other Deep Sea Drilling Project (DSDP) and Ocean Drilling Program (ODP) sites mentioned in the text. CGFZ = Charlie Gibbs Fracture Zone.

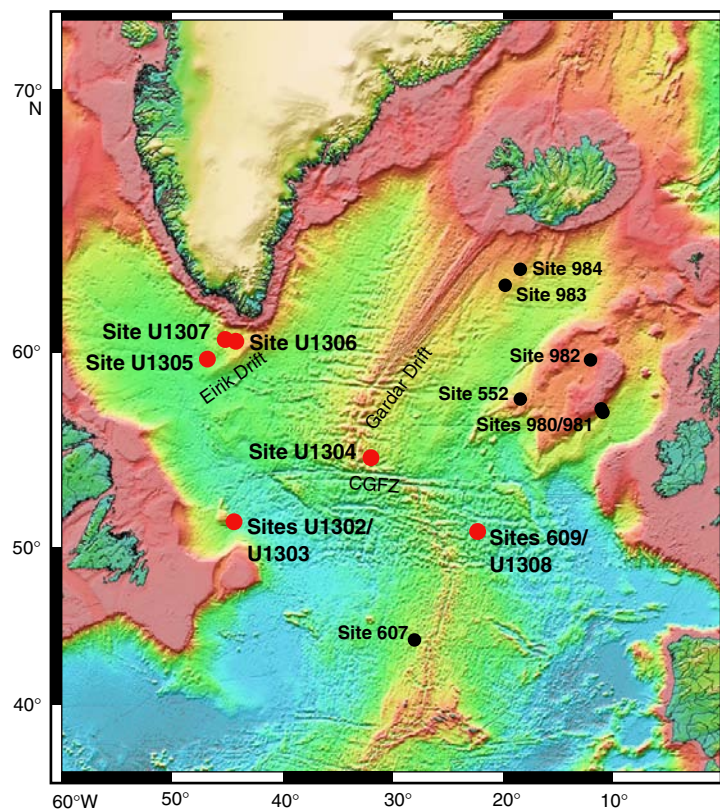


**Figure F2.** Location of Site U1308 lying between the eastern side of the mid-oceanic ridge (to the southwest) and the Isengard Ridge and Porcupine Abyssal Plain (to the northeast). Bathymetry from Smith and Sandwell (1994).

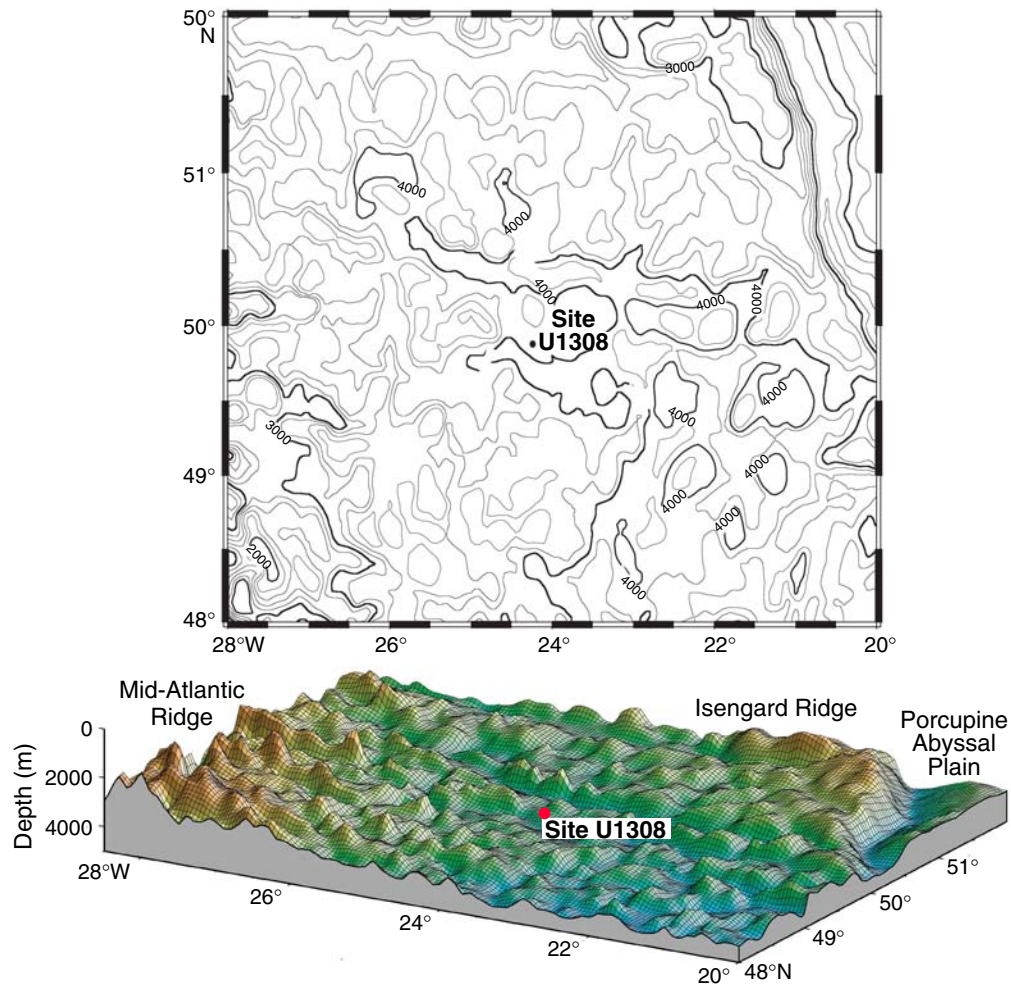


Figure F3. Abundances of quartz, detrital carbonate, foraminifers, and nannofossils.

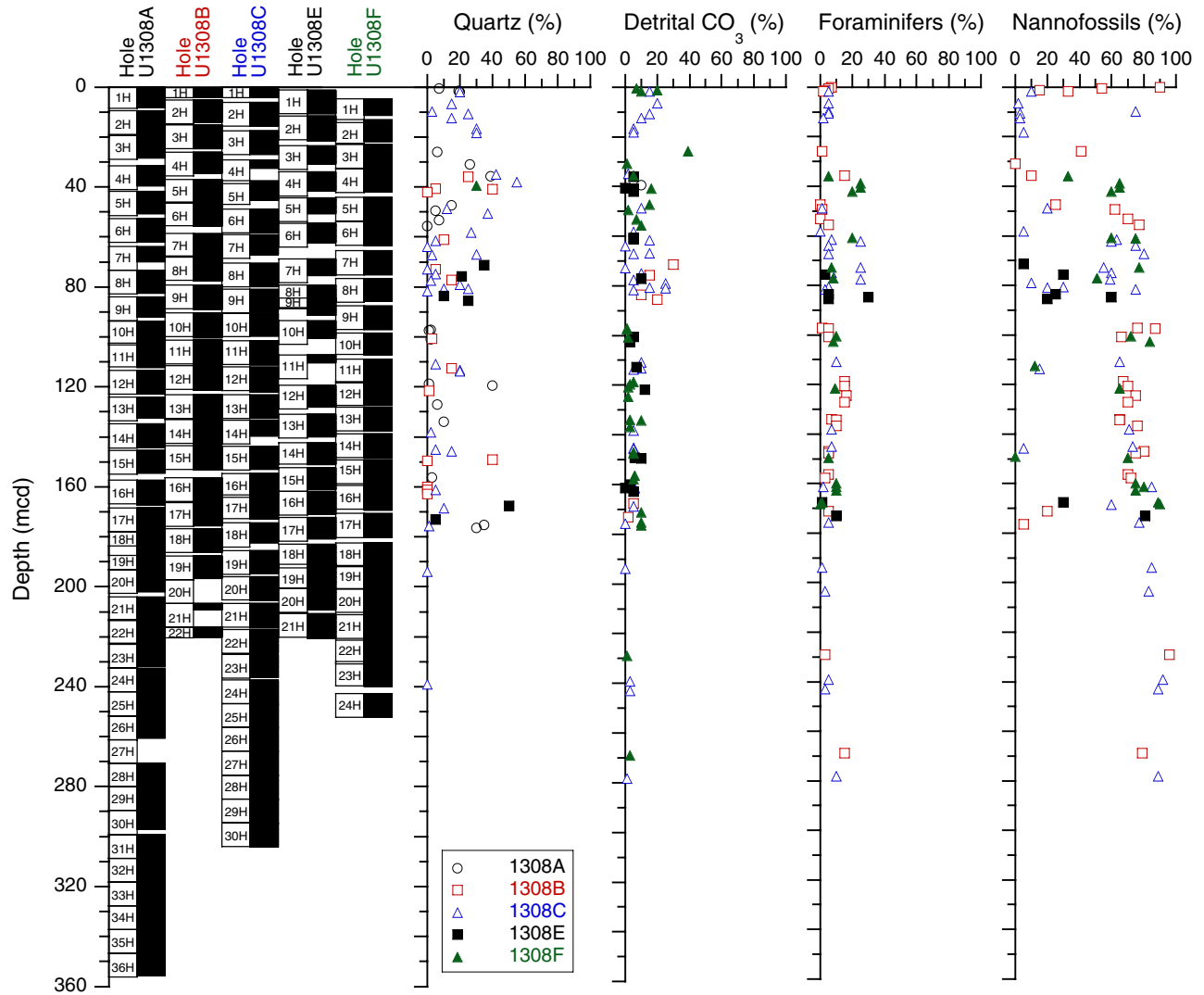




Figure F4. Abundance of gravel-sized grains (number of grains/10 cm length of core).

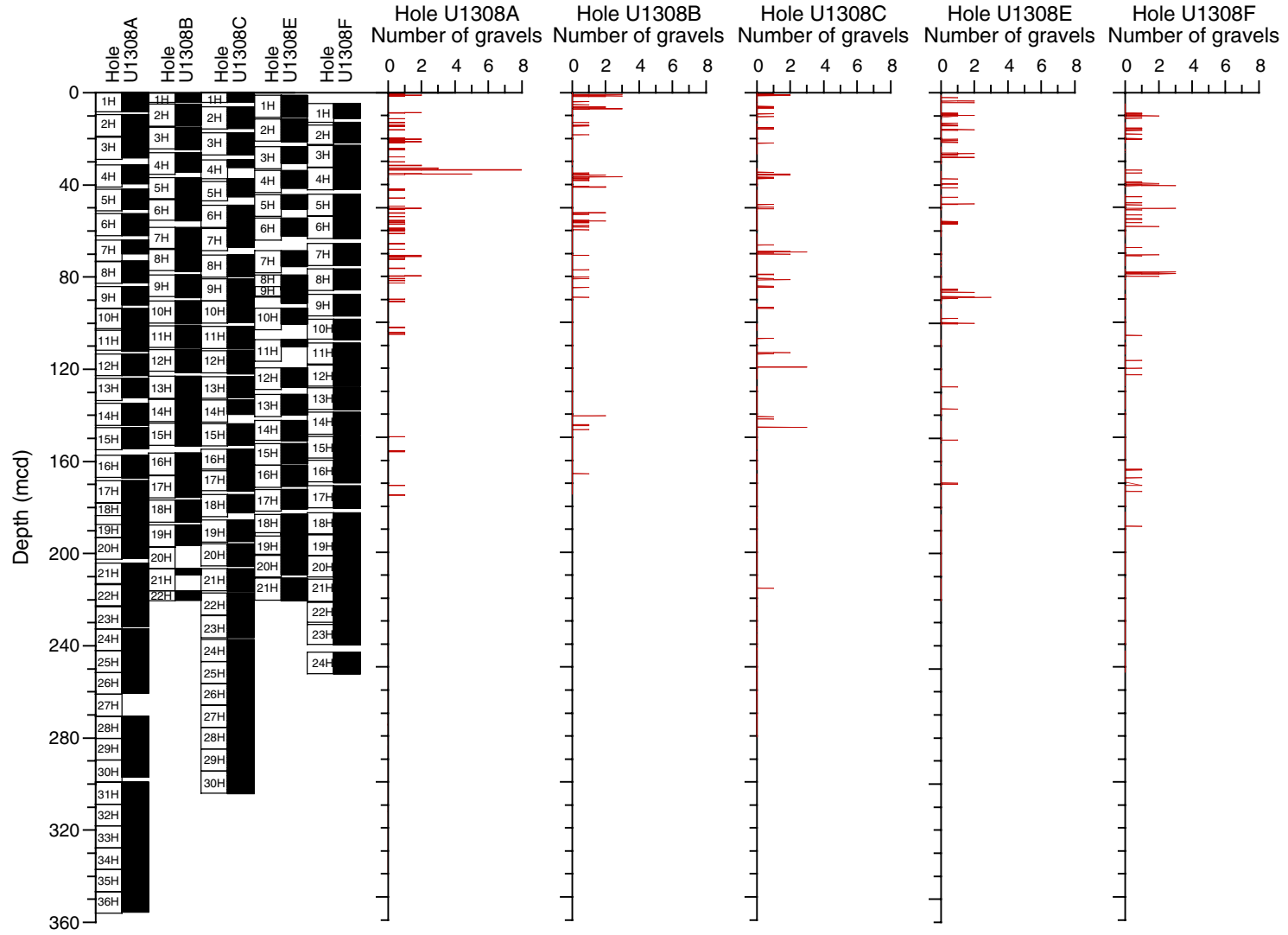
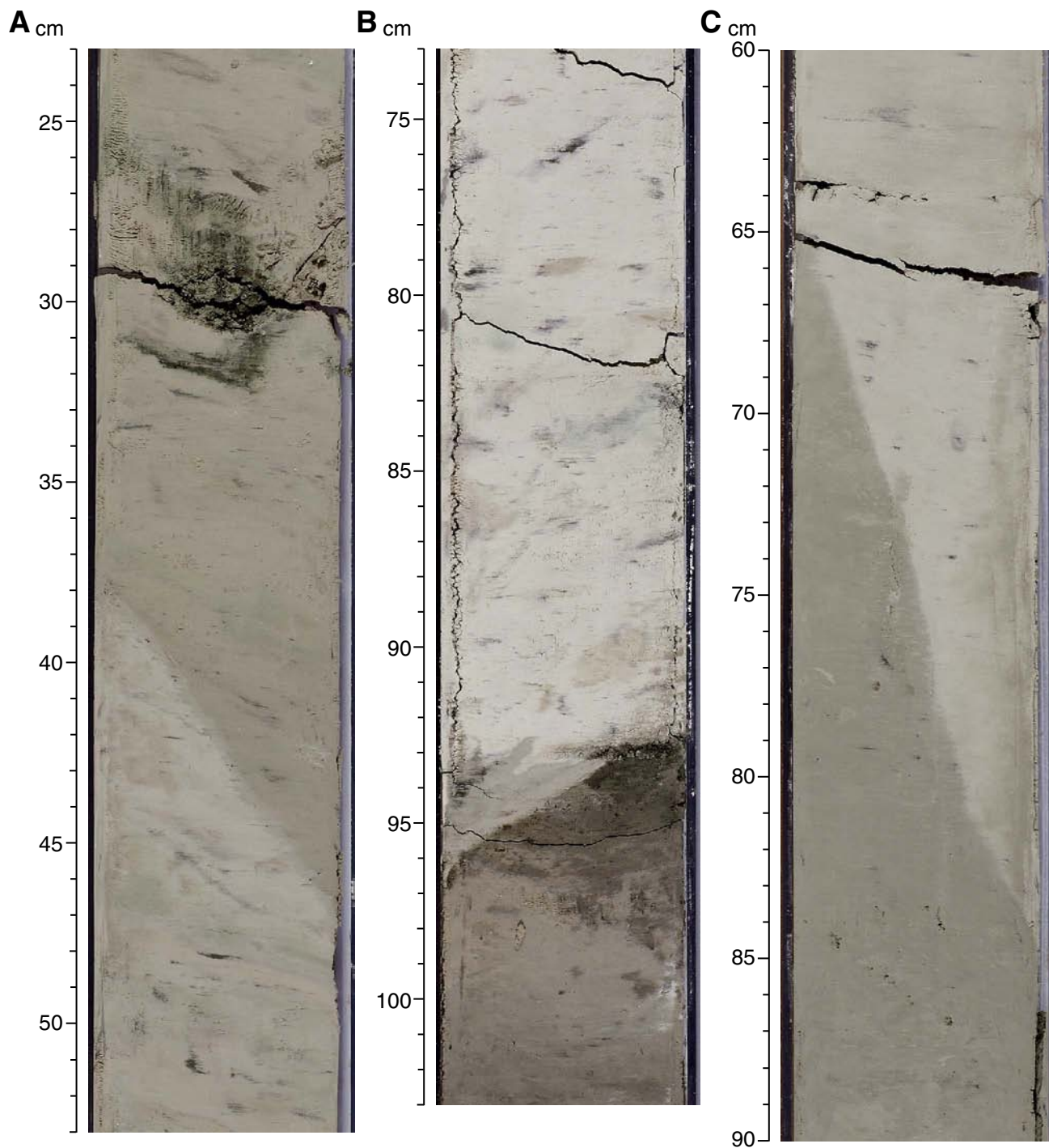


Figure F5. Sharp, inclined contacts between ~170 mcd and ~190 mcd. A. Interval 303-1308E-18H-6, 23–53 cm. B. Interval 303-U1308C-19H-3, 73–103 cm. C. Interval 303-U1308B-17H-2, 60–90 cm.



**Figure F6.** Sediment lightness ( $L^*$ ) values determined from color reflectance data. The Jaramillo Subchron ( $\sim 1$  Ma), Matuyama/Gauss boundary (2.58 Ma), top of the Mammoth Subchron (3.33 Ma), and lithologic units are shown.

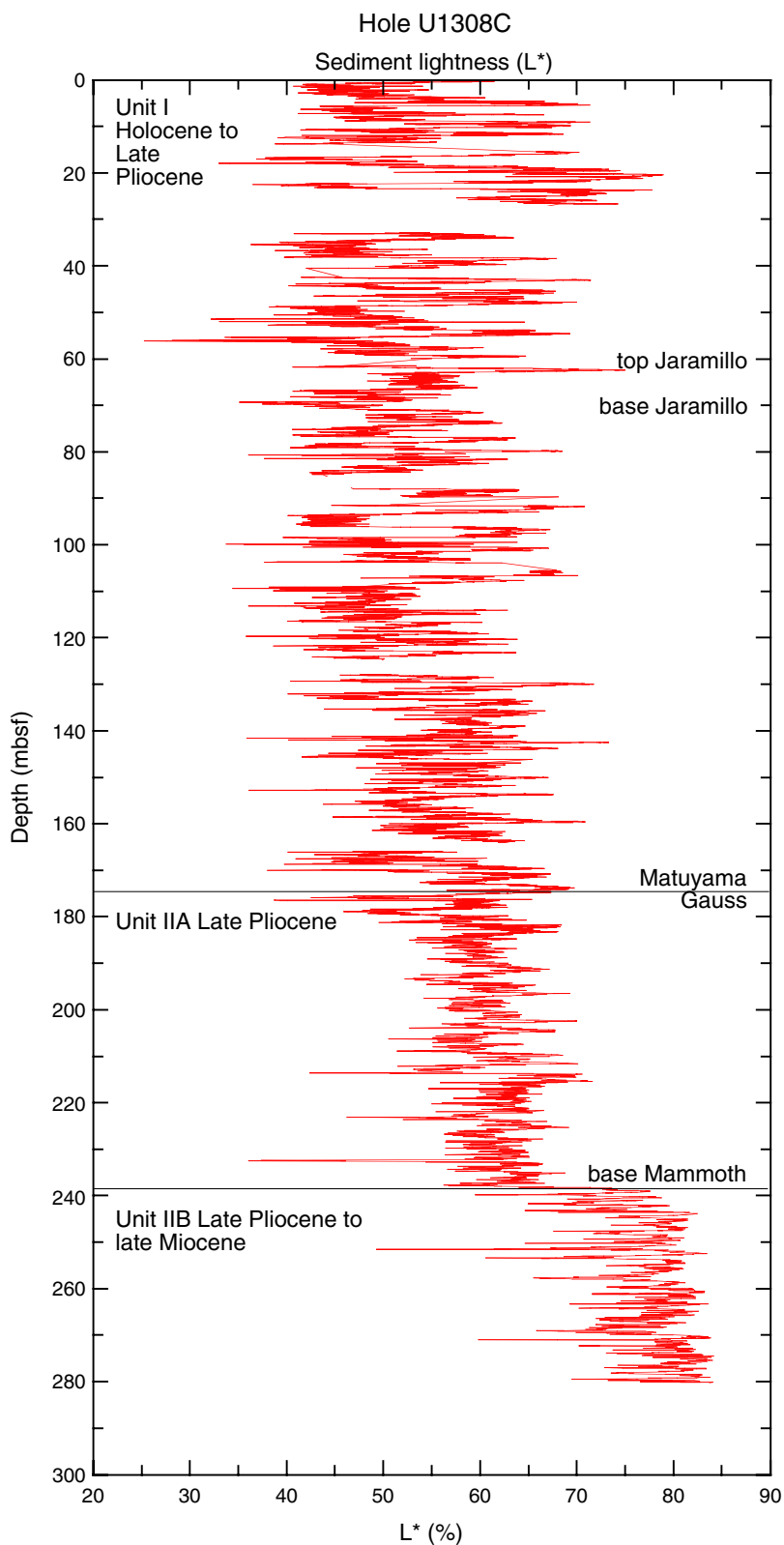
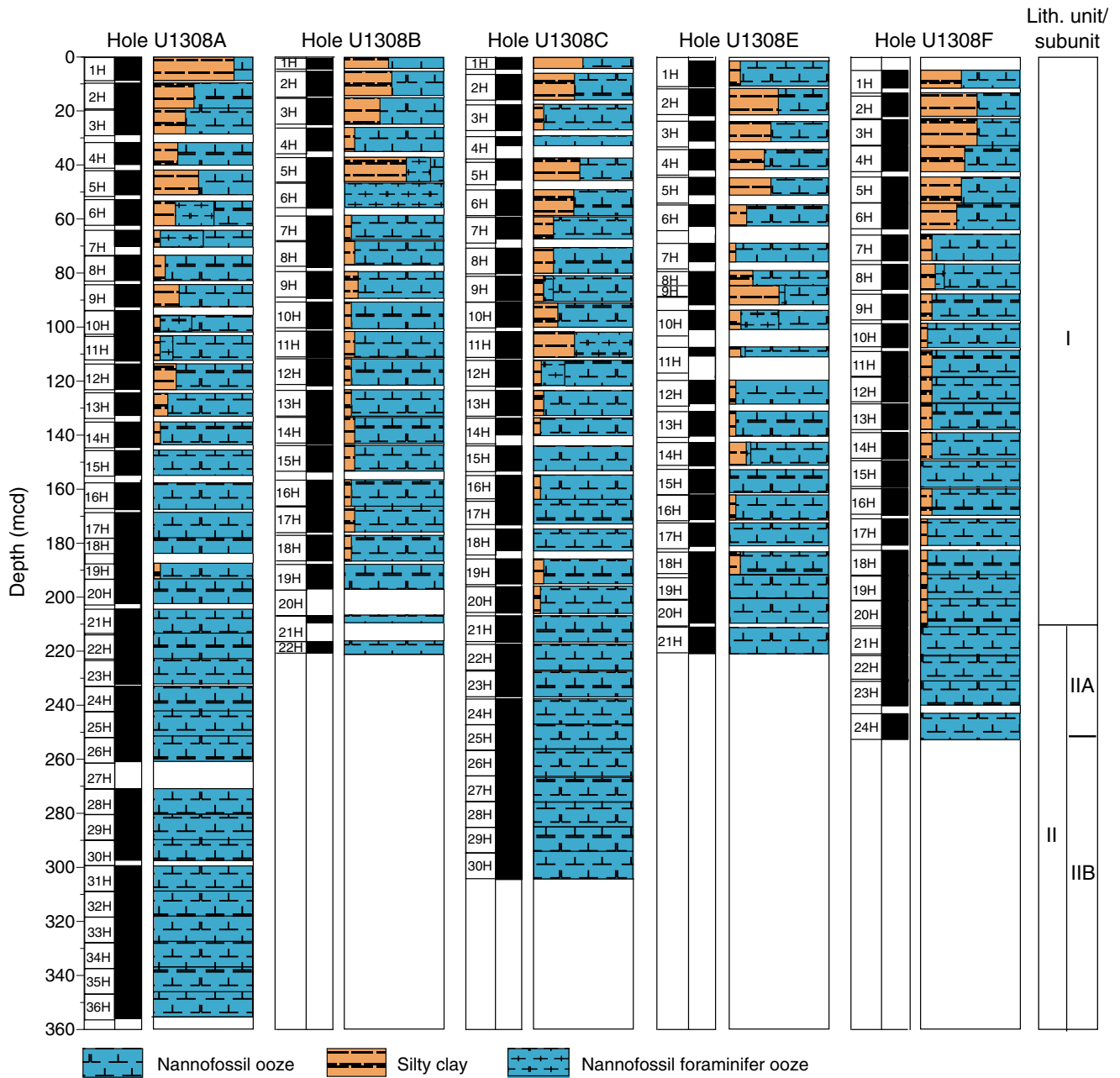
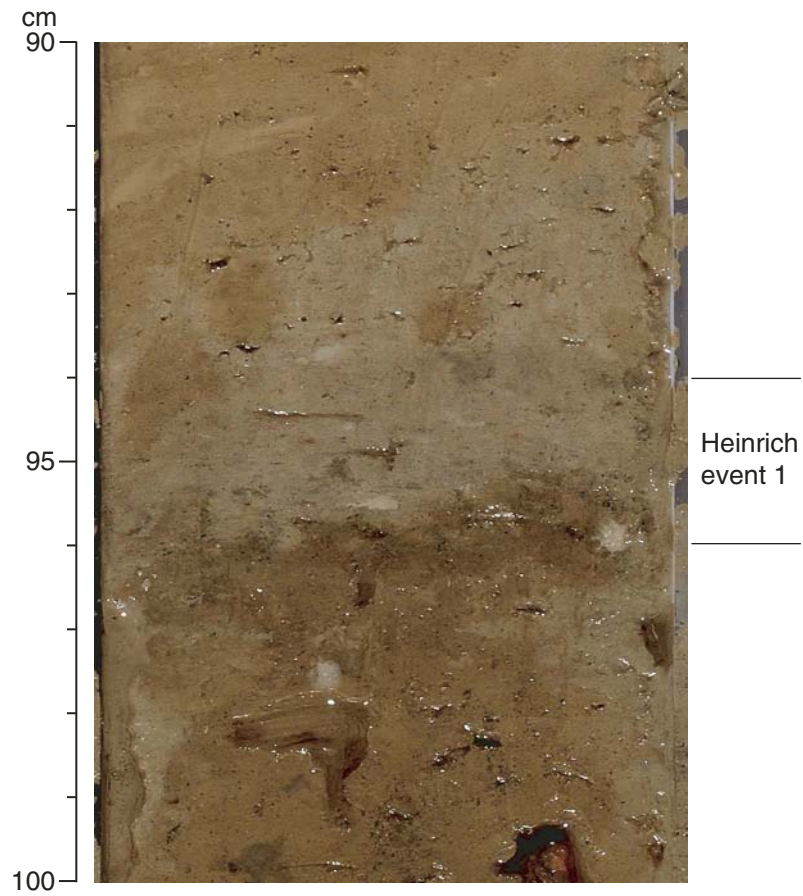


Figure F7. Graphic summary of the lithologies recovered at Site U1308.



**Figure F8.** Heinrich event 1 (interval 303-U1308C-1H-1, 90–100 cm). Note light color caused by detrital carbonate content, relatively sharp base, and bioturbated upper contact. Thickness is ~1–2 cm.





**Figure F9.** Heinrich event 2 (interval 303-U1308A-1H-1, 115–130 cm). Note light color caused by detrital carbonate content, relatively sharp base, and bioturbated upper contact. Thickness is ~5 cm.



**Figure F10.** Heinrich event 4 (interval 303-U1308B-1H-2, 70–100 cm). Note light color caused by detrital carbonate content, relatively sharp base, and bioturbated upper contact. Thickness is ~10–11 cm.



**Figure F11.** Heinrich event 5 (interval 303-U1308B-1H-3, 6–26 cm). Note light color caused by detrital carbonate content, relatively sharp base, and bioturbated upper contact. Thickness is ~10 cm.

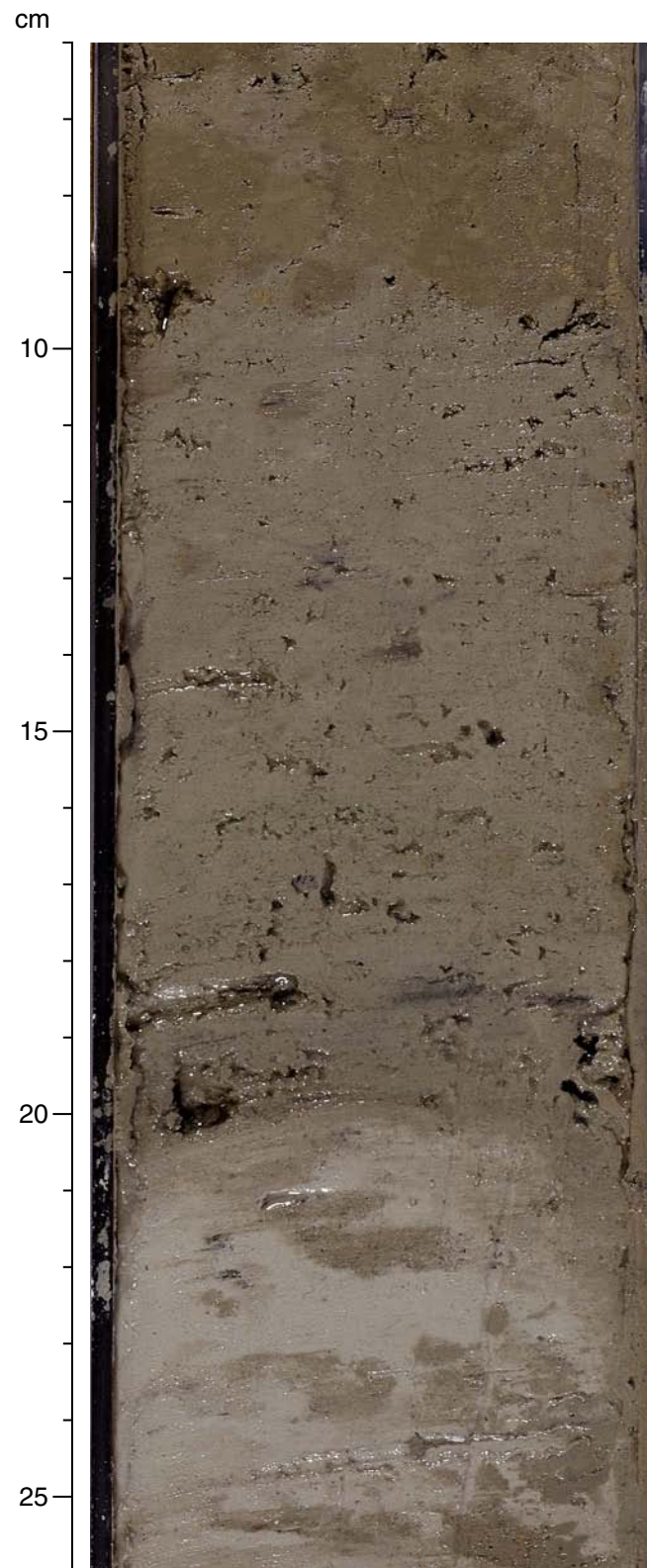




**Figure F12.** Chronostratigraphic correlation of Holes U1308A–U1308F based on calcareous nannofossils, diatoms, planktonic foraminifers, and dinocysts. Relationship to magnetostratigraphy is shown in the left panel. MIS = marine isotope stage, LO = last occurrence, FO = first occurrence.

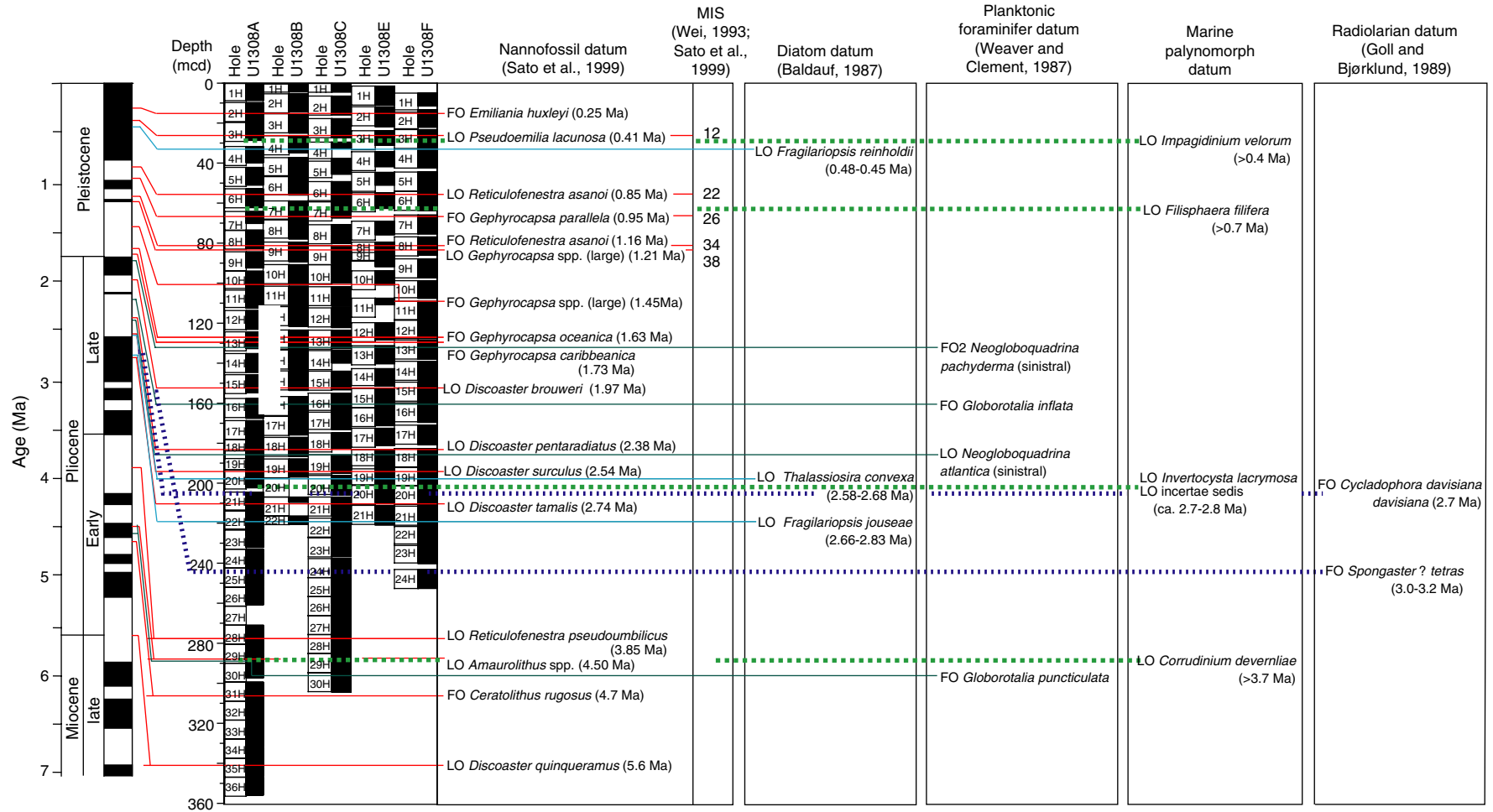




**Figure F13.** Site U1308 downcore relative abundance of calcareous nannofossils, planktonic foraminifers, diatoms, radiolarians, dinoflagellate cysts, and pollen.

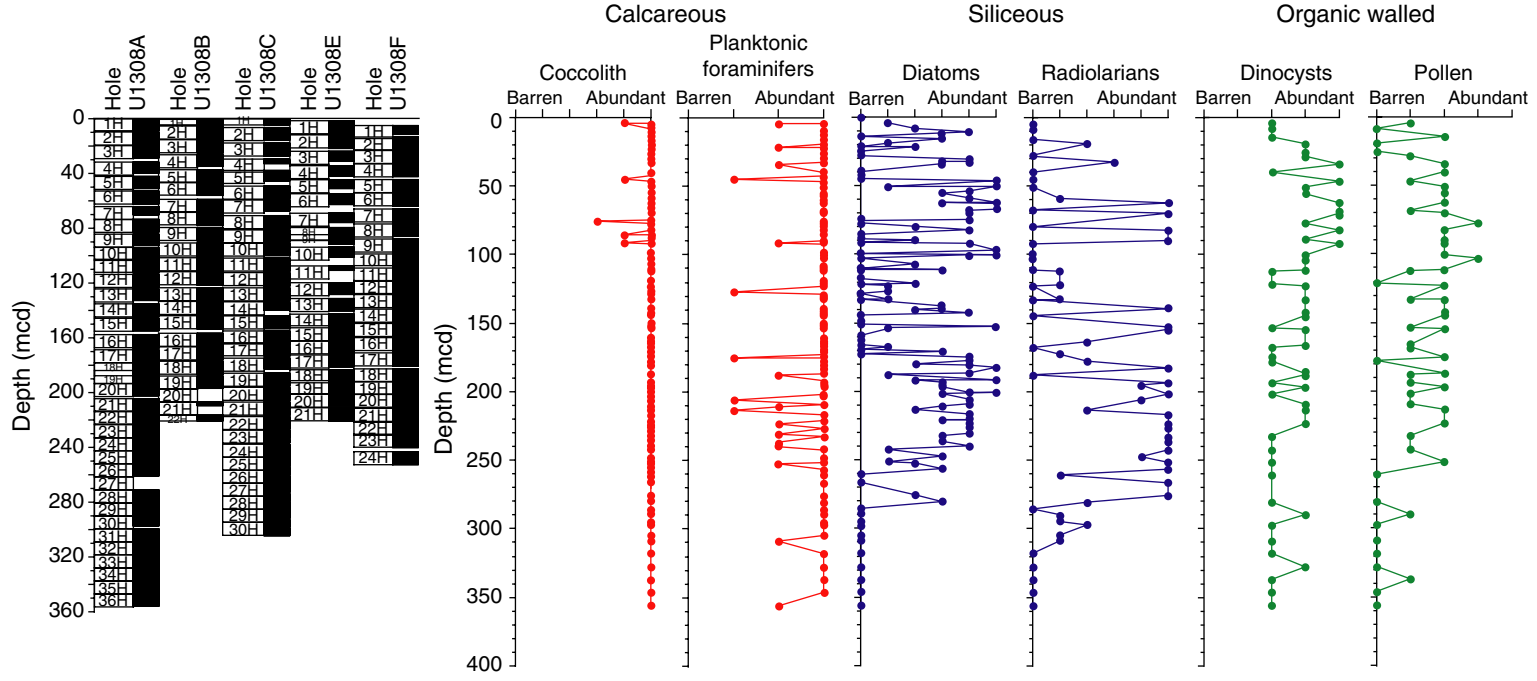




**Figure F14.** Site U1308 magnetization intensity before and after AF demagnetization versus depth. Green and orange curves indicate intensity before demagnetization and after demagnetization at AF peak field of 10 mT, respectively. Core recovery is shown in the left panel.

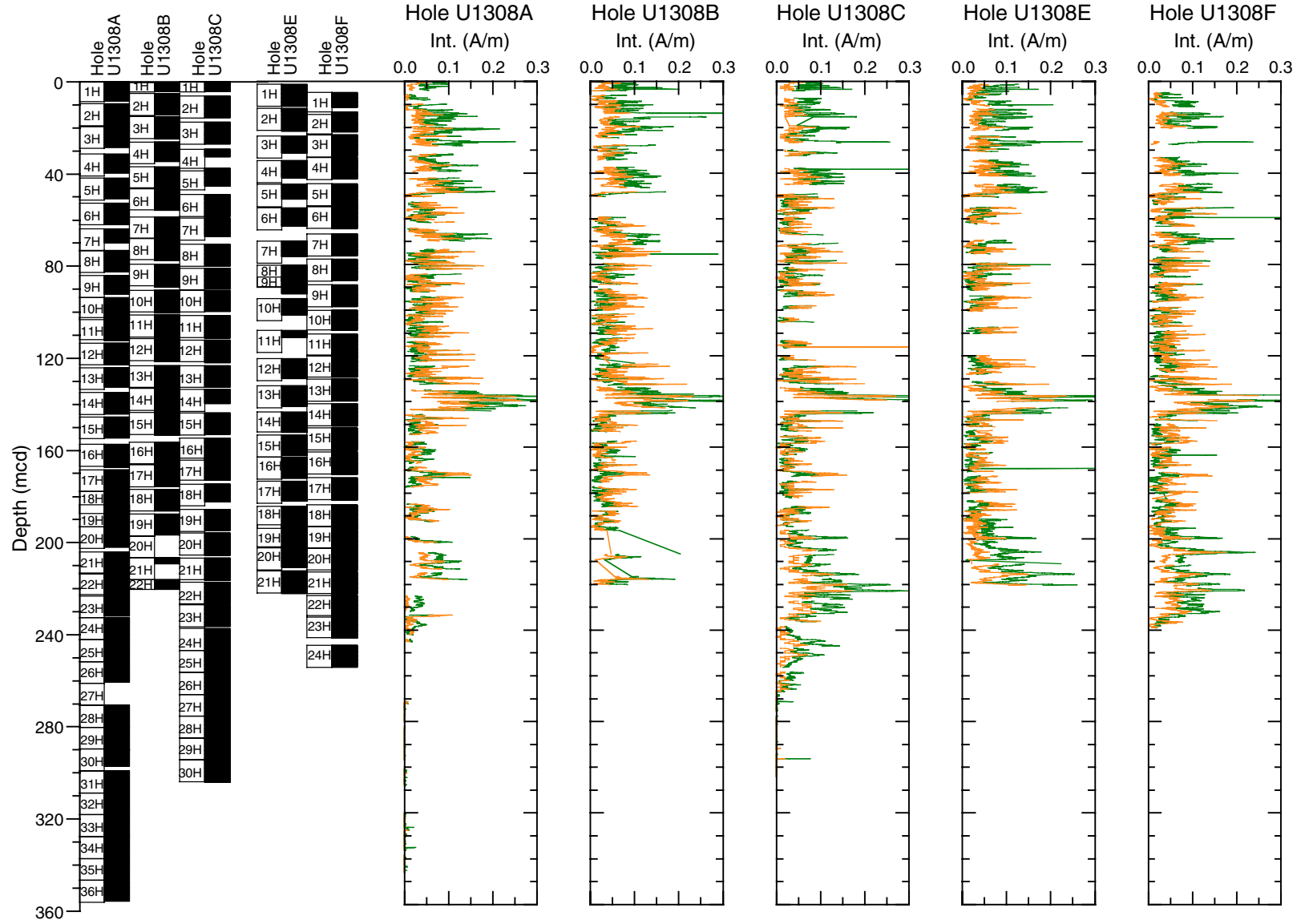




**Figure F15.** Site U1308 inclination of remanent magnetization after AF demagnetization at peak fields of 10 mT versus depth. Polarity timescale is shown for reference. Core recovery is shown in the left panel.

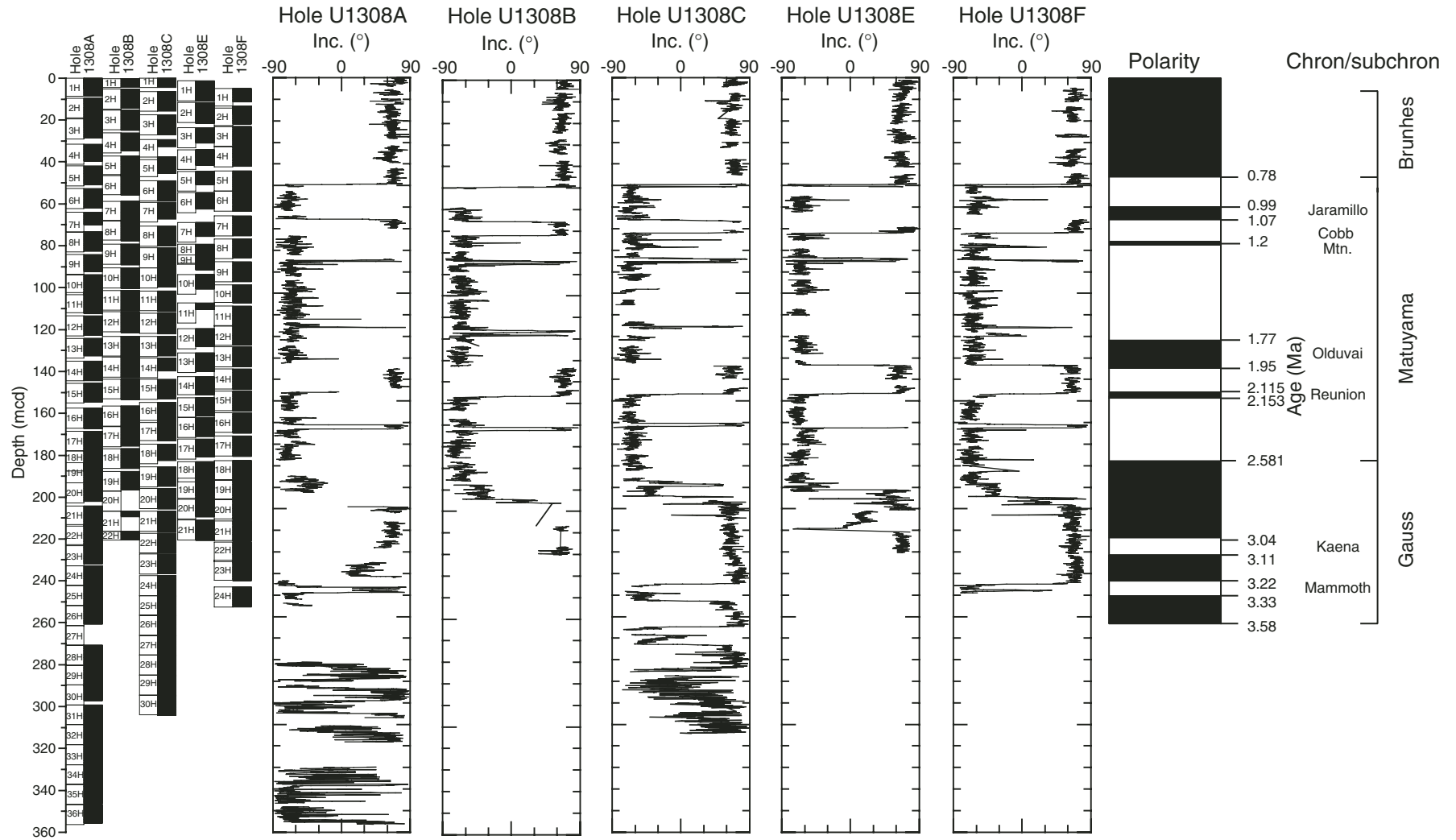




**Figure F16.** Site U1308 declination of remanent magnetization after AF demagnetization at peak fields of 10 mT versus depth. Black and blue symbols indicate declinations before and after Tensor tool correction, respectively. Polarity timescale is shown for reference. Core recovery is shown in the left panel.

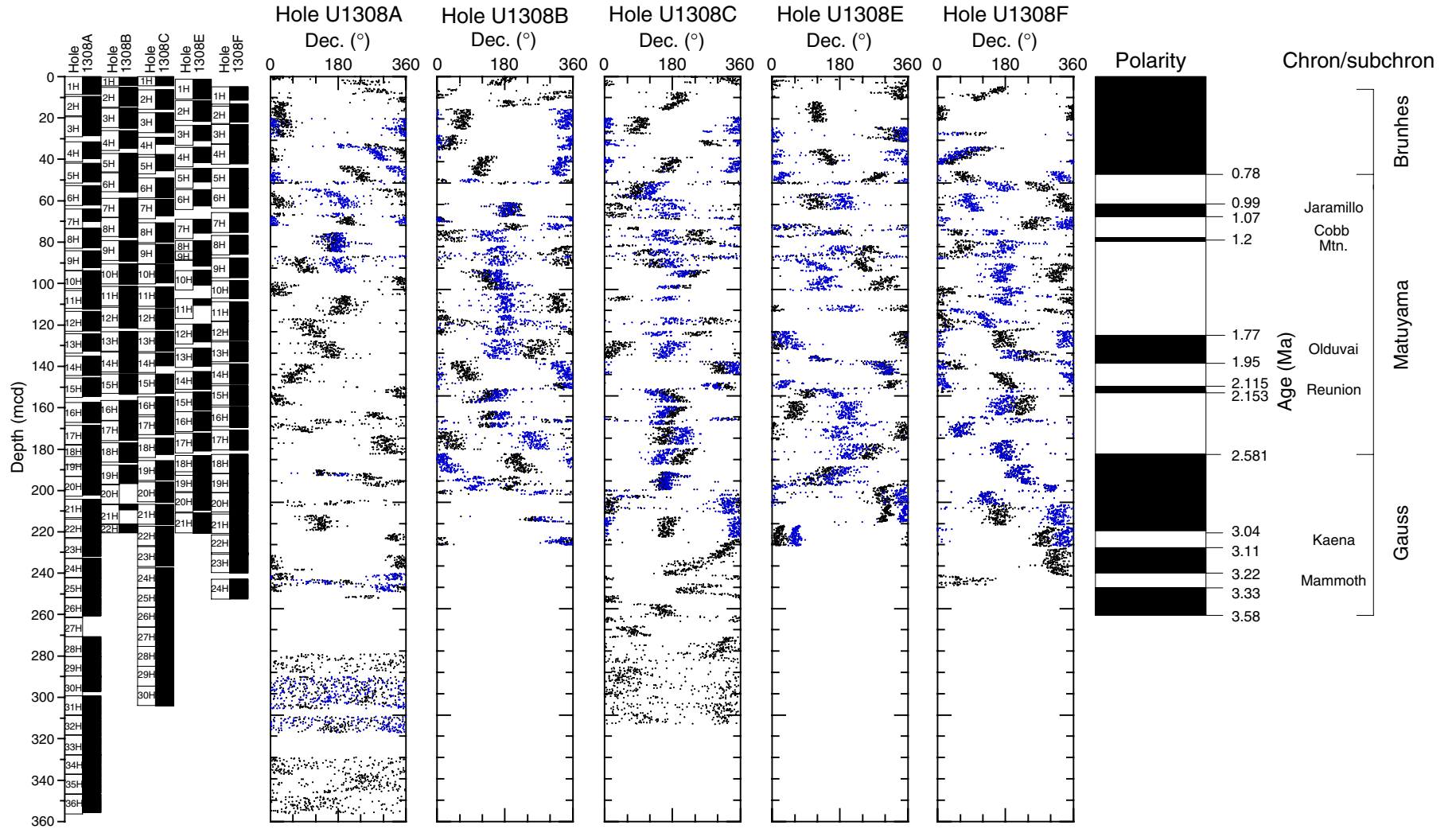




**Figure F17.** Lower panel: Magnetic susceptibility (MS) versus mcd for each hole drilled at Site U1308. Numbers below MS curve refer to the core of the MS record. Upper panel: Composite MS record indicating which hole was used to form the splice. **A.** 0–50 mcd. (Continued on next four pages.)

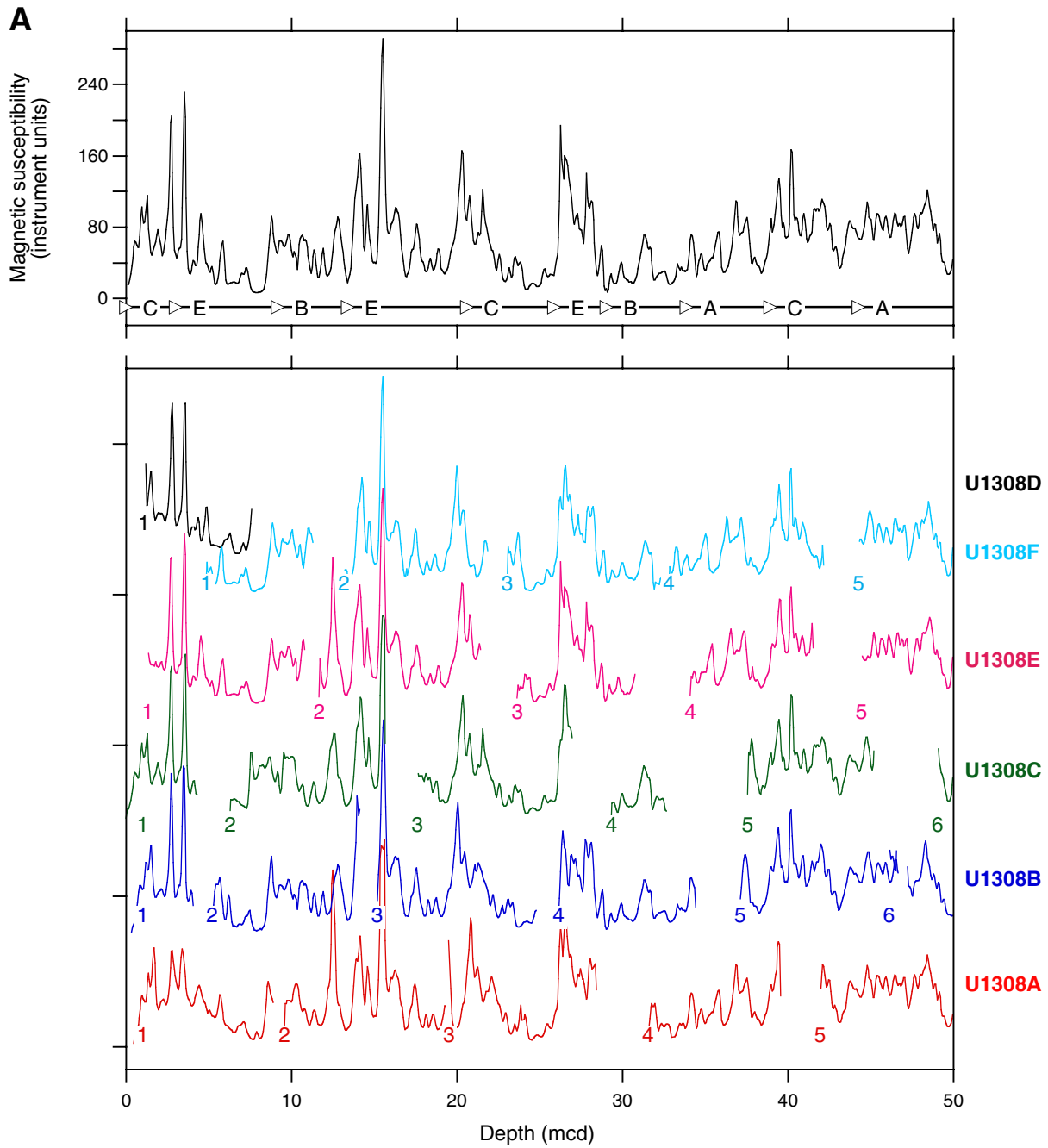


Figure F17 (continued). B. 50–100 mcd.

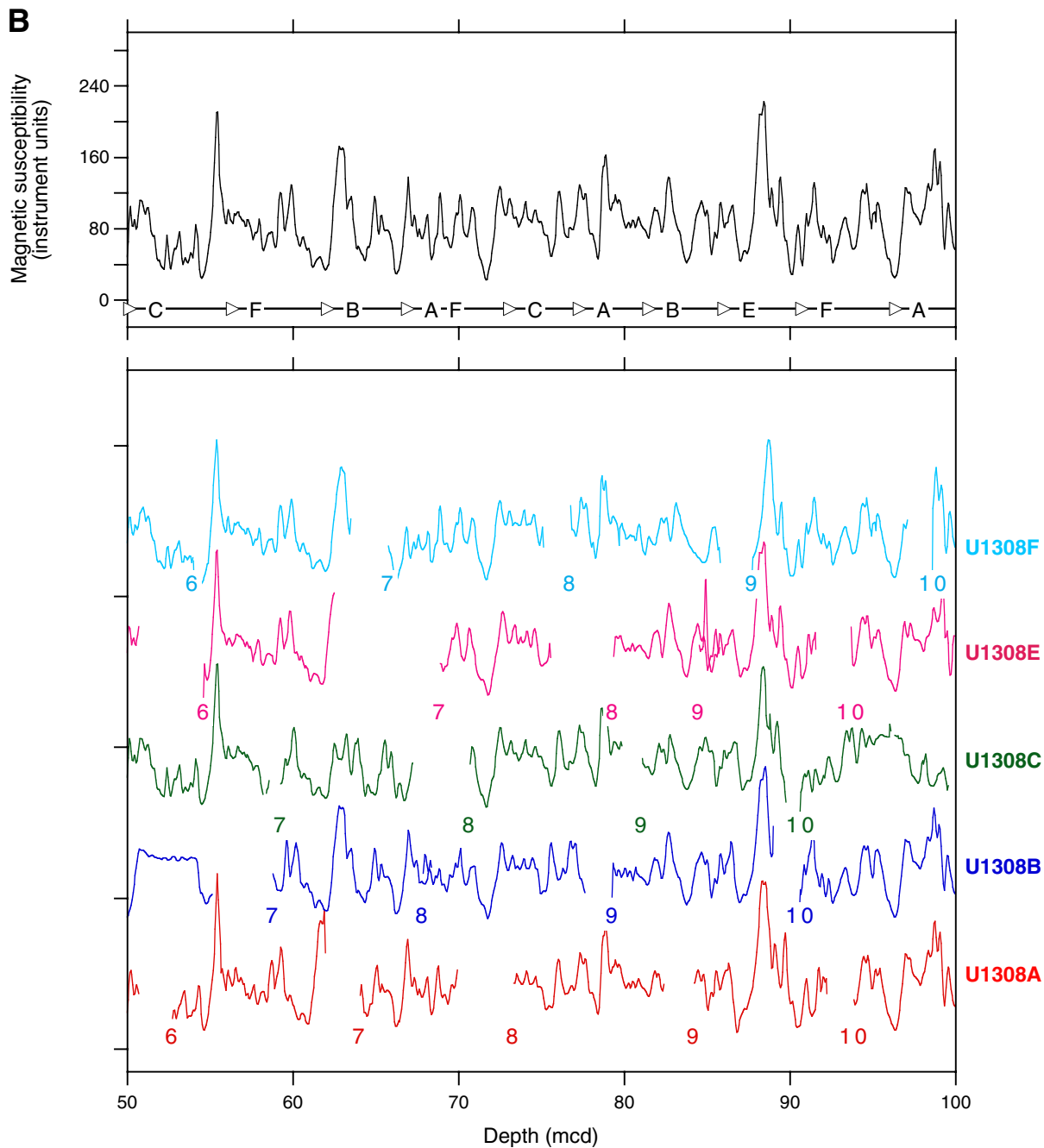


Figure F17 (continued). C. 100–150 mcd.

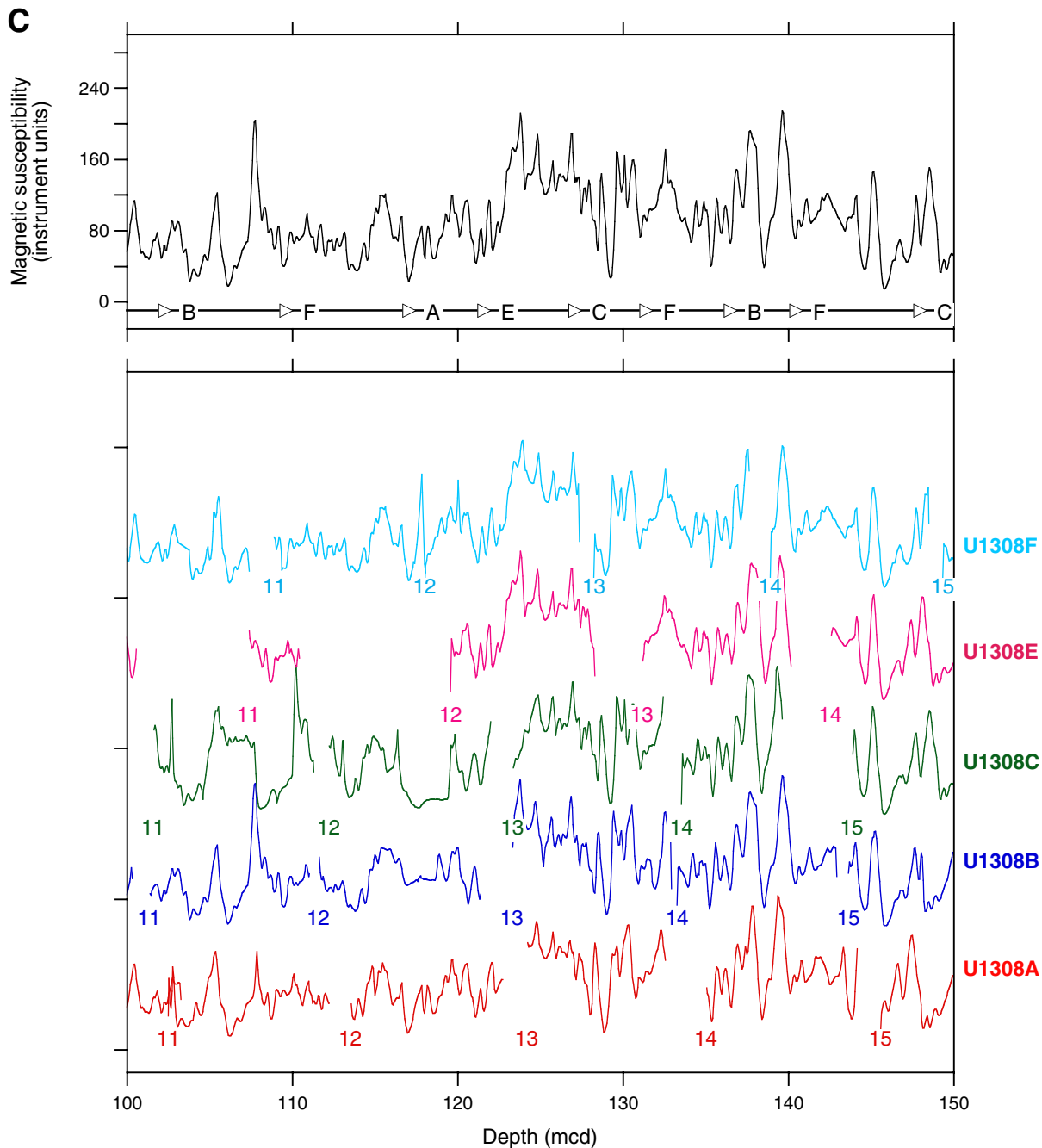


Figure F17 (continued). D. 150–200 mcd.

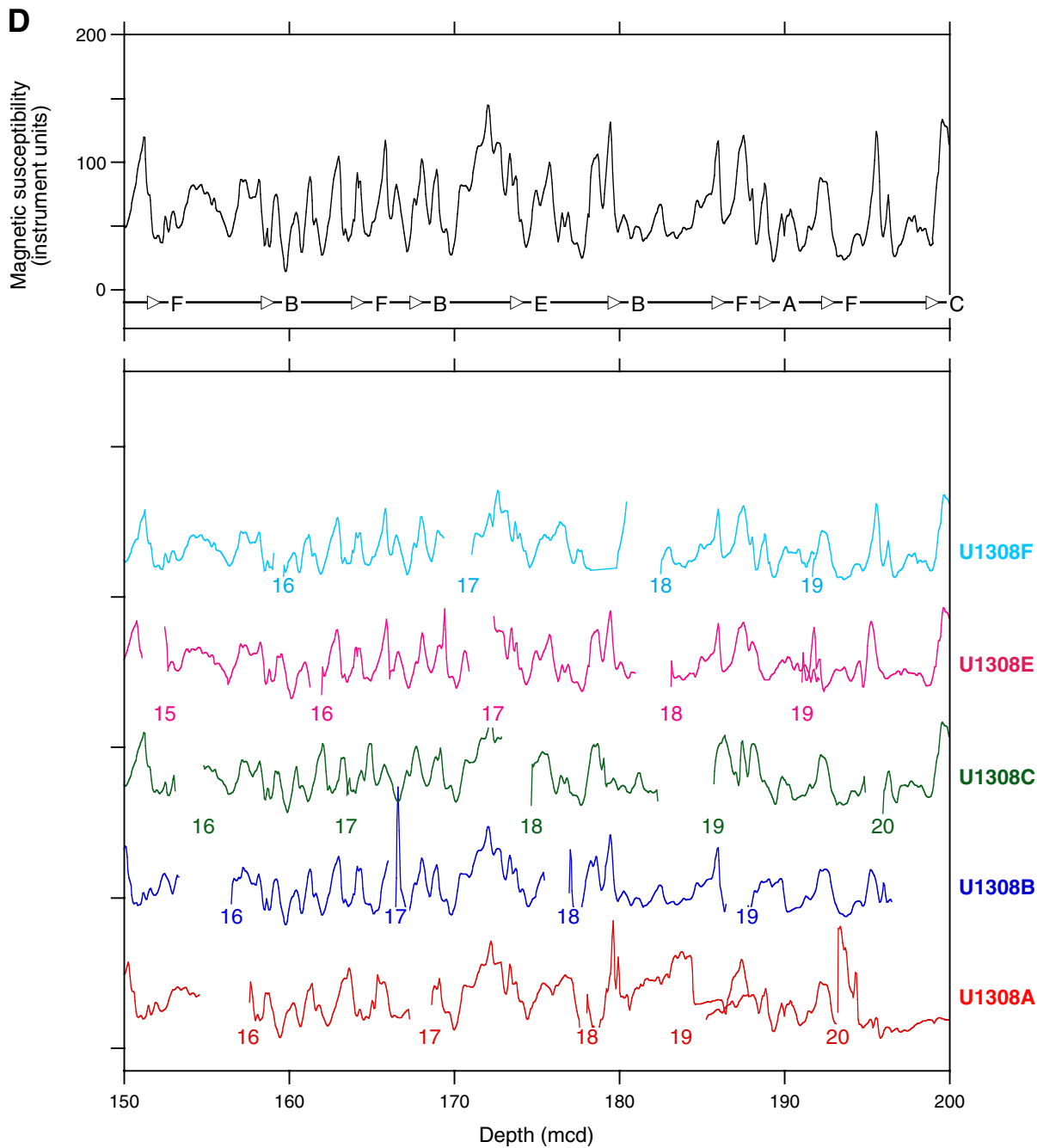
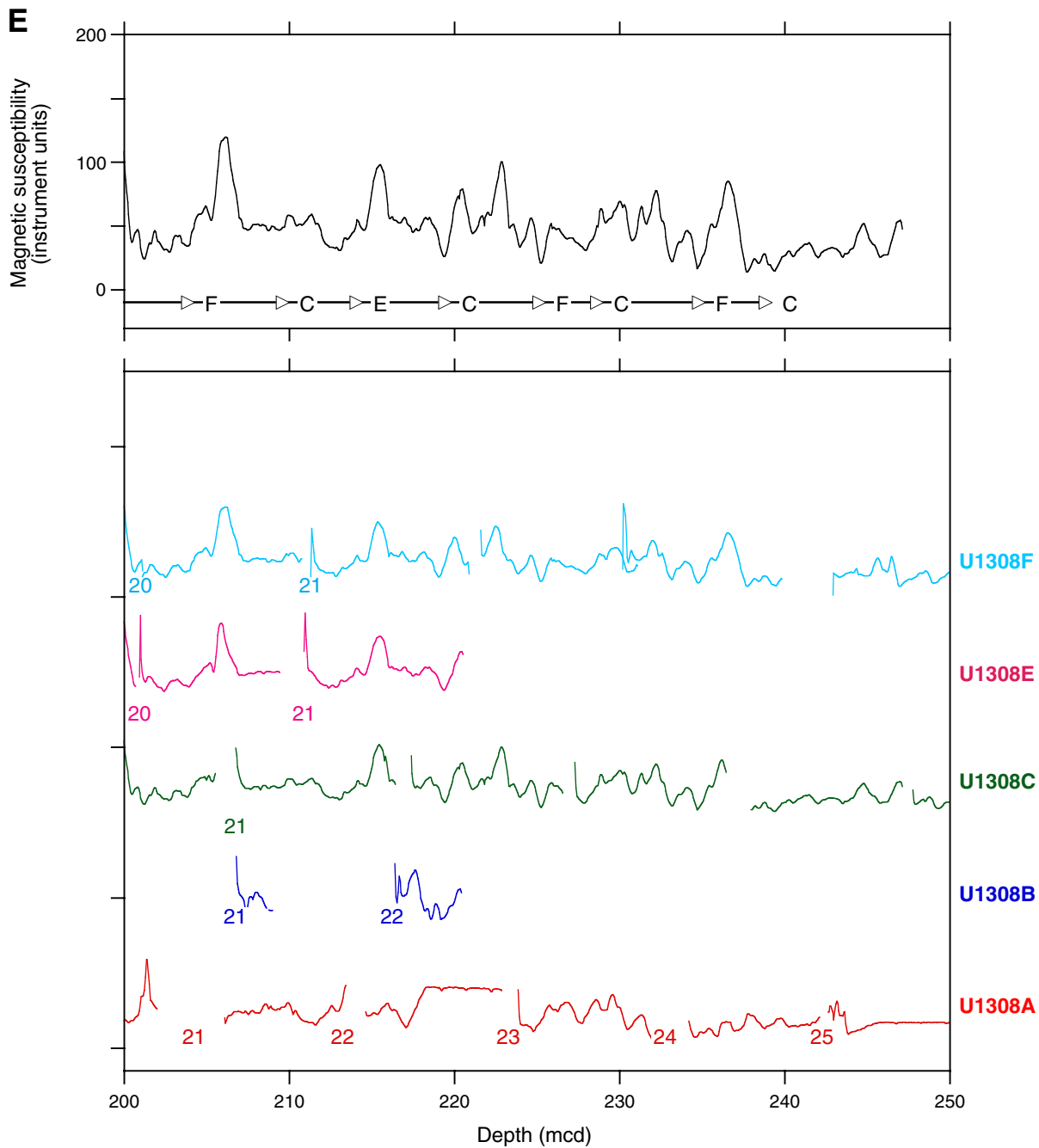
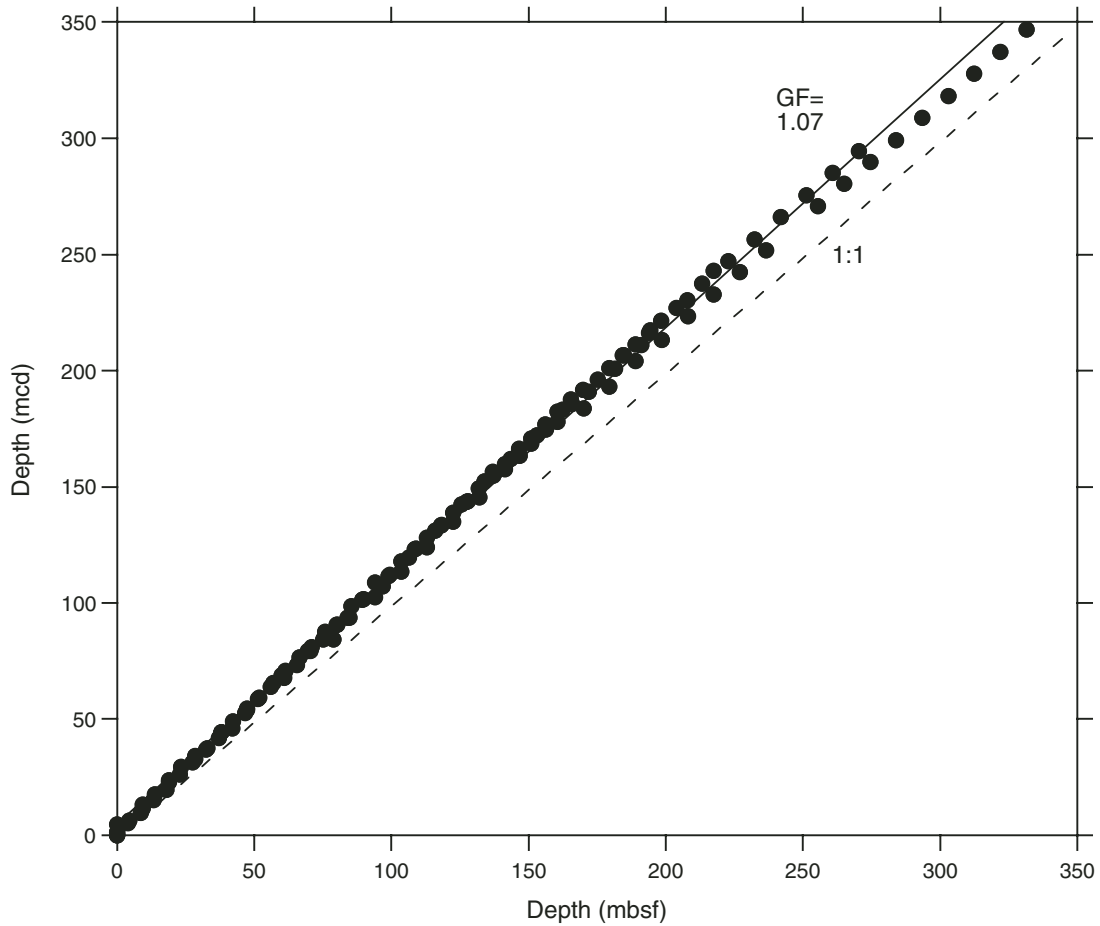


Figure F17 (continued). E. 200–250 mcd.



**Figure F18.** Meters composite depth versus meters below seafloor for tops of cores at Site U1308. The growth factor (GF = 1.07) is the slope of the regression line. On average, the mcd of the spliced section is 7% greater than mbsf.



**Figure F19.** Age versus depth for paleomagnetic datums for Site U1308. A mean sedimentation rate of 8.3 cm/k.y. was calculated by linear regression. Interval sedimentation rates derived from the paleomagnetic datums are represented by a solid line and range from 5.6 to 11.0 cm/k.y.

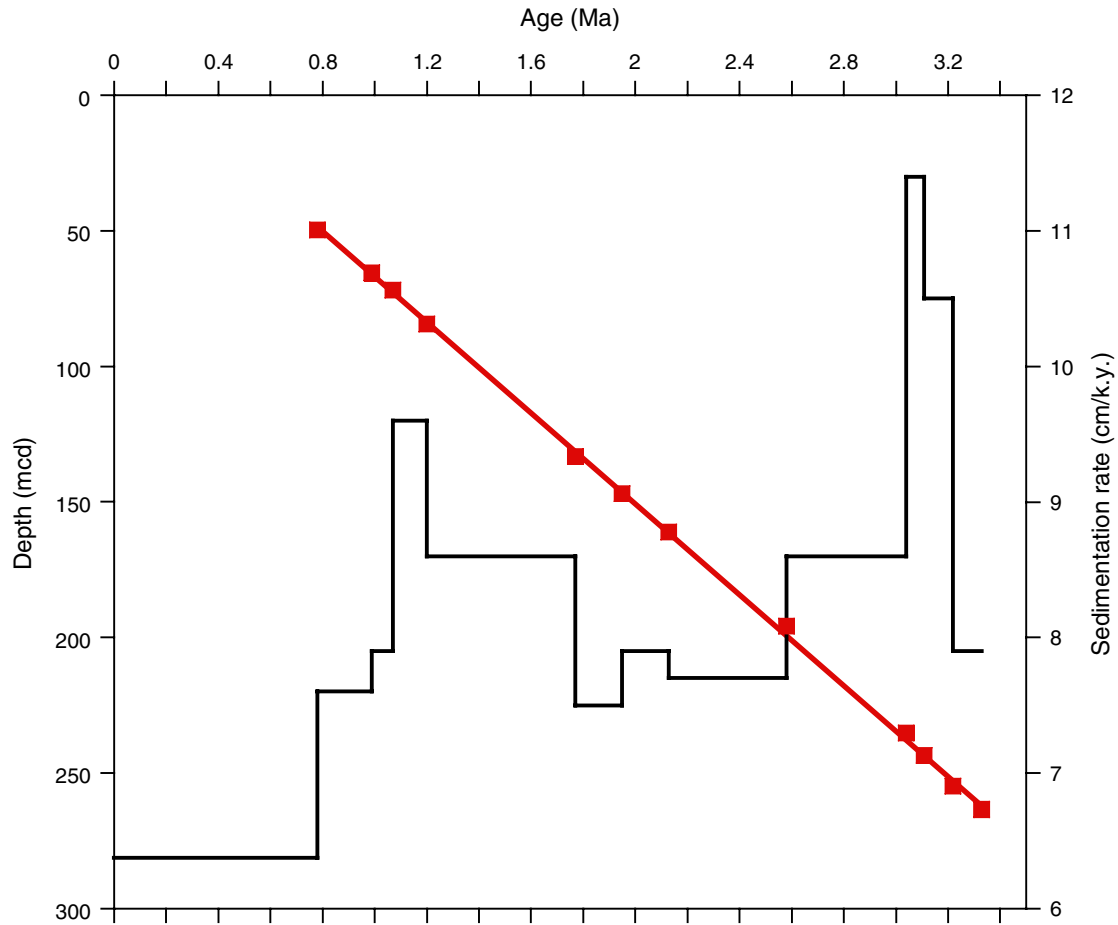
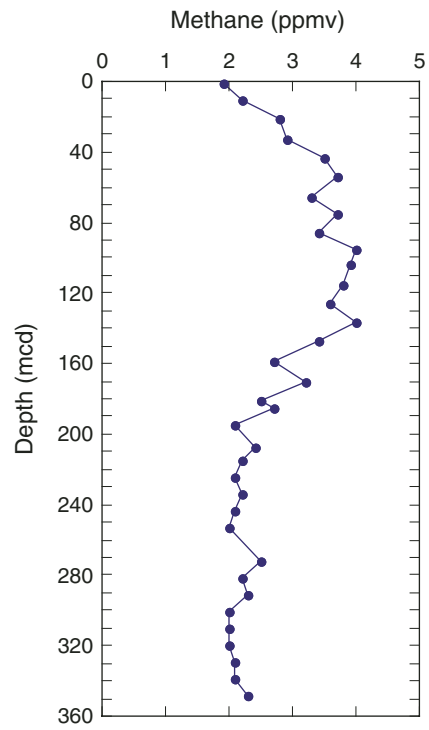
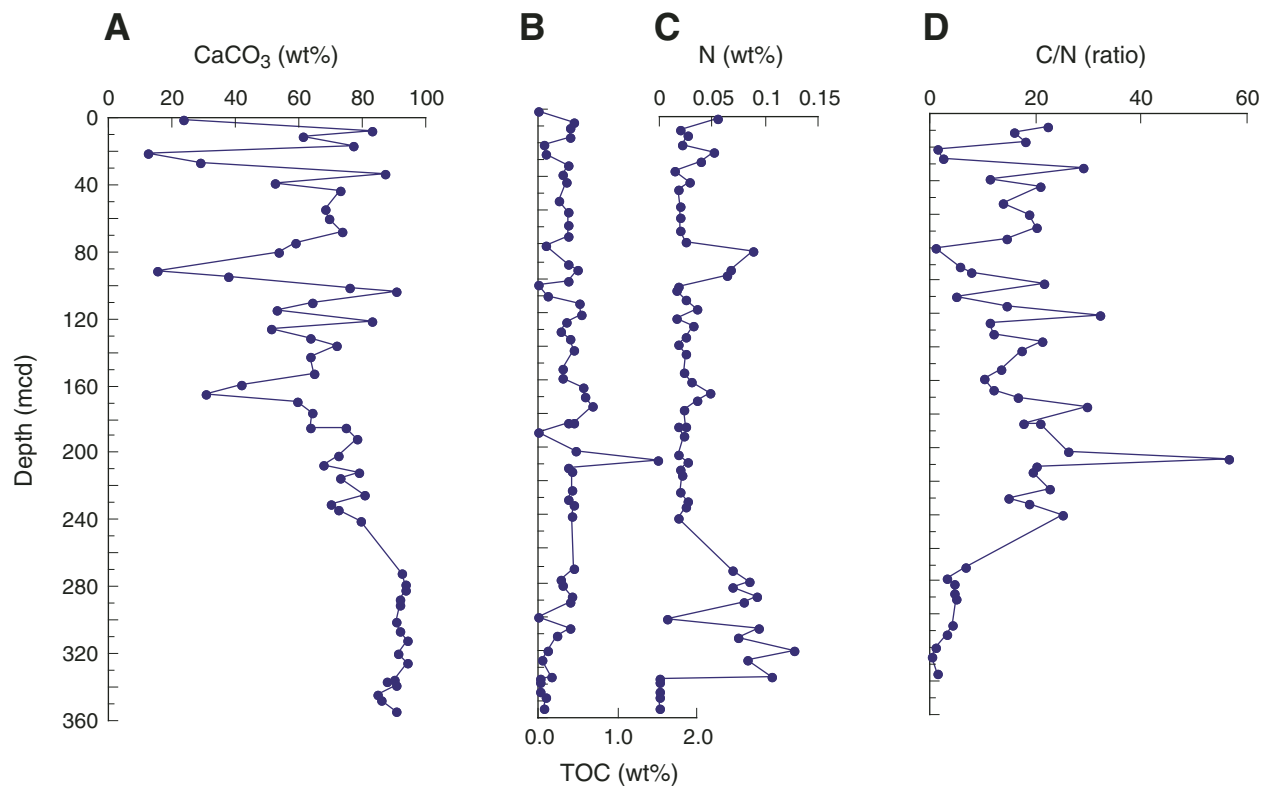


Figure F20. Headspace methane concentrations for Hole U1308A.





**Figure F21.** Site U1308 carbonate contents and elemental compositions. **A.** Calcium carbonate. **B.** Total organic carbon (TOC). **C.** Elemental nitrogen. **D.** Organic C/N ratio.



**Figure F22.** Profiles of chemical constituents in interstitial waters from Hole U1308A. A. Chloride. B. Sodium. C. pH. D. Boron. E. Alkalinity. F. Sulfate. G. Ammonium. H. Dissolved silica. I. Calcium. J. Strontium and Sr/Ca ratio. K. Lithium. L. Barium and sulfate. M. Magnesium. N. Potassium. O. Manganese. P. Iron.

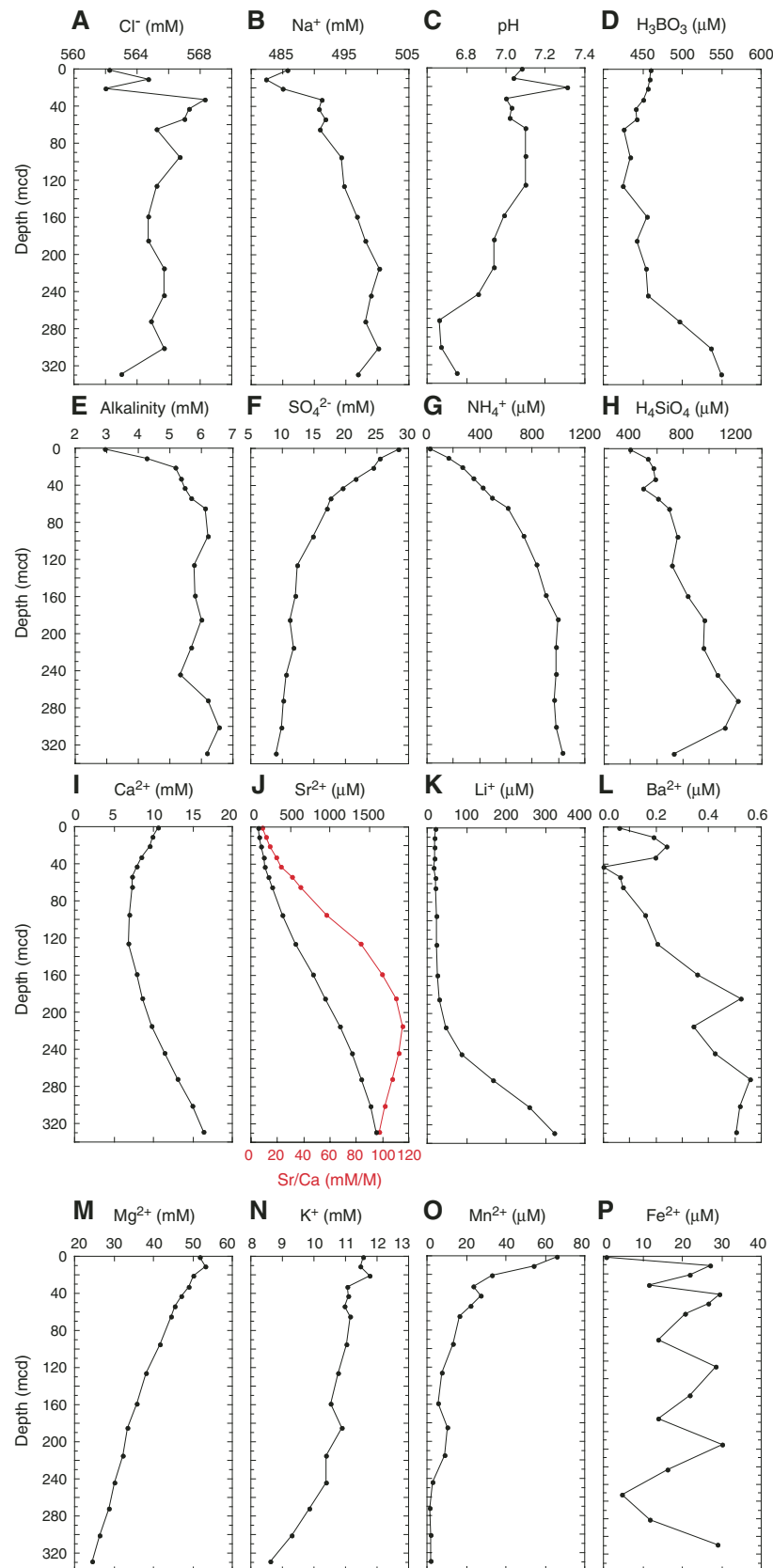




**Figure F23.** Site U1308 magnetic susceptibility (MS) records. Core recovery columns is represented on the left side of each plot. Black = multi-sensor track record, red = magnetic susceptibility core logger (MSCL) record.

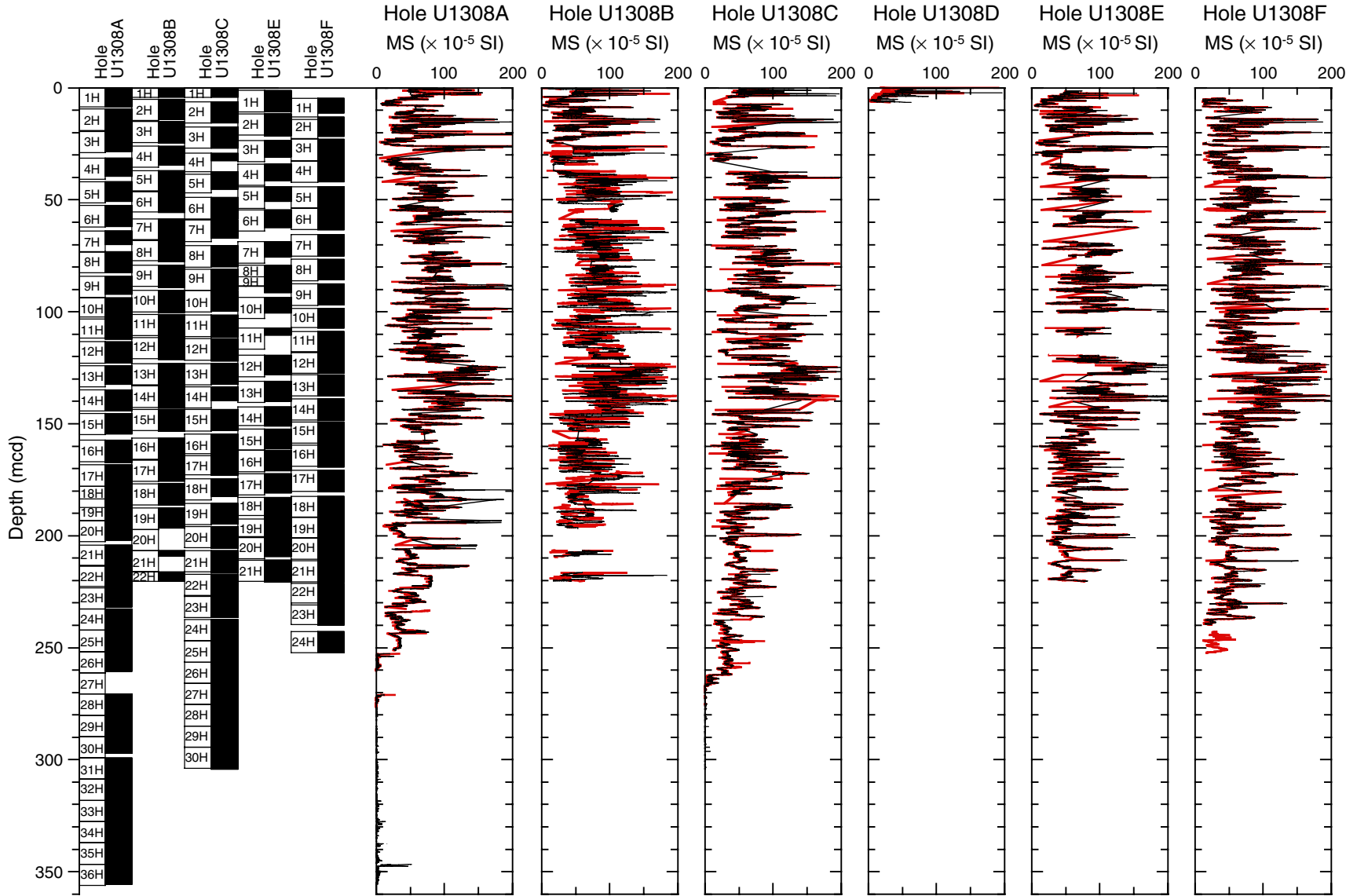


**Figure F24.** Combined gamma ray attenuation density measurements from the multisensor track and bulk density from discrete measurements (red circles), Site U1308.

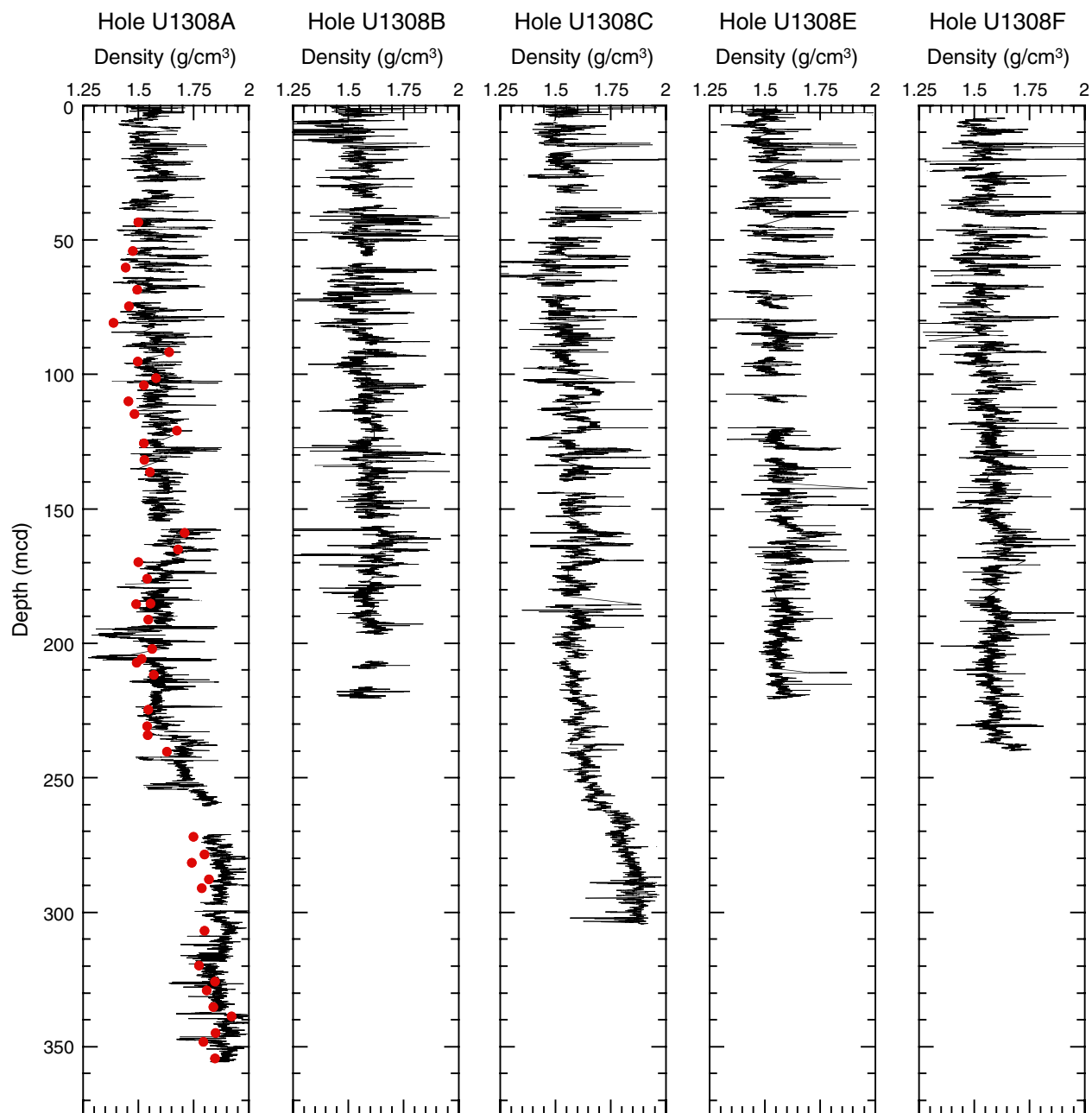


Figure F25. Natural gamma ray (NGR) counts from the multisensor track, Site U1308.

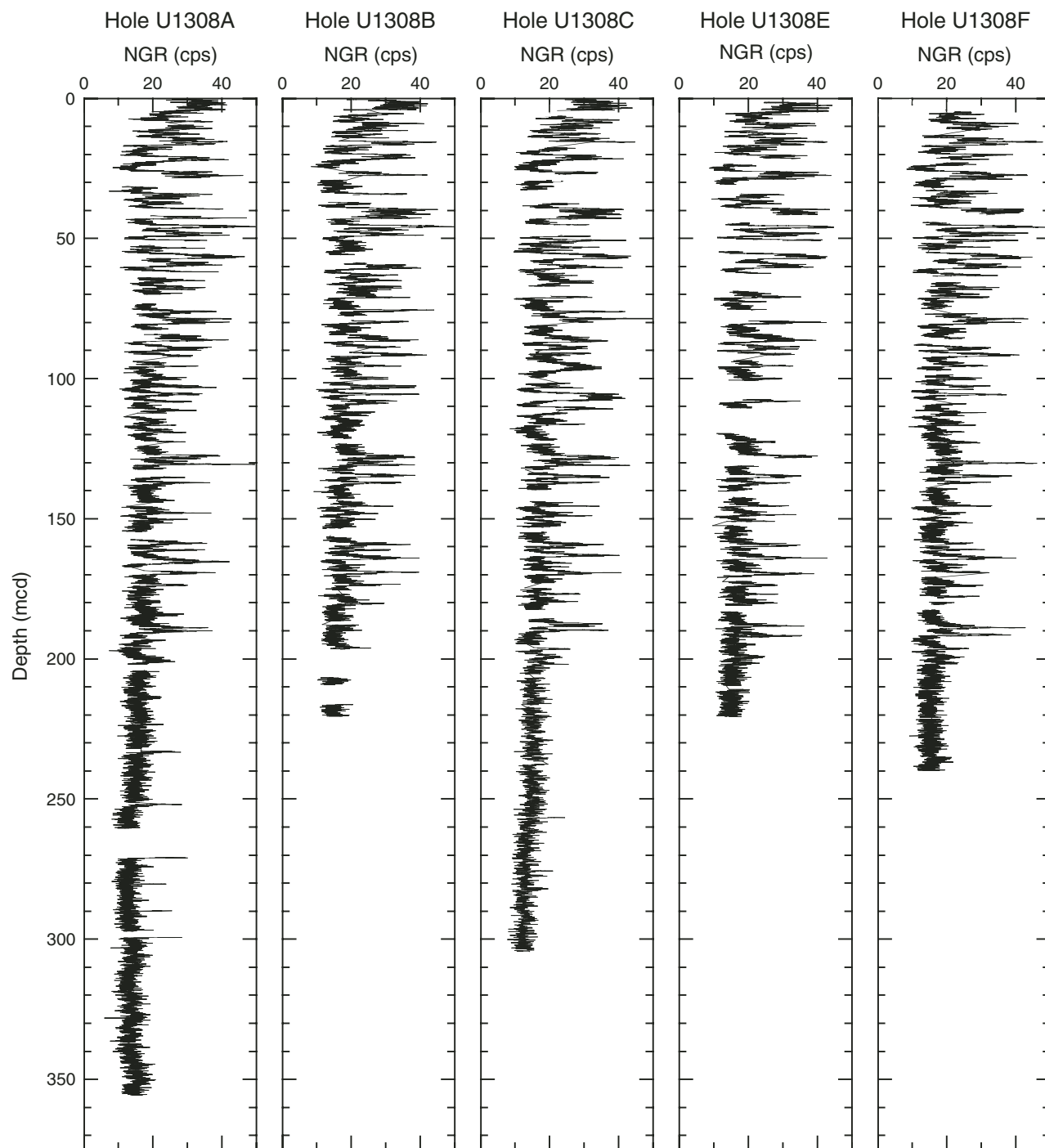


Figure F26. Downcore *P*-wave velocity records, Site U1308. Red circles = *P*-wave sensor number 3 velocity records.

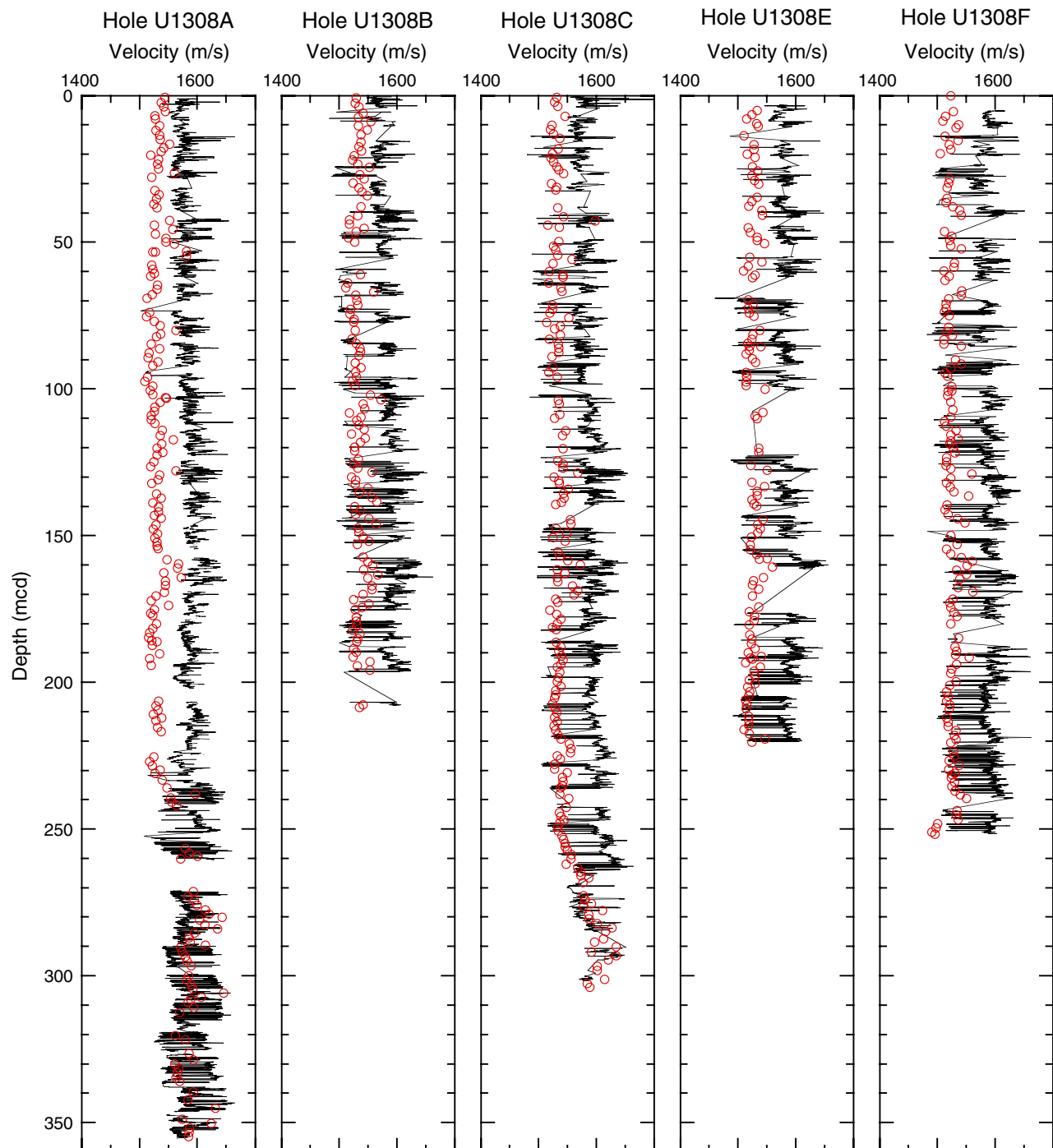
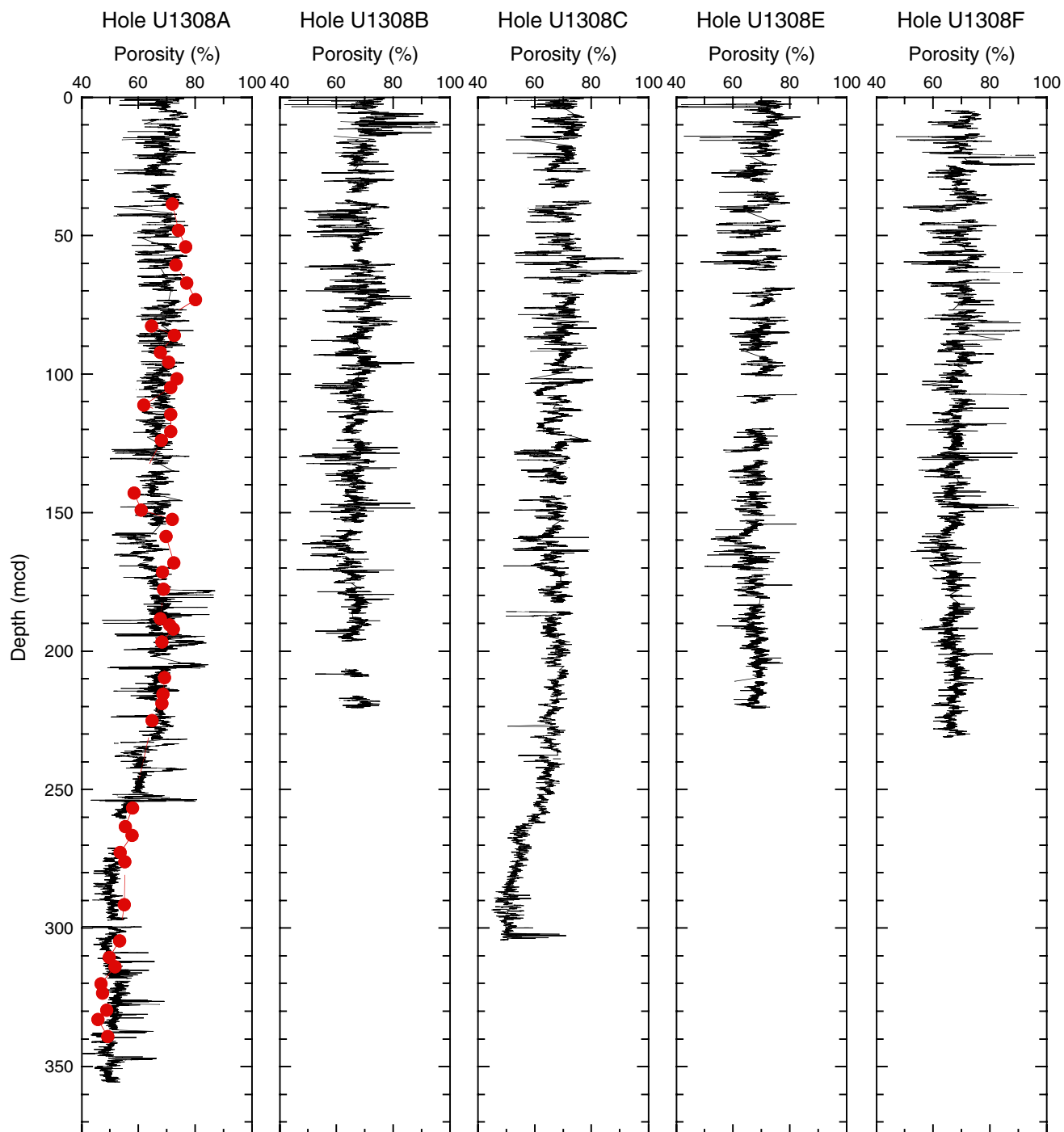
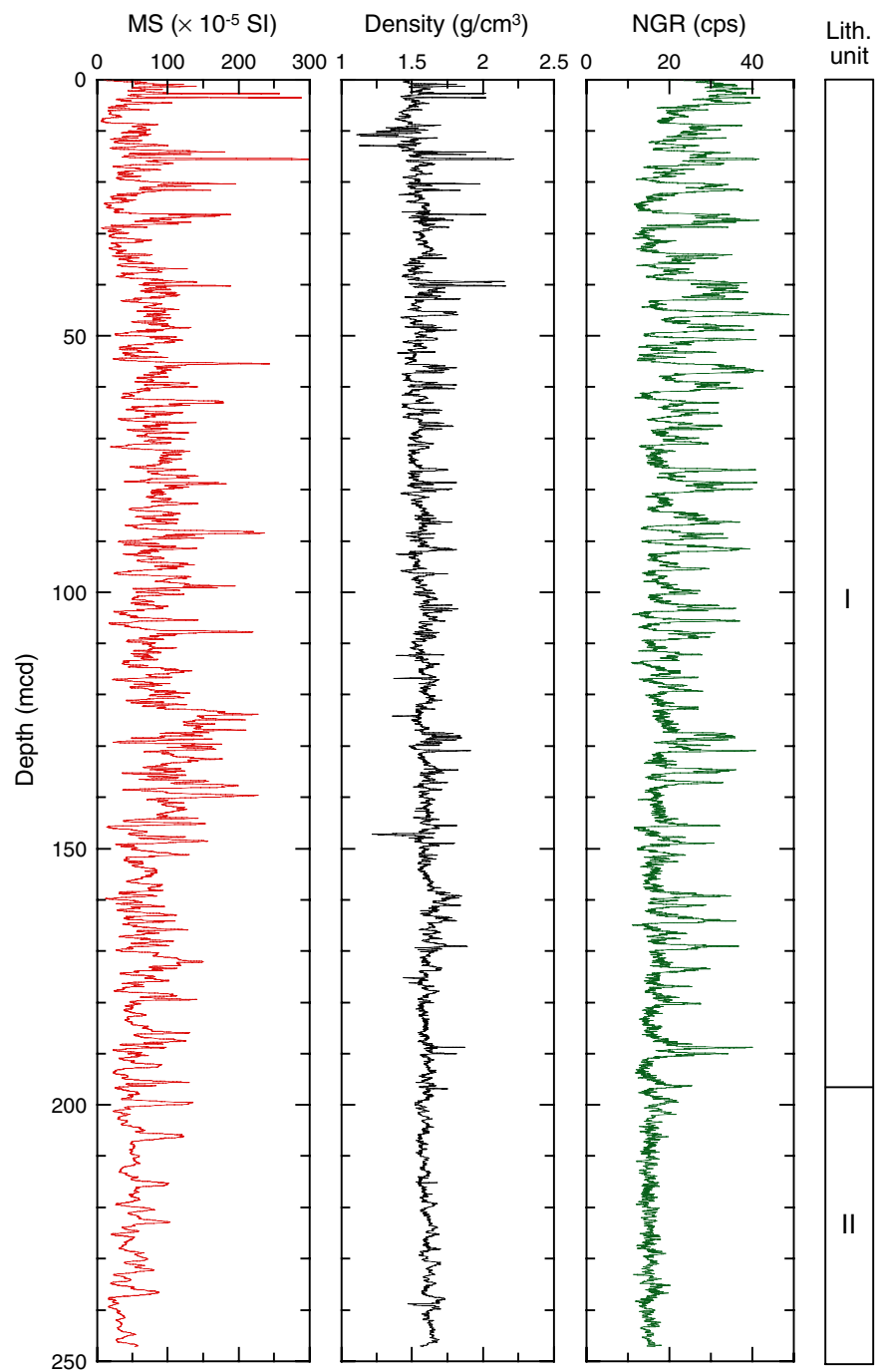


Figure F27. Downcore gamma ray attenuation–derived porosity calculations and discrete porosity measurements (red circles), Site U1308.



**Figure F28.** Combined plots of the smoothed spliced records of multisensor track-derived magnetic susceptibility (MS), gamma ray attenuation density and natural gamma ray NGR, Site U1308.





**Table T1.** Coring summary, Site U1308. (See table notes. Continued on next three pages.)**Hole U1308A**

Latitude: 49°52.6661'N  
 Longitude: 24°14.2875'W  
 Time on site (h): 242.00 (2230 h, 3 November 2004–0030 h, 14 November 2004)  
 Time on hole (h): 67.92 (2230 h, 3 November 2004–1825 h, 6 November 2004)  
 Seafloor (drill pipe measurement from rig floor, mbrf): 3882.3  
 Distance between rig floor and sea level (m): 11.3  
 Water depth (drill pipe measurement from sea level, m): 3871.0  
 Total depth (drill pipe measurement from rig floor, mbrf): 4223.4  
 Total penetration (mbsf): 341.1  
 Total length of cored section (m): 341.1  
 Total core recovered (m): 323.83  
 Core recovery (%): 94.9  
 Total number of cores: 36

**Hole U1308B**

Latitude: 49°52.6672'N  
 Longitude: 24°14.3126'W  
 Time on hole (h): 52.83 (1825 h, 6 November 2004–2315 h, 8 November 2004)  
 Seafloor (drill pipe measurement from rig floor, mbrf): 3882.4  
 Distance between rig floor and sea level (m): 11.3  
 Water depth (drill pipe measurement from sea level, m): 3871.1  
 Total depth (drill pipe measurement from rig floor, mbrf): 4080.7  
 Total penetration (mbsf): 198.3  
 Total length of cored section (m): 198.3  
 Total core recovered (m): 186.19  
 Core recovery (%): 93.9  
 Total number of cores: 22

**Hole U1308C**

Latitude: 49°52.6838'N  
 Longitude: 24°14.2867'W  
 Time on hole (h): 49.50 (2315 h, 8 November 2004–0045 h, 11 November 2004)  
 Seafloor (drill pipe measurement from rig floor, mbrf): 3884.0  
 Distance between rig floor and sea level (m): 11.3  
 Water depth (drill pipe measurement from sea level, m): 3872.7  
 Total depth (drill pipe measurement from rig floor, mbrf): 4163.9  
 Total penetration (mbsf): 279.9  
 Total length of cored section (m): 279.9  
 Total core recovered (m): 271.1  
 Core recovery (%): 96.9  
 Total number of cores: 30

**Hole U1308D**

Latitude: 49°52.6838'N  
 Longitude: 24°14.2867'W  
 Time on hole (h): 1.83 (0045 h, 11 November 2004–0235 h, 11 November 2004)  
 Seafloor (drill pipe measurement from rig floor, mbrf): 3885.1  
 Distance between rig floor and sea level (m): 11.3  
 Water depth (drill pipe measurement from sea level, m): 3873.8  
 Total depth (drill pipe measurement from rig floor, mbrf): 3891.8  
 Total penetration (mbsf): 6.7  
 Total length of cored section (m): 6.7  
 Total core recovered (m): 6.72  
 Core recovery (%): 100.3  
 Total number of cores: 1

**Hole U1308E**

Latitude: 49°52.6998'N  
 Longitude: 24°14.2866'W  
 Time on hole (h): 28.92 (0235 h, 11 November 2004–0730 h, 12 November 2004)  
 Seafloor (drill pipe measurement from rig floor, mbrf): 3882.3  
 Distance between rig floor and sea level (m): 11.3  
 Water depth (drill pipe measurement from sea level, m): 3871.0  
 Total depth (drill pipe measurement from rig floor, mbrf): 4082.8  
 Total penetration (mbsf): 200.5  
 Total length of cored section (m): 193.0  
 Total length of drilled intervals (m): 7.5  
 Total core recovered (m): 172.52  
 Core recovery (%): 89.4  
 Total number of cores: 21  
 Total number of drilled intervals: 3

Table T1 (continued).

## Hole U1308F

Latitude: 49°52.6996'N

Longitude: 24°14.3121'W

Time on hole (h): 41.00 (0730 h, 12 November 2004–0030 h, 14 November 2004)

Seafloor (drill pipe measurement from rig floor, mbrf): 3883.4

Distance between rig floor and sea level (m): 11.3

Water depth (drill pipe measurement from sea level, m): 3872.1

Total depth (drill pipe measurement from rig floor, mbrf): 4110.4

Total penetration (mbsf): 227.0

Total length of cored section (m): 227.0

Total core recovered (m): 228.55

Core recovery (%): 100.7

Total number of cores: 24

Core	Date (Nov 2004)	Local time (h)	Depth (mbsf)		Length (m)		Recovery (%)	Comments
			Top	Bottom	Cored	Recovered		
303-U1308A-								
1H	4	1030	0.0	8.6	8.6	8.62	100.2	Nonmagnetic barrel
2H	4	1135	8.6	18.1	9.5	10.05	105.8	Nonmagnetic barrel
3H	4	1235	18.1	27.6	9.5	9.11	95.9	Oriented; nonmagnetic barrel; split liner
4H	4	1340	27.6	37.1	9.5	8.29	87.3	Oriented; nonmagnetic barrel
5H	4	1435	37.1	46.6	9.5	9.00	94.7	Oriented; nonmagnetic barrel
6H	4	1535	46.6	56.1	9.5	9.53	100.3	Oriented; nonmagnetic barrel
7H	4	1635	56.1	65.6	9.5	6.11	64.3	Oriented; nonmagnetic barrel
8H	4	1740	65.6	75.1	9.5	9.44	99.4	Oriented; nonmagnetic barrel
9H	4	1840	75.1	84.6	9.5	8.29	87.3	Oriented; nonmagnetic barrel
10H	4	1940	84.6	94.1	9.5	9.70	102.1	Oriented; nonmagnetic barrel
11H	4	2045	94.1	103.6	9.5	10.02	105.5	Oriented; nonmagnetic barrel
12H	4	2150	103.6	113.1	9.5	9.56	100.6	Oriented; nonmagnetic barrel
13H	4	2245	113.1	122.6	9.5	8.56	90.1	Oriented; nonmagnetic barrel
14H	4	2355	122.6	132.1	9.5	9.51	100.1	Oriented; nonmagnetic barrel
15H	5	0115	132.1	141.6	9.5	9.25	97.4	Oriented; nonmagnetic barrel
16H	5	0245	141.6	151.1	9.5	10.06	105.9	Oriented; nonmagnetic barrel
17H	5	0420	151.1	160.6	9.5	9.36	98.5	Oriented; nonmagnetic barrel
18H	5	0710	160.6	170.1	9.5	10.13	106.6	Oriented; nonmagnetic barrel; two wireline trips due to parting of shear pin
19H	5	1030	170.1	179.6	9.5	9.57	100.7	Oriented; nonmagnetic barrel; crushed liner
20H	5	1320	179.6	189.1	9.5	9.07	95.5	Oriented; nonmagnetic barrel
21H	5	1450	189.1	198.6	9.5	9.48	99.8	Oriented; nonmagnetic barrel
22H	5	1615	198.6	208.1	9.5	9.94	104.6	Oriented; nonmagnetic barrel
23H	5	1750	208.1	217.6	9.5	8.83	93.0	Oriented; nonmagnetic barrel
24H	5	2030	217.6	227.1	9.5	9.63	101.4	Oriented; nonmagnetic barrel
25H	5	2145	227.1	236.6	9.5	9.34	98.3	Oriented; nonmagnetic barrel
26H	5	2305	236.6	246.1	9.5	9.01	94.8	Oriented; nonmagnetic barrel
27H	6	0100	246.1	255.6	9.5	0.00	0.0	No recovery
28H	6	0245	255.6	265.1	9.5	9.75	102.6	Oriented; nonmagnetic barrel
29H	6	0505	265.1	274.6	9.5	10.16	107.0	Oriented; nonmagnetic barrel
30H	6	0635	274.6	284.1	9.5	7.54	79.4	Oriented; nonmagnetic barrel; split liner
31H	6	0810	284.1	293.6	9.5	9.48	99.8	Oriented; nonmagnetic barrel
32H	6	1025	293.6	303.1	9.5	9.70	102.1	Oriented; nonmagnetic barrel
33H	6	1215	303.1	312.6	9.5	9.84	103.6	Nonmagnetic barrel
34H	6	1350	312.6	322.1	9.5	9.51	100.1	Nonmagnetic barrel
35H	6	1515	322.1	331.6	9.5	9.27	97.6	Nonmagnetic barrel
36H	6	1640	331.6	341.1	9.5	9.12	96.0	Nonmagnetic barrel
Totals:					341.1	323.83	94.9	
303-U1308B-								
1H	7	1350	0.0	4.0	4.0	4.04	101.0	Nonmagnetic barrel
2H	7	1510	4.0	13.5	9.5	9.21	97.0	Nonmagnetic barrel; split liner; core transferred to a pre-split liner; very disturbed
3H	7	1635	13.5	23.0	9.5	9.85	103.7	Oriented; nonmagnetic barrel
4H	7	1800	23.0	32.5	9.5	8.69	91.5	Oriented; nonmagnetic barrel
5H	7	1915	32.5	42.0	9.5	9.76	102.7	Oriented; nonmagnetic barrel
6H	7	2035	42.0	51.5	9.5	9.88	104.0	Oriented; nonmagnetic barrel; crushed liner
7H	7	2200	51.5	61.0	9.5	9.81	103.3	Oriented; nonmagnetic barrel
8H	7	2330	61.0	70.5	9.5	10.06	105.9	Oriented; nonmagnetic barrel
9H	8	0105	70.5	80.0	9.5	10.05	105.8	Oriented; nonmagnetic barrel
10H	8	0230	80.0	89.5	9.5	10.03	105.6	Oriented; nonmagnetic barrel
11H	8	0405	89.5	99.0	9.5	9.88	104.0	Oriented; nonmagnetic barrel
12H	8	0545	99.0	108.5	9.5	10.05	105.8	Oriented; nonmagnetic barrel
13H	8	0710	108.5	118.0	9.5	9.89	104.1	Oriented; nonmagnetic barrel; crushed liner

Table T1 (continued).

Core	Date (Nov 2004)	Local time (h)	Depth (mbsf)		Length (m)		Recovery (%)	Comments
			Top	Bottom	Cored	Recovered		
303-U1308B-								
14H	8	0850	118.0	127.5	9.5	9.91	104.3	Oriented; nonmagnetic barrel
15H	8	1020	127.5	137.0	9.5	9.94	104.6	Oriented; nonmagnetic barrel; crushed liner
16H	8	1215	137.0	146.5	9.5	9.83	103.5	Oriented; nonmagnetic barrel; crushed liner
17H	8	1350	146.5	156.0	9.5	9.44	99.4	Oriented; nonmagnetic barrel
18H	8	1525	156.0	165.5	9.5	9.67	101.8	Oriented; nonmagnetic barrel
19H	8	1655	165.5	175.0	9.5	9.15	96.3	Oriented; nonmagnetic barrel
20H	8	1805	175.0	184.5	9.5	0.02	0.2	Oriented; nonmagnetic barrel
21H	8	1915	184.5	194.0	9.5	2.72	28.6	Oriented; nonmagnetic barrel
22H	8	2050	194.0	198.3	4.3	4.31	100.2	Oriented; nonmagnetic barrel; shattered liner on entire core; core disturbed
Totals:					198.3	186.19	93.9	
303-U1308C-								
1H	9	0800	0.0	4.4	4.4	4.43	100.7	Nonmagnetic barrel
2H	9	0915	4.4	13.9	9.5	9.57	100.7	Nonmagnetic barrel
3H	9	1020	13.9	23.4	9.5	9.63	101.4	Oriented; nonmagnetic barrel; crushed liner
4H	9	1125	23.4	32.9	9.5	3.47	36.5	Oriented; nonmagnetic barrel; crushed liner
5H	9	1235	32.9	42.4	9.5	7.92	83.4	Oriented; nonmagnetic barrel
6H	9	1345	42.4	51.9	9.5	9.65	101.6	Oriented; nonmagnetic barrel; crushed liner
7H	9	1450	51.9	61.4	9.5	8.16	85.9	Oriented; nonmagnetic barrel; crushed liner; core very disturbed
8H	9	1555	61.4	70.9	9.5	9.50	100.0	Oriented; nonmagnetic barrel
9H	9	1710	70.9	80.4	9.5	9.12	96.0	Oriented; nonmagnetic barrel
10H	9	1820	80.4	89.9	9.5	9.33	98.2	Oriented; nonmagnetic barrel
11H	9	1925	89.9	99.4	9.5	9.94	104.6	Oriented; nonmagnetic barrel
12H	9	2040	99.4	108.9	9.5	10.08	106.1	Oriented; nonmagnetic barrel
13H	9	2155	108.9	118.4	9.5	9.40	99.0	Oriented; nonmagnetic barrel
14H	9	2300	118.4	127.9	9.5	6.31	66.4	Oriented; nonmagnetic barrel
15H	10	0015	127.9	137.4	9.5	9.45	99.5	Oriented; nonmagnetic barrel; crushed liner
16H	10	0140	137.4	146.9	9.5	9.13	96.1	Oriented; nonmagnetic barrel
17H	10	0240	146.9	156.4	9.5	9.75	102.6	Oriented; nonmagnetic barrel
18H	10	0350	156.4	165.9	9.5	7.90	83.2	Oriented; nonmagnetic barrel
19H	10	0500	165.9	175.4	9.5	9.36	98.5	Oriented; nonmagnetic barrel; crushed liner
20H	10	0615	175.4	184.9	9.5	9.82	103.4	Oriented; nonmagnetic barrel
21H	10	0725	184.9	194.4	9.5	9.97	105.0	Oriented; nonmagnetic barrel
22H	10	0930	194.4	203.9	9.5	9.63	101.4	Drillover barrel with AHC
23H	10	1105	203.9	213.4	9.5	9.60	101.1	Drillover barrel with PHC
24H	10	1255	213.4	222.9	9.5	9.93	104.5	Drillover barrel with PHC
25H	10	1425	222.9	232.4	9.5	9.81	103.3	Drillover barrel with PHC
26H	10	1555	232.4	241.9	9.5	9.95	104.7	Drillover barrel with PHC
27H	10	1730	241.9	251.4	9.5	9.97	105.0	Drillover barrel with PHC
28H	10	1835	251.4	260.9	9.5	10.18	107.2	
29H	10	2000	260.9	270.4	9.5	10.18	107.2	Drillover barrel with PHC; bent core barrel
30H	10	2315	270.4	279.9	9.5	9.96	104.8	Drillover barrel with PHC; bent core barrel
Totals:					279.90	271.10	96.86	
303-U1308D-								
1H	11	0245	0.0	6.7	6.7	6.72	100.3	2.2 m between Sections 3 and 4 discarded due to heavy disturbance by crushed liner
Totals:					6.7	6.72	100.3	
303-U1308E-								
1H	11	0400	0.0	9.5	9.5	9.67	101.8	Nonmagnetic barrel
2H	11	0530	9.5	19.0	9.5	10.05	105.8	Nonmagnetic barrel
3H	11	0640	19.0	28.5	9.5	7.46	78.5	Oriented; nonmagnetic barrel
4H	11	0745	28.5	38.0	9.5	7.61	80.1	Oriented; nonmagnetic barrel
5H	11	0850	38.0	47.5	9.5	6.52	68.6	Oriented; nonmagnetic barrel
6H	11	0950	47.5	57.0	9.5	8.08	85.1	Oriented; nonmagnetic barrel
*****Drilled 57.0 to 60.0 mbsf*****								
7H	11	1110	60.0	69.5	9.5	6.96	73.3	Oriented; nonmagnetic barrel
8H	11	1225	69.5	79.0	9.5	6.72	70.7	Oriented; nonmagnetic barrel
9H	11	1355	79.0	83.0	4.0	7.27	181.8	Oriented; nonmagnetic barrel; core overlapped 5.5 m with Core 8H
*****Drilled 83.0 to 84.0 mbsf*****								
10H	11	1515	84.0	93.5	9.5	7.29	76.7	Oriented; nonmagnetic barrel
*****Drilled 93.5 to 97.0 mbsf*****								
11H	11	1635	97.0	106.5	9.5	3.34	35.2	Oriented; nonmagnetic barrel
12H	11	1810	106.5	116.0	9.5	8.78	92.4	Oriented; nonmagnetic barrel; crushed liner at bottom
13H	11	1940	116.0	125.5	9.5	9.18	96.6	Oriented; nonmagnetic barrel

Table T1 (continued).

Core	Date (Nov 2004)	Local time (h)	Depth (mbsf)		Length (m)		Recovery (%)	Comments
			Top	Bottom	Cored	Recovered		
303-U1308E-								
14H	11	2055	125.5	134.0	8.5	8.84	104.0	Oriented; nonmagnetic barrel
15H	11	2210	134.0	143.5	9.5	8.93	94.0	Oriented; nonmagnetic barrel; crushed liner at bottom
16H	11	2320	143.5	153.0	9.5	9.22	97.1	Oriented; nonmagnetic barrel
17H	12	0030	153.0	162.5	9.5	8.78	92.4	Oriented; nonmagnetic barrel
18H	12	0140	162.5	172.0	9.5	9.29	97.8	Oriented; nonmagnetic barrel
19H	12	0250	172.0	181.5	9.5	9.93	104.5	Oriented; nonmagnetic barrel
20H	12	0435	181.5	191.0	9.5	8.69	91.5	
21H	12	0610	191.0	200.5	9.5	9.91	104.3	
				Cored:	193.0	172.52	89.4	
				Drilled:	7.5			
				Total:	200.5			
303-U1308F-								
1H	12	1125	0.0	9.5	9.5	6.62	69.7	Nonmagnetic barrel; crushed liner
2H	12	1220	9.5	19.0	9.5	8.89	93.6	Nonmagnetic barrel; crushed liner
3H	12	1330	19.0	28.5	9.5	9.59	101.0	Oriented; nonmagnetic barrel; crushed liner
4H	12	1440	28.5	38.0	9.5	9.42	99.2	Oriented; nonmagnetic barrel; crushed liner
5H	12	1550	38.0	47.5	9.5	9.92	104.4	Oriented; nonmagnetic barrel; crushed liner
6H	12	1655	47.5	57.0	9.5	9.71	102.2	Oriented; steel core barrel; crushed liner
7H	12	1810	57.0	66.5	9.5	9.67	101.8	Oriented; nonmagnetic barrel; crushed liner
8H	12	1915	66.5	76.0	9.5	9.29	97.8	Oriented; nonmagnetic barrel; crushed liner
9H	12	2020	76.0	85.5	9.5	9.58	100.8	Oriented; nonmagnetic barrel; crushed liner
10H	12	2125	85.5	94.0	8.5	8.93	105.1	Oriented; nonmagnetic barrel; crushed liner
11H	12	2235	94.0	103.5	9.5	9.40	99.0	Oriented; nonmagnetic barrel
12H	12	2340	103.5	113.0	9.5	9.62	101.3	Oriented; nonmagnetic barrel
13H	13	0050	113.0	122.5	9.5	9.66	101.7	Oriented; nonmagnetic barrel; crushed liner
14H	13	0155	122.5	132.0	9.5	9.84	103.6	Oriented; nonmagnetic barrel; crushed liner
15H	13	0305	132.0	141.5	9.5	9.91	104.3	Oriented; nonmagnetic barrel
16H	13	0410	141.5	151.0	9.5	9.96	104.8	Oriented; nonmagnetic barrel
17H	13	0515	151.0	160.5	9.5	9.84	103.6	Oriented; nonmagnetic barrel; crushed liner
18H	13	0620	160.5	170.0	9.5	9.63	101.4	Oriented; nonmagnetic barrel
19H	13	0725	170.0	179.5	9.5	9.68	101.9	Oriented; nonmagnetic barrel
20H	13	0835	179.5	189.0	9.5	10.05	105.8	Oriented; nonmagnetic barrel
21H	13	0940	189.0	198.5	9.5	9.87	103.9	Oriented; nonmagnetic barrel
22H	13	1100	198.5	208.0	9.5	9.89	104.1	Drillover barrel
23H	13	1240	208.0	217.5	9.5	9.97	105.0	Drillover barrel
24H	13	1405	217.5	227.0	9.5	9.61	101.2	Drillover barrel
				Totals:	227.0	228.55	100.7	

Note: AHC = active heave compensator, PHC = passive heave compensator.











Table T5. Distribution of calcareous nannofossils, Hole U1308D.

Core, section	Age (Ma)	Abundance	Preservation	<i>Calcidiscus leptoporus</i>	<i>Coccolithus streckerii</i>	<i>Coccolithus pelagicus</i>	<i>Emiliania huxleyi</i>	<i>Gephyrocapsa oceanica</i>	<i>Gephyrocapsa</i> spp. (small)	<i>Helicosphaera carteri</i>	<i>Helicosphaera hyalina</i>	<i>Reticulofenestra</i> spp. (small)	<i>Umbilicosphaera sibogae</i>	<i>Arkangeliskella cymbiformis</i>
303-U1308D-1H-CC	0-0.25	F	M	R	+	R	F	+	F	R	+	+	+	r

Notes: Abundance: F = few, R = rare, + = present, r = reworked. Preservation: M = moderate.



Table T6. Distribution of calcareous nannofossils, Hole U1308E.

Core, section	Age (Ma)	Abundance	Preservation	<i>Calcidiscus leptoporus</i>	<i>Calcidiscus macintyreii</i>	<i>Coccolithus streckerii</i>	<i>Coccolithus pelagicus</i>	<i>Cyclolithella annula</i>	<i>Discoaster brouweri</i>	<i>Discoaster pentaradiatus</i>	<i>Discoaster surculus</i>	<i>Discoaster tamalis</i>	<i>Discoaster triradiatus</i>	<i>Discoaster</i> spp.	<i>Discolithina japonica</i>	<i>Discolithina</i> spp.	<i>Emiliana huxleyi</i>	<i>Gephyrocapsa caribbeanica</i>	<i>Gephyrocapsa oceanica</i>	<i>Gephyrocapsa parallela</i>	<i>Gephyrocapsa</i> spp. (large)	<i>Gephyrocapsa</i> spp. (small)	<i>Helicosphaera carteri</i>	<i>Helicosphaera hyalina</i>	<i>Helicosphaera sellii</i>	<i>Pseudoemiliana lacunosa</i>	<i>Reticulofenestra asanoi</i>	<i>Reticulofenestra ampla</i>	<i>Reticulofenestra</i> spp. (small)	<i>Rhabdosphaera clavigera</i>	<i>Rhabdosphaera stylifera</i>	<i>Scapholithus fossilis</i>	<i>Syracosphaera pulchra</i>	<i>Umbilicosphaera sibogae</i>	Reworked species				
																																			<i>Arkangelskiella cymbiformis</i>	<i>Biscutum magnum</i>	<i>Gartnerago obliquum</i>	<i>Prediscosphaera cretacea</i>	<i>Watznaueria barnesae</i>
303-U1308E-																																							
1H-CC	0~0.25	A	M	R	R	F	+								+	F																							
2H-CC	0.25~0.41	A	M	R		R													F	+		R																	
3H-CC	0.41~0.85	A	G	R		+	R								+	+																							
4H-CC	0.41~0.85	A	M	R																R	+																		
5H-CC	0.41~0.85	A	M	R		+	R																																
6H-CC	0.85~0.95	A	M	R		+	R																																
7H-CC	0.95~1.16	F	M	+																																			
8H-CC	0.95~1.16	C	M	R		+	R																																
9H-CC	1.21~1.45	C	M	R																																			
10H-CC	1.45~1.65	A	M	R			R																																
11H-CC	1.45~1.65	A	M	R			F																																
12H-CC	1.73~1.97	A	M	R	+	+	F																																
13H-CC	1.73~1.97	A	M	R	R	+	F	+																															
14H-CC	1.73~1.97	A	M	R	R	+	R	+																															
15H-CC	1.97~2.38	A	M	R	R	+	R	+																															
16H-CC	1.97~2.38	A	M	R	R	+	R		+					R	R	R	R	R																					
17H-CC	1.97~2.38	A	M	R	R	+	F							R	R	R	R	R																					
18H-CC	2.38~2.54	A	M	R	R	+	R								R	R	R	R																					
19H-CC	2.54~2.74	A	M	R	R	+	R								R	R	R	R																					
20H-CC	2.54~2.74	A	M	R	R	+	R								R	R	R	R																					
21H-CC	2.78~3.85	A	M	R	R	+	R								R	R	R	R								R													

Notes: Abundance: A = abundant, C = common, F = few, R = rare, + = present, r = reworked. Preservation: G = good, M = moderate.







Table T9. Distribution of planktonic foraminifers, Hole 1308B.

Core	Preservation	Overall abundance	<i>Globigerina bulloides</i>	<i>Globigerina decoraperta</i>	<i>Globigerina falconensis</i>	<i>Globigerina nepenthes</i>	<i>Globigerinella calida</i>	<i>Globigerinella siphonifera</i>	<i>Globigerinita glutinata</i>	<i>Globigerinita uvula</i>	<i>Globigerinoides conglobatus</i>	<i>Globigerinoides extremus</i>	<i>Globigerinoides obliquus</i>	<i>Globigerinoides ruber</i>	<i>Globigerinoides sacculifer</i>	<i>Globigerinoides tenella</i>	<i>Globorotalia conomiozea</i>	<i>Globorotalia crassaformis</i>	<i>Globorotalia crassula</i>	<i>Globorotalia hirsuta</i>	<i>Globorotalia inflata</i>	<i>Globorotalia margaritae</i>	<i>Globorotalia puncticulata</i>	<i>Globorotalia scitula</i>	<i>Globorotalia truncatulinoides</i>	<i>Globorotalia turrida</i>	<i>Hastigerina pelagica</i>	<i>Neogloboquadrina atlantica (d)</i>	<i>Neogloboquadrina atlantica (s)</i>	<i>Neogloboquadrina dutertrei</i>	<i>Neogloboquadrina incompta</i>	<i>Neogloboquadrina pachyderma (d)</i>	<i>Neogloboquadrina pachyderma (s)</i>	<i>Orbulina universa</i>	<i>Turborotalita quinqueloba (d)</i>	<i>Turborotalita quinqueloba (s)</i>	Biozone					
U1308B-																																										
1H	VG	C	A	R					P																																	
2H	VG	A	A				P		P	P				P						P	R																					
3H	VG	A	A		P				R	R	R			R																												
4H	VG	A	A						R	R	R																															
5H	VG	A	A		F		R	R	R	R					P																											
6H	G	A	A		R		R	F	R	R				R				P																								
7H	VG	A	D				R	R	F																																	
8H	G	A	A						R	P																																
9H	G	A	R															R																								
10H	VG	A	D					R	P																																	
11H	VG	A	D					A	R					R																												
12H	G	A	D					A	F																																	
13H	VG	A	A		P			A	P					F																												
14H	G	A	A		P		P	A	R					F																												
15H	VG	A	R		F				F	F				R																												
16H	G	A	A		P	R			R	R				P				R																								
17H	G	A	F		P	R			F	R																																
18H	M	A	R			R			P	R				P				R	A	R																						
19H	M	A				R			R									P																								
20H	M	R	R		P	F			P									P																								
21H	M	A				R			P	A								P	P																							
22H	M	A	A			P			A									R																								

Notes: Abundance: D = dominant, A = abundant, C = common, F = few, R = rare, P = present. Preservation: VG = very good, G = good, M = moderate (see "Foraminifers" in the "Site U1302–U1308 methods" chapter). d = dextral, s = sinistral.



Table T10. Distribution of planktonic foraminifers, Hole 1308C.

Core	Preservation	Overall abundance	<i>Globigerina bulloides</i>	<i>Globigerina decoraperta</i>	<i>Globigerina falconensis</i>	<i>Globigerina nepenthes</i>	<i>Globigerinella calida</i>	<i>Globigerinella siphonifera</i>	<i>Globigerinita glutinata</i>	<i>Globigerinita uvula</i>	<i>Globigerinoides conglobatus</i>	<i>Globigerinoides extremus</i>	<i>Globigerinoides obliquus</i>	<i>Globigerinoides ruber</i>	<i>Globigerinoides sacculifer</i>	<i>Globigerinoides tenella</i>	<i>Globorotalia conomiozea</i>	<i>Globorotalia crassaformis</i>	<i>Globorotalia crassula</i>	<i>Globorotalia hirsuta</i>	<i>Globorotalia inflata</i>	<i>Globorotalia margaritae</i>	<i>Globorotalia puncticulata</i>	<i>Globorotalia scitula</i>	<i>Globorotalia truncatulinoides</i>	<i>Globorotalia tumida</i>	<i>Hastigerina pelagica</i>	<i>Neogloboquadrina atlantica (d)</i>	<i>Neogloboquadrina atlantica (s)</i>	<i>Neogloboquadrina dutertrei</i>	<i>Neogloboquadrina incompta</i>	<i>Neogloboquadrina pachyderma (d)</i>	<i>Neogloboquadrina pachyderma (s)</i>	<i>Orbulina universa</i>	<i>Turborotalita quinqueloba (d)</i>	<i>Turborotalita quinqueloba (s)</i>	Biozone						
303-U1308C-																																											
1H	G	A	A					P	R																																		
2H	VG	A	A						F																																		
3H	G	A	R		P																																						
4H	G	A	A		R		R		P																																		
5H	M	R	R		P				P	R																																	
6H	G	A	A		F		P	P	P	R																																	
7H	G	A	R																																								
8H	G	A	A		R		P	R	P	R																																	
9H	G	A	F		R		P	P	P	R			P																														
10H	G	A	A		F		R		P	R																																	
11H	G	A	R					R																																			
12H	G	A	A		P		R	R	F																																		
13H	VG	A	A		P				R																																		
14H	VG	A	A	R			F		R																																		
15H	G	A	A				P	R																																			
16H	VG	A	F		P			A																																			
17H	G	A	A		R			R		P																																	
18H	G	A	D	P				A																																			
19H	G	A	F	R				F																																			
20H	M	R			R			A	R	P																																	
21H	M	A	R					F	P																																		
22H	M	A	A	R	R			A																																			
23H	M	C			R			F	R																																		
24H	M	A	P		R			R																																			
25H	M	A	A		P			A																																			
26H	M	A	R		F			R		P																																	
27H	M	A			F		P	P																																			
28H	M	A	R		R			P		P																																	
29H	M	A	A	R	R			A																																			
30H	M	A	A	R	P			R																																			

Notes: Abundance: D = dominant, A = abundant, C = common, F = few, R = rare, P = present. Preservation: VG = very good, G = good, M = moderate (see "Foraminifers" in the "Site U1302–U1308 methods" chapter). d = dextral, s = sinistral.



Table T11. Distribution of planktonic foraminifers, Hole U1308E.

Core	Overall abundance	Preservation	<i>Globigerina bulloides</i>	<i>Globigerina decoraperta</i>	<i>Globigerina falconensis</i>	<i>Globigerina nepenthes</i>	<i>Globigerinella calida</i>	<i>Globigerinella siphonifera</i>	<i>Globigerinita glutinata</i>	<i>Globigerinita uvula</i>	<i>Globigerinoides conglobatus</i>	<i>Globigerinoides extremus</i>	<i>Globigerinoides obliquus</i>	<i>Globigerinoides ruber</i>	<i>Globigerinoides sacculifer</i>	<i>Globigerinoides tenella</i>	<i>Globorotalia conomiozea</i>	<i>Globorotalia crassaformis</i>	<i>Globorotalia crassula</i>	<i>Globorotalia hirsuta</i>	<i>Globorotalia inflata</i>	<i>Globorotalia margaritae</i>	<i>Globorotalia puncticulata</i>	<i>Globorotalia scitula</i>	<i>Globorotalia truncatulinoides</i>	<i>Globorotalia tumida</i>	<i>Hastigerina pelagica</i>	<i>Neogloboquadrina atlantica (d)</i>	<i>Neogloboquadrina atlantica (s)</i>	<i>Neogloboquadrina dutertrei</i>	<i>Neogloboquadrina incompta</i>	<i>Neogloboquadrina pachyderma (d)</i>	<i>Neogloboquadrina pachyderma (s)</i>	<i>Orbulina universa</i>	<i>Turborotalita quinqueloba (d)</i>	<i>Turborotalita quinqueloba (s)</i>	Biozone			
303-U1308E-																																								
1H	A	M	A					P													F																			
2H	C	M	P																																					
3H	A	G	A	R			R	P													D		P	P																
4H	A	M	F					P													F																			
5H	A	M	R																																					
6H	A	G	P	R							P							P																						
7H	A	G	R	R				P	R				P	P																										
8H	A	G	R					P										P																						
9H	C	G	R																																					
10H	A	G	A	R			P	R	P					P														P	P											
11H	A	G	A	R			R	R										R		R	D																			
12H	A	G	F	R				R	A									P			A							R												
13H	A	G	R	R			P	P	R	P				P						P	A								P											
14H	A	G	F	F				F	P										R		D																			
15H	A	G	A	R				F						P																										
16H	A	G	A					A										R																						
17H	A	G	A	R				F						F																										
18H	A	M	A					R																																
19H	A	G	D	P				F																																
20H	A	G	A	P				R																																
21H	A	M	A	P				A																																

Notes: Abundance: D = dominant, A = abundant, C = common, F = few, R = rare, P = present. Preservation: G = good, M = moderate (see "Foraminifers" in the "Site U1302–U1308 methods" chapter). d = dextral, s = sinistral.



Table T12. Distribution of planktonic foraminifers, Hole U1308F.

Core	Overall abundance	Preservation	<i>Globigerina bulloides</i>	<i>Globigerina decoraperta</i>	<i>Globigerina falconensis</i>	<i>Globigerina nepenthes</i>	<i>Globigerinella calida</i>	<i>Globigerinella siphonifera</i>	<i>Globigerinita glutinata</i>	<i>Globigerinita uvula</i>	<i>Globigerinoides conglobatus</i>	<i>Globigerinoides extremus</i>	<i>Globigerinoides obliquus</i>	<i>Globigerinoides ruber</i>	<i>Globigerinoides sacculifer</i>	<i>Globigerinoides tenella</i>	<i>Globorotalia conomiozea</i>	<i>Globorotalia crassaformis</i>	<i>Globorotalia crassula</i>	<i>Globorotalia hirsuta</i>	<i>Globorotalia inflata</i>	<i>Globorotalia margaritae</i>	<i>Globorotalia puncticulata</i>	<i>Globorotalia scitula</i>	<i>Globorotalia truncatulinoides</i>	<i>Globorotalia tumida</i>	<i>Hastigerina pelagica</i>	<i>Neogloboquadrina atlantica (d)</i>	<i>Neogloboquadrina atlantica (s)</i>	<i>Neogloboquadrina dutertrei</i>	<i>Neogloboquadrina incompta</i>	<i>Neogloboquadrina pachyderma (d)</i>	<i>Neogloboquadrina pachyderma (s)</i>	<i>Orbulina universa</i>	<i>Turborotalita quinqueloba (d)</i>	<i>Turborotalita quinqueloba (s)</i>	Biozone			
303-U1308F-																																								
1H	A	G	A	R				R										P		F									R		F	D	P		R					
2H	A	G	A	R				F										P		A			R	P						A	A	P	F	F						
3H	A	G	A					R										R	P	D			P	F			P	P		A	R	P	P		P					
4H	A	G	F	R				R												D										A	D	P	P	R						
5H	A	G	R	P	R			R	F											A				R	P					R	A	P	A	A						
6H	A	G	A	R				R	P											D										A	A	P								
7H	A	G	A	R				R	R	P			F	P				F		D			P	P					A	R		R	R					<i>N. pachyderma (s)</i>		
8H	A	G	F					R					F	P				F		D			P	P					A	R		R	R							
9H	A	G	R	F				F		P			F		R			P		A			R	R					D	R	P	R	P							
10H	A	G	D	R				R	F				F							D				P					A	R	P	P	R							
11H	A	G	A					A	F				F					R		D									R	R	R		R							
12H	R	G	F						R				P							A			P						A	D			R	R						
13H	A	M	A						F									R		D			P	P					D											
14H	A	G	A	P				P	R					P						A				F					D	R		A	R					<i>G. inflata</i>		
15H	A	G	A						R											D				P					D	R										
16H	A	M	A					P	F									R		F									D	P			P							
17H	A	G	A						A									F		A				P					D				P							
18H	A	G	D					R	P					P				A					R						A	P	R									
19H	A	M	D						F														R	P					D	A	F	R								
20H	C	M	R	F				F	R									P	R	R			A	F					A	A	P	R	R							
21H	A	M	P	R				F		P				P			R	P	P				D	R					A	R	P	R	P					<i>N. atlantica – G. puncticulata</i>		
22H	C	M		P				A	R									P					D	R					R	A		A	F							
23H	C	M						F	F							P	F			A									F	A	P	P	A	F						
24H	C	M	P	R							P						R		A	P			D	P					F	A										

Notes: Abundance: D = dominant, A = abundant, C = common, F = few, R = rare, P = present. Preservation: G = good, M = moderate (see "Foraminifers" in the "Site U1302–U1308 methods" chapter). d = dextral, s = sinistral.



Table T13. Distribution of benthic foraminifers, Holes U1308A.

Core	<i>Bolivina</i> spp.	<i>Bolivina translucens</i>	<i>Cassidulina crassa</i>	<i>Cassidulina minuta</i>	<i>Chilostomella</i> spp.	<i>Cibicides</i> spp.	<i>Cibicides wuellerstorfi</i>	<i>Eggerelloides bradyi</i>	<i>Ehrenbergina</i> spp.	<i>Elphidium</i> spp.	<i>Epistominella exigua</i>	<i>Fissurina</i> spp.	<i>Gavelinopsis praegeri</i>	<i>Globobulimina</i> spp.	<i>Globocassidulina</i> sp.	<i>Gyrodina</i> spp.	<i>Hoeglundina elegans</i>	<i>Lagena</i> spp.	<i>Lenticulina</i> spp.	<i>Melonis barleeanum</i>	<i>Melonis pompilioides</i>	<i>Nonion</i> spp./ <i>Astronion</i> spp.	<i>Nuttallides umbonifera</i>	<i>Oridorsalis umbonatus</i>	<i>Pullenia bulloides</i>	<i>Pullenia quinqueloba</i>	<i>Pyrgo</i> spp./ <i>Biloculina</i> spp.	<i>Sphaeroidina bulloides</i>	<i>Stainforthia</i> sp.	<i>Uvigerina peregrina</i>	Indeterminate <i>Lagena</i>	Indeterminate <i>Miliolina</i>	Indeterminate <i>Rotalina</i>	Indeterminate <i>Textulariina</i>	Total			
303-U1308A-1H																																				1		
2H						1										1					1		2													4		
3H		1					1																														9	
4H	1							2								1				1				1	1	1		1									10	
5H							1						1																								5	
6H									1				1													1	1											8
7H					1	1					1														1												6	
8H					1																																5	
9H																		1	1		1	3				1							4				8	
10H							1											1				1															5	
11H																						1															2	
12H																											2											3
13H																																						0
14H											1															1												3
15H																																						2
16H						1										1																						2
17H																										1	1											4
18H		1	2				1	1					3									1			1												11	
19H							1					1										1			2													8
20H				2		1					8	2	1	1								1		2														18
21H											4	3	1											3	1	1	1	1										17
22H												1						1				1			1													6
23H																																						0
24H				1																																		3
25H																																						0
26H						1																																2
27H																																						0
28H																																						2
29H																																						4
30H			3	3																																		13
31H							1	1						4								1	1	1	2	1											13	
32H	2					3	1															1	1	1	1												19	
33H						4	4		1		1	2				3		1		1		1	5	5	1	1	2										34	
34H	2					1	2					1											3	2														19
35H	1		1																				1	2	2	1												15
36H	2					1	3	5	1			5		16		5	2	1	2			8	22	6	9	8	1										116	

Note: Numbers are total observations, which are not calibrated.



Table T14. Distribution of benthic foraminifers, Hole U1308B.

Core	<i>Bolivina</i> spp. <i>Bolivina translucens</i> <i>Cassidulina crassa</i> <i>Cassidulina minuta</i> <i>Chilostomella</i> spp.	<i>Cibicides</i> spp. <i>Cibicides wuellerstorfi</i> <i>Eggerelloides bradyi</i> <i>Ehrenbergina</i> spp. <i>Elphidium</i> spp.	<i>Epistominella exigua</i> <i>Fissurina</i> spp. <i>Gavelinopsis praegeri</i> <i>Globobulimina</i> spp. <i>Globocassidulina</i> sp.	<i>Gyroidina</i> spp. <i>Hoeglundina elegans</i> <i>Lagena</i> spp. <i>Lenticulina</i> spp. <i>Melonis barleeaanum</i>	<i>Melonis pompilioides</i> Nonion spp./ <i>Astronion</i> spp. <i>Nuttallides umbonifera</i> <i>Oridorsalis umbonatus</i> <i>Pullenia bulloides</i>	<i>Pullenia quinqueloba</i> <i>Pyrgo</i> spp./ <i>Biloculina</i> spp. <i>Sphaeroidina bulloides</i> <i>Stainforthia</i> sp. <i>Uvigerina peregrina</i>	Indeterminate Lagenina Indeterminate Millolina Indeterminate Rotalina Indeterminate Textularina	Total
303-U1308B-								
1H			1			3		4
2H						2		2
3H				1				2
4H					1			2
5H								0
6H						1		1
7H						1		3
8H		1				1		6
9H	1	1			1	1	2	6
10H		1	1					4
11H					1			2
12H						1	1	4
13H						1		2
14H			1		1	1	1	4
15H					1			2
16H				1	1	1	1	4
17H		1	2	1			1	13
18H					1	1		7
19H		1	1		1			4
20H		1			1	1	1	5
21H			1				1	3

Note: Numbers are total observations, which have not been calibrated.

Table T15. Distribution of benthic foraminifers, Hole U1308C.

Core	<i>Bolivina</i> spp.	<i>Bolivina translucens</i>	<i>Cassidulina crassa</i>	<i>Cassidulina minuta</i>	<i>Chilostomella</i> spp.	<i>Cibicides</i> spp.	<i>Cibicides wuellerstorfi</i>	<i>Eggerelloides bradyi</i>	<i>Ehrenbergina</i> spp.	<i>Elphidium</i> spp.	<i>Epistominella exigua</i>	<i>Fissurina</i> spp.	<i>Gavelinopsis praegeri</i>	<i>Globobulimina</i> spp.	<i>Globocassidulina</i> sp.	<i>Gyroldina</i> spp.	<i>Hoeglundina elegans</i>	<i>Lagena</i> spp.	<i>Lenticulina</i> spp.	<i>Melonis barleeaanum</i>	<i>Melonis pompilioides</i>	<i>Nonion</i> spp./ <i>Astronion</i> spp.	<i>Nuttallides umbonifera</i>	<i>Oridorsalis umbonatus</i>	<i>Pullenia bulloides</i>	<i>Pullenia quinqueloba</i>	<i>Pyrgo</i> spp./ <i>Biloculina</i> spp.	<i>Sphaeroidina bulloides</i>	<i>Stainforthia</i> sp.	<i>Uvigerina peregrina</i>	Indeterminate Lagenina	Indeterminate Miliolina	Indeterminate Rotalina	Indeterminate Textularina	Total			
303-U1308C-																																						
1H																						1				1		2								4		
2H																											1										5	
3H					1	1	1				1																										10	
4H																																					0	
5H		1																																			1	
6H														1																							2	
7H							4																														8	
8H											1												1			1	2										5	
9H																							1										1				3	
10H													1																								2	
11H		1												1													1										4	
12H													1							1			1				2										7	
13H																							1														1	
14H																																					3	
15H							1																		1												3	
16H											2																										3	
17H																							1			1											7	
18H																		1																			2	
19H						1																															1	
20H											1		1		2								1	1		1											8	
21H													2		1								2														7	
22H													1		1																						7	
23H																											1											3
24H							2																															7
25H								2			1																	1										5
26H												1																										2
27H																																						2
28H						1																																1
29H																																						2
30H							1	1								1																						4

Note: Numbers are total observations, which are not calibrated.

Table T16. Distribution of benthic foraminifers, Hole U1308D and U1308E.

Core	<i>Bolivina</i> spp.	<i>Bolivina translucens</i>	<i>Cassidulina crassa</i>	<i>Cassidulina minuta</i>	<i>Chilostomella</i> spp.	<i>Cibicides</i> spp.	<i>Cibicides wuellerstorfi</i>	<i>Eggerelloides bradyi</i>	<i>Ehrenbergina</i> spp.	<i>Elphidium</i> spp.	<i>Epistominella exigua</i>	<i>Fissurina</i> spp.	<i>Gavelinopsis praegeri</i>	<i>Globobulimina</i> spp.	<i>Globocassidulina</i> sp.	<i>Gyroldina</i> spp.	<i>Hoeglundina elegans</i>	<i>Lagena</i> spp.	<i>Lenticulina</i> spp.	<i>Melonis barleeaanum</i>	<i>Melonis pompilioides</i>	<i>Nonion</i> spp./ <i>Astronion</i> spp.	<i>Nuttallides umbonifera</i>	<i>Oridorsalis umbonatus</i>	<i>Pullenia bulloides</i>	<i>Pullenia quinqueloba</i>	<i>Pyrgo</i> spp./ <i>Biloculina</i> spp.	<i>Sphaeroidina bulloides</i>	<i>Stainforthia</i> sp.	<i>Uvigerina peregrina</i>	Indeterminate Lagenina	Indeterminate Millolina	Indeterminate Rotalina	Indeterminate Textularina	Total			
303-U1308D-1H																1																				2		
303-U1308E-1H																									1				1								3	
2H							1				1																										2	
3H							1																														4	
4H							1							1																							3	
5H													1																								2	
6H						1																			1	1												3
7H													1																								2	
8H																										1			2								3	
9H																1								1	1					1								3
10H																							1		1						1							3
11H																									1													2
12H																														1								2
13H																							2										1					3
14H							1					1																										2
15H											3			1																								4
16H											1																											2
17H												1																										2
18H		1																				1																3
19H											4		1		3											1												10
20H																																						2
21H											1																							1				3

Note: Numbers are total observations, which have not been calibrated.

Table T17. Distribution of benthic foraminifers, Hole U1308F.

Core	<i>Bolivina</i> spp.	<i>Bolivina translucens</i>	<i>Cassidulina crassa</i>	<i>Cassidulina minuta</i>	<i>Chilostomella</i> spp.	<i>Cibicides</i> spp.	<i>Cibicides wuellerstorfi</i>	<i>Eggerelloides bradyi</i>	<i>Ehrenbergina</i> spp.	<i>Elphidium</i> spp.	<i>Epistominella exigua</i>	<i>Fissurina</i> spp.	<i>Gavelinopsis praegeri</i>	<i>Globbulimina</i> spp.	<i>Globocassidulina</i> sp.	<i>Gyroldina</i> spp.	<i>Hoeglundina elegans</i>	<i>Lagena</i> spp.	<i>Lenticulina</i> spp.	<i>Meloris barleanum</i>	<i>Meloris pompilioides</i>	<i>Nonion</i> spp.	<i>Nuttallides umbonifera</i>	<i>Oridorsalis umbonatus</i>	<i>Pullenia bulloides</i>	<i>Pullenia quinqueloba</i>	<i>Pyrgo</i> spp.	<i>Sphaeroidina bulloides</i>	<i>Stainforthia</i> sp.	<i>Uvigerina peregrina</i>	Indeterminate Lagenina	Indeterminate Miliolina	Indeterminate Rotalina	Indeterminate Textularina	Total		
303-U1308F-1H											1																									1	
2H							1						1								1					2										6	
3H																				1						1										3	
4H			2								2			1							1					1										9	
5H																									1											1	
6H								2																							5					7	
7H						1																														1	
8H														1																			1			6	
9H																									1											2	
10H																																		1		1	
11H																											1									2	
12H																																				0	
13H			1								1	1														1	1									8	
14H						1														1																5	
15H																																				7	
16H								1																	4	1			1								7
17H																								1	2	2											7
18H												1																								4	
19H																	3																			3	
20H			1								5		3			3										2	1									17	
21H									1			2			2											1										14	
22H			1									1																								2	
23H		1	1	2																																13	
24H		1													3											1										1	

Note: Numbers are total observations, which are not calibrated.

Table T18. Distribution of diatoms and silicoflagellates, Hole U1308A. (See table notes. Continued on next five pages.)

Core, section, interval (cm)	Diatoms																																
	Abundance	Preservation	<i>Achnanthes</i> sp.	<i>Actinocyclus curvatulus</i>	<i>Actinocyclus ellipticus</i>	<i>Actinocyclus octonarius</i>	<i>Actinocyclus oculatus</i>	<i>Actinocyclus</i> spp.	<i>Actinopterychus senarius</i>	<i>Alveus marinus</i>	<i>Amphora</i> sp.	<i>Azpeitia africana</i>	<i>Azpeitia neocrenulata</i>	<i>Azpeitia nodulifera</i>	<i>Azpeitia tabularis</i>	<i>Bacteriastrium hyalinum</i>	<i>Bacteriastrium</i> sp.	<i>Cavitatus jousearnus</i>	RS <i>Chaetoceros cinctus</i>	RS <i>Chaetoceros compressus</i>	RS <i>Chaetoceros constrictus</i>	RS <i>Chaetoceros coronatus</i>	RS <i>Chaetoceros debilis</i>	RS <i>Chaetoceros diadema</i>	RS <i>Chaetoceros lorenzianus</i>	RS <i>Chaetoceros</i> spp.	<i>Chaetoceros setae</i>	<i>Cocconeis</i> spp.	<i>Coscinodiscus asteromphalus</i>	<i>Coscinodiscus argus</i>	<i>Coscinodiscus marginatus</i>	<i>Coscinodiscus radiatus</i>	
303-U1308A-1H-1, 2	A	G		T	T				T								T		R		R	T	T	F	*							T	
1H-1, 20	C	M		T													T		T	T	T		T	R	*								
1H-1, 68	C	M		T	T				*										T	T	T		T	R	*				R			T	
1H-1, 137	C	M		F				T											T		T		T	R	*							T	
1H-2, 33	R	P																	T					T	T	*				T		T	
1H-CC	R	M		R					*																T					*		*	
2H-4, 20	B																																
2H-5, 90	B																																
2H-5, 144	C	M		T					T										T				T	T	*					T	T		
2H-7, 44	C	G		R								T							T		T		T	T	*					T	T	*	
2H-CC	T	P																											*				
3H-6, 30	B																																
3H-CC	B																																
4H-3, 33	B																																
4H-CC	B																																
5H-3, 70	B																																
5H-CC	T	P																							T	T							
6H-1, 79	B																																
6H-2, 129	R	P		T																T			T										
6H-5, 60	T	P																		T							*						
6H-7, 45	C	M		T		T									T								T		R	*	*	T					
6H-CC	A	M		T		T														T			T	T	R	*	*				T	T	
7H-CC	C	M			T			T		T		T							T				T	T	R	*	*				T	T	
8H-CC	C	M						T		T									T		T		T		R					T			
9H-CC	C	M																	T		T										T		
10H-CC	B																																
11H-3, 5	B																																
11H-3, 30	B																																
11H-5, 8	C	M							T											T							*					T	
11H-CC	B																																
12H-2, 6	C	M		T											T																T	T	
12H-4, 124	T	M													T																		
12H-CC	T	P																															
13H-4, 122	B																																
13H-5, 60	B																																
13H-6, 25	T	M																															
13H-CC	B																																
14H-2, 52	B																																
14H-3, 145	F	M		F		T														T					T	*						T	
14H-CC	B																																
15H-2, 42	C	M	T	T																				T									
15H-2, 73	B																																
15H-4, 19	T	M																															
15H-CC	T	M		T				*	*					*	*																	*	
16H-4, 100	B																																
16H-5, 10	B																																
16H-CC	T	P																															
17H-4, 73	B																																
17H-5, 64	F	G		T											T																		
17H-CC	C	G						T																									
18H-CC	T	P																															









Table T18 (continued).

Core, section, interval (cm)	Diatoms																																			
	Abundance	Preservation	<i>Achnanthes</i> sp.	<i>Actinocyclus curvatulus</i>	<i>Actinocyclus ellipticus</i>	<i>Actinocyclus octonarius</i>	<i>Actinocyclus oculatus</i>	<i>Actinocyclus</i> spp.	<i>Actinopterychus senarius</i>	<i>Alveus marinus</i>	<i>Amphora</i> sp.	<i>Azpeitia africana</i>	<i>Azpeitia neocrenulata</i>	<i>Azpeitia nodulifera</i>	<i>Azpeitia tabularis</i>	<i>Bacteriastrium hyalinum</i>	<i>Bacteriastrium</i> sp.	<i>Cavitatus jousearnus</i>	RS <i>Chaetoceros cinctus</i>	RS <i>Chaetoceros compressus</i>	RS <i>Chaetoceros constrictus</i>	RS <i>Chaetoceros coronatus</i>	RS <i>Chaetoceros debilis</i>	RS <i>Chaetoceros diadema</i>	RS <i>Chaetoceros lorenzianus</i>	RS <i>Chaetoceros</i> spp.	<i>Chaetoceros setae</i>	<i>Cocconeis</i> spp.	<i>Coscinodiscus asteromphalus</i>	<i>Coscinodiscus argus</i>	<i>Coscinodiscus marginatus</i>	<i>Coscinodiscus radiatus</i>				
303-U1308A-19H-1, 115	B																																			
19H-4, 60	B																																			
19H-5, 30	B																																			
19H-CC	F	M		*					*																		T							*		
20H-CC	F	M			T																					T	*	T	T						T	
21H-CC	R	M			T								T	T												T	T	*								
22H-CC	C	M			T							T		T		T								T		T	*									
23H-CC	F	M			T			T	T					T							T	T		T		T	*	T						T	T	
24H-CC	T	M			T																															
25H-2, 40	B																																			
25H-CC	T	M			T																															
26H-CC	B																																			
28H-CC	F	M												*				*									*	T						*		
29H-3, 81	B																																			
29H-CC	B																																			
30H-CC	B																																			
31H-2, 80	B																																			
31H-CC	B																																			
32H-CC	B																																			
33H-CC	B																																			
34H-CC	B																																			
35H-CC	B																																			
36H-CC	B																																			

Notes: Abundance: A = abundant, C = common, F = few, R = rare, T = trace, B = barren. Preservation: G = good, M = moderate, P = poor. RS = resting spore. \* = fragment present.



Table T18 (continued).

Core, section, interval (cm)	Diatoms																																				
	Abundance	Preservation	<i>Cymbella</i> sp.	<i>Ethmodiscus</i> sp.	<i>Fragilariopsis doliolus</i>	<i>Fragilariopsis fossilis</i>	<i>Fragilariopsis jouseae</i>	<i>Fragilariopsis oceanica</i>	<i>Fragilariopsis reinholdii</i>	<i>Fragilariopsis</i> spp.	<i>Hemidiscus cuneiformis</i>	<i>Navicula</i> sp.	<i>Neodenticula seminiae</i>	<i>Nitzschia bicapitata</i>	<i>Nitzschia kolaczekii</i>	<i>Nitzschia interruptestrata</i>	<i>Nitzschia sicula</i>	<i>Nitzschia</i> spp.	<i>Opephora</i> sp.	<i>Paralia sulcata</i>	<i>Planktoniella sol</i>	<i>Porosira glacialis</i>	<i>Proboscia alata</i>	<i>Proboscia alata</i> f. <i>indica</i>	<i>Proboscia barboi</i>	<i>Proboscia curvirostris</i>	<i>Rhizosolenia bergonii</i>	<i>Rhizosolenia hebetata</i> f. <i>hiemalis</i>	<i>Rhizosolenia hebetata</i> f. <i>semispina</i>	<i>Rhizosolenia hebetata</i> f. <i>subacuta</i>	<i>Rhizosolenia praebergonii</i>	<i>Rhizosolenia styliformis</i>					
303-U1308A-																																					
19H-1, 115	B																																				
19H-4, 60	B																																				
19H-5, 30	B																																				
19H-CC	F	M				T		*		T						*																					
20H-CC	F	M		*		T		T		T			T																							T	
21H-CC	R	M						T		T			T													*?										T	
22H-CC	C	M						T		T																										T	
23H-CC	F	M		*				T		T									T																	T	
24H-CC	T	M								T																										T	
25H-2, 40	B																																				
25H-CC	T	M						T		T																										T	
26H-CC	B																																				
28H-CC	F	M				*	*?	*	*	*			*	*				*	*																		
29H-3, 81	B																																				
29H-CC	B																																				
30H-CC	B																																				
31H-2, 80	B																																				
31H-CC	B																																				
32H-CC	B																																				
33H-CC	B																																				
34H-CC	B																																				
35H-CC	B																																				
36H-CC	B																																				

Table T18 (continued).

Core, section, interval (cm)	Diatoms										Silicoflagellates																												
	Abundance	Preservation	<i>Rhizosolenia</i> spp.	<i>Roperia tessellata</i>	<i>Stellarima</i> sp.	<i>Stephanodiscus niagarae</i> (?)	<i>Stephanopyxis turris</i>	<i>Thalassionema bacillare</i>	<i>Thalassionema frauenfeldii</i>	<i>Thalassionema nitzschioides</i> var. <i>nitzschioides</i>	<i>Thalassionema nitzschioides</i> var. <i>inflata</i>	<i>Thalassionema nitzschioides</i> var. <i>parva</i>	<i>Thalassiosira bipora</i>	<i>Thalassiosira convexa</i> var. <i>convexa</i>	<i>Thalassiosira eccentrica</i>	<i>Thalassiosira ferelineata</i>	<i>Thalassiosira gravida</i>	<i>Thalassiosira gravida</i> spore	<i>Thalassiosira jacksonii</i>	<i>Thalassiosira jouseae</i>	<i>Thalassiosira leptopus</i>	<i>Thalassiosira lineata</i>	<i>Thalassiosira nordenskioldii</i>	<i>Thalassiosira oestrupii</i> var. <i>oestrupii</i>	<i>Thalassiosira oestrupii</i> var. <i>venrickae</i>	<i>Thalassiosira poroseriata</i>	<i>Thalassiosira sackettii</i> f. <i>plana</i>	<i>Thalassiosira trifulta</i>	<i>Thalassiosira</i> spp.	<i>Thalassiothrix</i> / <i>Lioloma</i> complex	<i>Bachmannocena elliptica elliptica</i>	<i>Dictyocha fibula</i>	<i>Distephanus speculum</i>	<i>Actiniscus pentasterias</i>					
303-U1308A-19H-1, 115	B																																						
19H-4, 60	B																																						
19H-5, 30	B																																						
19H-CC	F	M						T	T	T	T	*		*						T	T																		
20H-CC	F	M					T	T	T	T	T									T	T																		
21H-CC	R	M		*			T	T	T	T	T																												
22H-CC	C	M					T	T	T	T	T																												
23H-CC	F	M		*			T	T	T	T	T																												
24H-CC	T	M																																					
25H-2, 40	B																																						
25H-CC	T	M					T																																
26H-CC	B																																						
28H-CC	F	M	*				T		R		*										*	*		*			*		*										
29H-3, 81	B																																						
29H-CC	B																																						
30H-CC	B																																						
31H-2, 80	B																																						
31H-CC	B																																						
32H-CC	B																																						
33H-CC	B																																						
34H-CC	B																																						
35H-CC	B																																						
36H-CC	B																																						

Table T19. Distribution of diatoms and silicoflagellates, Hole U1308B. (Continued on next three pages.)

Core, section, interval (cm)	Diatoms																																			
	Abundance	Preservation	<i>Actinocyclus curvatulus</i>	<i>Actinocyclus ellipticus</i>	<i>Actinocyclus octonarius</i>	<i>Actinocyclus oculatus</i>	<i>Actinocyclus</i> spp.	<i>Actinoptychus vulgaris</i>	<i>Alveus marinus</i>	<i>Asteromphalus arachne</i>	<i>Asteromphalus flabellatus</i>	<i>Asteromphalus imbricatus</i>	<i>Azpeitia africana</i>	<i>Azpeitia barronii</i>	<i>Azpeitia neocrenulata</i>	<i>Azpeitia nodulifera</i>	<i>Azpeitia tabularis</i>	<i>Bacteriastrium</i> sp.	<i>Cavitatus jouseanus</i>	RS <i>Chaetoceros affinis</i>	RS <i>Chaetoceros cinctus</i>	RS <i>Chaetoceros compressus</i>	RS <i>Chaetoceros debilis</i>	RS <i>Chaetoceros diadema</i>	RS <i>Chaetoceros</i> spp.	<i>Chaetoceros setae</i>	<i>Cocconeis costata</i>	<i>Cocconeis</i> spp.	<i>Coscinodiscus asteromphalus</i>	<i>Coscinodiscus argus</i>	<i>Coscinodiscus marginatus</i>	<i>Coscinodiscus radiatus</i>				
303-U1308B-1H-CC	T	P																					T	T	T											
2H-CC	B																																			
3H-CC	B																																			
4H-CC	F	M	T					T							T			T		T	T			T	R	*		T								
5H-5, 30	F	M	T																			T				T	*									
5H-6, 60	B																																			
5H-6, 100	B																																			
5H-7, 60	A	M						T	T		T					T	T	T					T	T	T	*				T	T					
5H-CC	A	M	T					T	T		T				R		T	R					T	T	T	*				T	T	T				
6H-CC	F	M	T					T	T				T							T	T		T	T	T	*										
7H-7, 30	F	M	T					T	T																	T	*									
7H-7, 60	B																																			
7H-CC	C	M	T					T							T								T	R	T	T	*		*		T					
8H-CC	B																																			
9H-2, 85	B																																			
9H-5, 64	B																																			
9H-CC	B																																			
10H-CC	A	G						*	*										*							R										
11H-CC	F	M						T	*						T										T		*							T		
12H-2, 10	B																																			
12H-3, 65	C	M	R					T																												
12H-CC	R	P																																		
13H-3, 116	B																																			
13H-CC	B																																			
14H-3, 67	B																																			
14H-CC	C	G						*	*																											
15H-CC	T	P						T																												
16H-CC	B																																			
17H-2, 113	B																																			
17H-2, 113	B																																			
17H-CC	C	M	T						T	T									T					T										T	T	
18H-3, 95	A	G	R																																	
18H-4, 80	A	G	R																							T										
18H-5, 81	F	M	T																																	
18H-CC	C	M	T																																	
19H-2, 125	C	M	R																																	
19H-CC	F	M	T																																	
20H-CC	C	M	R																																	
20H-CC	C	M	R																																	
21H-CC	C	M	T	T	T																															
22H-CC	C	M	R																																	

Notes: Abundance: A = abundant, C = common, F = few, R = rare, T = trace, B = barren. Preservation: G = good, M = moderate, P = poor. RS = resting spore. \* = fragment present.



Table T19 (continued).

Core, section, interval (cm)	Diatoms																																			
	Abundance	Preservation	<i>Delphineis surirella</i>	<i>Ethmodiscus</i> sp.	<i>Fragilariopsis doliolus</i>	<i>Fragilariopsis fossilis</i>	<i>Fragilariopsis oceanica</i>	<i>Fragilariopsis pseudocylindrica</i>	<i>Fragilariopsis reinholdii</i>	<i>Grammatophora marina</i>	<i>Hemidiscus cuneiformis</i>	<i>Hemidiscus karstenii</i>	<i>Navicula</i> sp.	<i>Neodenticula seminiae</i>	<i>Nitzschia bicapitata</i>	<i>Nitzschia capuluspalae</i>	<i>Nitzschia kolaczekii</i>	<i>Nitzschia interruptestrata</i>	<i>Nitzschia sicula</i>	<i>Nitzschia</i> sp.	<i>Nitzschia</i> sp. aff. <i>sicula</i>	<i>Odontella aurita</i>	<i>Paralia sulcata</i>	<i>Planktoniella sol</i>	<i>Pleurosigma</i> sp.	<i>Porosira glacialis</i>	<i>Proboscia alata</i>	<i>Proboscia curvirostris</i>	<i>Rhizosolenia acuminata</i>	<i>Rhizosolenia bergonii</i>	<i>Rhizosolenia hebetata</i> f. <i>hiemalis</i>	<i>Rhizosolenia hebetata</i> f. <i>semispina</i>				
303-U1308B-																																				
1H-CC	T	P																T	*																	
2H-CC	B																																			
3H-CC	B																																			
4H-CC	F	M			T	T		*																												
5H-5, 30	F	M				T		R																												
5H-6, 60	B																																			
5H-6, 100	B																																			
5H-7, 60	A	M		*		R		T	T						T																					
5H-CC	A	M			T	F		T	T			*		T	T																					
6H-CC	F	M			T									T	T																					
7H-7, 30	F	M												T																						
7H-7, 60	B																																			
7H-CC	C	M			T	T		T	T					F		T																				
8H-CC	B																																			
9H-2, 85	B																																			
9H-5, 64	B																																			
9H-CC	B																																			
10H-CC	A	G			R	F		T	*						T																					
11H-CC	F	M			T	T		R	*								*																			
12H-2, 10	B																																			
12H-3, 65	C	M				T		R	T																											
12H-CC	R	P																																		
13H-3, 116	B																																			
13H-CC	B																																			
14H-3, 67	B																																			
14H-CC	C	G			*?	T																														
15H-CC	T	P				*		*																												
16H-CC	B																																			
17H-2, 113	B																																			
17H-2, 113	B																																			
17H-CC	C	M		*				T	T	T					T																					
18H-3, 95	A	G						R																												
18H-4, 80	A	G		*		T		F	R																											
18H-5, 81	F	M				T		R	T																											
18H-CC	C	M		*		T		T	T																											
19H-2, 125	C	M						T	T																											
19H-CC	F	M				T																														
20H-CC	C	M			T			T	T						T																					
21H-CC	C	M	T			T			T						T																					
22H-CC	C	M			T	T	T		T						T																					





Table T19 (continued).

Core, section, interval (cm)	Diatoms		Silicoflagellates				
	Abundance	Preservation	<i>Bacillmannocena elliptica elliptica</i>	<i>Dictyochoa fibula</i>	<i>Distephanus quinarius</i>	<i>Distephanus speculum</i>	<i>Actiniscus pentasterias</i>
303-U1308B-							
1H-CC	T	P					
2H-CC	B						
3H-CC	B						
4H-CC	F	M		T	T	T	
5H-5, 30	F	M		T			
5H-6, 60	B						
5H-6, 100	B						
5H-7, 60	A	M	T	T	T		
5H-CC	A	M		T	T	T	
6H-CC	F	M		T		T	
7H-7, 30	F	M			T		
7H-7, 60	B						
7H-CC	C	M		T	T		
8H-CC	B						
9H-2, 85	B						
9H-5, 64	B						
9H-CC	B						
10H-CC	A	G					
11H-CC	F	M					
12H-2, 10	B						
12H-3, 65	C	M		T			
12H-CC	R	P					
13H-3, 116	B						
13H-CC	B						
14H-3, 67	B						
14H-CC	C	G					
15H-CC	T	P					
16H-CC	B						
17H-2, 113	B						
17H-2, 113	B						
17H-CC	C	M		T	T	T	
18H-3, 95	A	G		T	T		
18H-4, 80	A	G		T	T	T	
18H-5, 81	F	M				T	
18H-CC	C	M		T	T		
19H-2, 125	C	M	*	T	T		
19H-CC	F	M		T	T	T	
20H-CC	C	M			T	R	T
21H-CC	C	M					
22H-CC	C	M					

Table T20. Distribution of diatoms and silicoflagellates, Hole U1308C. (This table is available in an [oversized format](#).)







Table T21 (continued).

Core, section, interval (cm)	Diatoms						Silicoflagellates												
	Abundance	Preservation	<i>Thalassionema nitzschioides</i> var. <i>nitzschioides</i>	<i>Thalassionema nitzschioides</i> var. <i>inflata</i>	<i>Thalassionema nitzschioides</i> var. <i>parva</i>	<i>Thalassiosira bipora</i>	<i>Thalassiosira eccentrica</i>	<i>Thalassiosira ferelineata</i>	<i>Thalassiosira gravida</i> spore	<i>Thalassiosira leptopus</i>	<i>Thalassiosira lineata</i>	<i>Thalassiosira oestrupii</i> var. <i>oestrupii</i>	<i>Thalassiosira oestrupii</i> var. <i>venrickae</i>	<i>Thalassiosira</i> spp.	<i>Thalassiothrix/Lioloma</i> complex	<i>Dictyocha fibula</i>	<i>Distephanus quinarius</i>	<i>Distephanus speculum</i>	<i>Actiniscus pentasterias</i>
303-U1308E-																			
1H-CC	C	M	T									T	T						
2H-CC	B																		
3H-CC	C	M	*	*	T	T				T	R								
4H-CC	B																		
5H-CC	A	M	*						T	*	T								
6H-CC	F	M	T						*		T		T	T					
7H-CC	B																		
8H-CC	B																		
9H-2, 35	B																		
9H-4, 15	B																		
9H-4, 130	R	M										T						T	
9H-5, 60	B																		
9H-CC	B																		
10H-CC	C	M			T							T	T		T	T			
11H-CC	B																		
12H-CC	B																		
13H-CC	R	M	T	T	T				T		T	T						T	
14H-CC	B																		
15H-CC	B																		
16H-CC	F	M	R					T			T		T	T	T	T			
17H-CC	C	M	T									T		T	R				
18H-4, 64	B																		
18H-CC	R	P	T											T	*				
19H-1, 108	B																		
19H-CC	C	M	F									T			R				
20H-CC	C	G	R	T					T	T	T		T	T					
21H-CC	F	G	T	T								T						T	













Table T23 (continued).

Core, section	Abundance	Preservation	<i>Lampromitra</i> sp.	<i>Lipmanella</i> spp.	<i>Peridium</i> spp.	<i>Pseudodictyophimus</i> spp.	Other plagioteuthids	<i>Bathropyraxis</i> spp.	<i>Cornutella</i> spp.	<i>Cycladophora davisiana davisiana</i>	<i>Cycladophora bicornis</i>	<i>Dictyophimus</i> spp.	<i>Eucecryphalus</i> spp.	<i>Eucyrtidium acuminatum</i>	<i>Eucyrtidium calvertense?</i>	<i>Eucyrtidium hexastichum</i>	<i>Eucyrtidium teucheri</i>	<i>Lithocampe punctatum</i>	<i>Litharachnium</i> spp.	<i>Pterocanium</i> spp.	Other theopeerids	<i>Carpocanistrum</i> spp.	<i>Anthocyrtidium</i> spp.	<i>Lamprocyclas maritima</i>	<i>Lamprocyrtis (?) hannai</i>	<i>Pterocorys zancleus</i>	<i>Theocorythium trachelium</i>	<i>Botryostrobus acquilonariss</i>	<i>Botryostrobus auritus/australis</i>	<i>Phormostichoartus cf. corbula</i>	<i>Siphocampe</i> spp.	<i>Stichocorys seriata</i>	<i>Spirocyrts</i> spp.	Radiolarian zone						
303-U1308C-																																								
1H-CC	B																																							
2H-CC	B																																							
3H-CC	B																																							
4H-CC	F	M								R														T									T			<i>C. d. davisiana</i>				
5H-CC	B																																				?			
6H-CC	T	P																																						
7H-CC	B																																							
8H-CC	B																																							
9H-CC	A	P								T					R					R			T					A	R								<i>C. d. davisiana</i>			
10H-CC	B																																							
11H-CC	B																																							
12H-CC	T	P																																						
13H-CC	T	M																																						
14H-CC	A	G	T			T		T	F	T	T	T	R	R	R	T	R	T	T	R	R	T	F	T	F	R		T			T	R					<i>C. d. davisiana</i>			
15H-CC	A	G	R	T		R		T	F	T	T	T	T	F	T	T	T	T	T	F	R	T	R	R	T	R	F	R	T											
16H-CC	R	M																																						
17H-CC	T	P																																						
18H-CC	A	M			T	T	R	T	F	T		T	R	R									R	T		F		T		R			T				<i>C. d. davisiana</i>			
19H-CC	C	P					T	R	T																		T		T											
20H-CC	C	P					R	T																			F		T		R	T					<i>S. ?tetras</i>			
21H-CC	A	M	T				F		T			R	T	T	R								R			R						R								
22H-CC	A	M	F	T		T	T	T	T	T	T	T	R	R	F	R							R			F		T				T	T							
23H-CC	A	P	T				T	T	T	T	T	T		F	T									T	T	T	R		T											
24H-CC	C	A	R	T		F	F	T	T	T	T	T	T	R	T	T	T						T	T	T	R		T												
25H-CC	A	M	R	T		F	F	T		T		R	R	T	T	R								R	R	T	F		T											
26H-CC	A	P																																						
27H-CC	A	M			T	T	T	R	T			T			R												R		T											
28H-CC	B																																							
29H-CC	T	P																																						
30H-CC	T	P																																						

Table T24. Distribution of palynomorphs, Hole U1308A. (Continued on next page.)

Core, section	Marine			Terrestrial			Reworked			Dinocyst assemblages																							
	Preservation	Dinocysts*	Foraminifer organic linings Tasmanites	Pollen	Spores of Pteridophytes	Spores of Sphagnum	Acritarchs	Dinocysts	Bisaccate pollen	Trilete spores	<i>Brigantedinium</i> spp.	<i>Brigantedinium simplex</i>	<i>Islandinium minutum</i>	<i>Echinidinium aculeatum</i>	<i>Lejeunecysta sabrina</i>	<i>Selenopemphix nephroides</i>	<i>Impagidinium aculeatum</i>	<i>Impagidinium cf. paradoxum</i>	<i>Impagidinium patulum</i>	<i>Impagidinium sphaericum</i>	<i>Impagidinium striolatum</i>	<i>Impagidinium pallidum</i>	<i>Impagidinium cf. japonicum</i>	<i>Impagidinium velorum</i>	<i>Impagidinium</i> spp.	<i>Bitectatodinium tepikeense</i>	<i>Operculodinium centrocarpum</i>	<i>Operculodinium centrocarpum</i> (short process form)	<i>Operculodinium janduchenei</i>	<i>Nematosphaeropsis labyrinthus</i>			
303-U1308A-																																	
1H-CC	G	x																															
2H-CC	G	XX									r																						
3H-CC	G	XX		r																													
4H-CC	G	x		x			r	x	x	x	P																						
5H-CC	G	XX		x			r			x	x																						
6H-CC	G	XXX		x																													
7H-CC	G	XXX	x	x						x	x	x	r																				
8H-CC	G	XXX		x	r	r																											
9H-CC	G	XXX		x		x																											
10H-CC	G	XX	x	r	XX	x																											
11H-CC	M	x		r																													
12H-CC	G	XX		x																													
13H-CC	G	XX		r																													
14H-CC	M	XX	x	x	r																												
15H-CC	G	XX		x																													
16H-CC	M	x		r																													
17H-CC	M	x																															
18H-CC	M	XX		r																													
19H-CC	G	x		r		r																											
20H-CC	G	x	r	r	r																												
21H-CC	M	XX	r	r	x																												
22H-CC	G	XX		x																													
23H-CC	G	x		r		r																											
24H-CC	G	x		r																													
25H-CC	G	x	r	x																													
26H-CC	M	x																															
28H-CC	M	x																															
29H-CC	M	XX		r																													
30H-CC	M	x																															
31H-CC	M	x																															
32H-CC	M	x																															
33H-CC	M	XX																															
34H-CC	M	x		r																													
35H-CC	M	x																															
36H-CC	M	x																															

Notes: \* = *Cymatiosphaera* and incertae sedis sp. 1 included. Absolute abundances: XXX = abundant, XX = common, x = few, r = rare. Relative abundance of dinocyst taxa: XXX = dominant, XX = common, x = few, r = rare, P = presence, o = single occurrence.





Table T24 (continued).

Core, section	Dinocyst assemblages																																					
	<i>Pyxidinospis reticulata</i>	<i>Polysphaeridium zoharyi</i>	<i>Lingulodinium machaerophorum</i>	<i>Ataxodinium choanum</i>	<i>Achomosphaera</i> spp.	<i>Achomosphaera andalousiense</i>	<i>Spiniferites</i> cf. <i>bentorii</i>	<i>Spiniferites delicatus</i>	<i>Spiniferites elongatus</i>	<i>Spiniferites membranaceus</i>	<i>Spiniferites mirabilis-hyperhacanthus</i>	<i>Spiniferites ramosus</i>	<i>Spiniferites</i> spp.	<i>Corrudinium?</i> <i>labradori</i>	cf. <i>Filsphaera filifera</i>	<i>Operculodinium</i> cf. <i>crassum</i>	cf. <i>Batiacasphaera</i> sp.	<i>Ataxiodinium zevenboomii</i>	cf. <i>Pyxidinospis braboi</i>	<i>Nematosphaeropsis</i> sp. 1 de Vernal and Mudie, 1989	<i>Operculodinium eirikianum</i>	<i>Invertocysta lacrymosa</i>	<i>Tectatodinium pellitum</i>	<i>Ataxodinium confusum</i>	<i>Corrudinium devernaliae</i>	<i>Muraticysta microornata</i>	<i>Habibacysta tectata</i>	<i>Batiacasphaera sphaerica</i>	<i>Operculodinium</i> cf. <i>tegillatum</i>	<i>Pyxidinospis vesiculata</i>	<i>Cymatosphaera?</i> <i>invaginata</i>	<i>Incertae sedis</i> sp. 1 de Vernal and Mudie, 1989						
303-U1308A-																																						
1H-CC	o	?																																				
2H-CC	r		x			r																																
3H-CC		?																																				
4H-CC		?			o																																	
5H-CC		?						x		r																												
6H-CC					r					x		x	x	x																								
7H-CC								x	x	r																												
8H-CC					r		x	x								x																						
9H-CC										XXX						r																						
10H-CC						r				XXX						x	r																					
11H-CC										P						o																						
12H-CC					r			r	r							x																						
13H-CC						r				r	r					x	r																		x			
14H-CC										r						x																			r			
15H-CC					r											r																			XXX	r		
16H-CC										P																									o			
17H-CC																o	P																		o			
18H-CC																		P																		o		
19H-CC					o					P							P																			o		
20H-CC										o																										P	o	
21H-CC																x																				x		
22H-CC						r										x																				XX		
23H-CC										o	o	P																								P	P	
24H-CC										o						o	o										P	P								P	P	
25H-CC																o																				P	P	
26H-CC																																						
28H-CC																																						
29H-CC																																					P	P
30H-CC																																					P	P
31H-CC																																						
32H-CC																																						
33H-CC																																					P	P
34H-CC																																						
35H-CC																																						
36H-CC																																						





**Table T25.** Distribution of palynomorphs, Hole U1308B. (Continued on next page.)

Core, section	Marine			Terrestrial			Reworked			Dinocyst assemblages																																						
	Preservation	Dinocysts*	Foraminifer organic linings Tasmanites	Pollen	Spores of Pteridophytes	Spores of <i>Sphagnum</i>	Acritarchs	Dinocysts	Bisaccate pollen	Trilete spores	<i>Brigantedinium</i> spp.	<i>Brigantedinium simplex</i>	<i>Impagidinium aculeatum</i>	<i>Impagidinium cf. paradoxum</i>	<i>Impagidinium patulum</i>	<i>Impagidinium sphaericum</i>	<i>Impagidinium striatum</i>	<i>Impagidinium pallidum</i>	<i>Impagidinium cf. japonicum</i>	<i>Impagidinium velorum</i>	<i>Impagidinium</i> spp.	<i>Bitectatodinium tepikeiense</i>	<i>Bitectatodinium spongium</i>	<i>Operculodinium centrocarpum</i>	<i>Operculodinium centrocarpum</i> (short process form)	<i>Operculodinium janduchenei</i>	<i>Nematosphaeropsis labyrinthus</i>	<i>Pyxidimopsis reticulata</i>	<i>Polysphaeridium zoharyi</i>	<i>Lingulodinium machaerophorum</i>	<i>Achomosphaera</i> spp.	<i>Achomosphaera andalusiense</i>	<i>Spiniferites belerius</i>	<i>Spiniferites cf. bentorii</i>	<i>Spiniferites delicatus</i>	<i>Spiniferites elongatus</i>	<i>Spiniferites membranaceus</i>	<i>Spiniferites mirabilis-hyperhacanthus</i>	<i>Spiniferites</i> spp.	<i>Cornulinium? labradori</i>								
303-U1308B-																																																
1H-CC	G	x		r			r	x	x																																							
2H-CC	G	x		x																																												
3H-CC	G	XX																																														
4H-CC	G	XXX	x																																													
5H-CC	G	XXX		r	r	r																																										
6H-CC	G	XX		x																																												
7H-CC	G	XXX		r																																												
8H-CC	G	XX		XX			XX	x	r		x	XX	x	XX							XX	x	XX																									
9H-CC	G	XX		x			r	r				XXX	r	XXX							r	r	r	r	XX																							
10H-CC	G	XX		x								XXX	x	x							r	r	XX	r																								
11H-CC	M	XX		x		r						XX	x	r							x	x	x																									
12H-CC	M	x										P																																				
13H-CC	G	XX		x		r						XXX	x																																			
14H-CC	M	XX		x								x	x	x																																		
15H-CC	M	x		r								P	P																																			
16H-CC	M	XX		r								r	x	r																																		
17H-CC	M	x		x																																												
18H-CC	M	XX		x								x	r																																			
19H-CC	M	XX		x								XX	r																																			
21H-CC	M	XX		r								XX	r																																			

Notes: \* = *Cymatiosphaera* and incertae sedis sp. 1 included. Absolute abundances: XXX = abundant, XX = common, x = few, r = rare. Relative abundance of dinocyst taxa: XXX = dominant, XX = common, x = few, r = rare, P = presence, o = single occurrence.



Table T25 (continued).

Core, section	Dinocyst assemblages											
	<i>cf. Filisphaera filifera</i>	<i>Operculodinium cf. crassum</i>	<i>cf. Batiacasphaera</i> sp.	<i>Ataxiodinium zevenboomii</i>	<i>Nematosphaeropsis</i> sp. 1 de Vernal and Mudie, 1989	<i>Invertocysta lacrymosa</i>	<i>Muraticysta microomata</i>	<i>Habibacysta tectata</i>	<i>Operculodinium cf. tegillatum</i>	<i>Pyxidinoopsis vesiculata</i>	<i>Cymatiosphaera? invaginata</i>	<i>Incertae sedis</i> sp. 1 de Vernal and Mudie, 1989
303-U1308B-												
1H-CC												
2H-CC												
3H-CC	r											
4H-CC												
5H-CC												
6H-CC												
7H-CC												
8H-CC	r	x										
9H-CC		r										
10H-CC												
11H-CC	r											
12H-CC												
13H-CC	r			r								r
14H-CC	r							?				
15H-CC												
16H-CC	r	x										r
17H-CC	o	o						o				
18H-CC		r						x				r
19H-CC		r			x							r
21H-CC						?			r	r	r	r



Table T26 Polarity zonation, Holes U1308A, U1308B, U1308C, U1308E, and U1308F.

Polarity chron interpretation	Age (Ma)	Interval	Hole U1308A			Hole U1308B			Hole U1308C			Hole U1308E			Hole U1308F		
			Core, section, interval (cm)	Depth (mbsf)	Depth (mcd)	Core, section, interval (cm)	Depth (mbsf)	Depth (mcd)	Core, section, interval (cm)	Depth (mbsf)	Depth (mcd)	Core, section, interval (cm)	Depth (mbsf)	Depth (mcd)	Core, section, interval (cm)	Depth (mbsf)	Depth (mcd)
			303-U1308A-			303-U1308B-			303-U1308C-			303-U1308E			303-U1308F-		
C1n (b) Matuyama/ Brunhes	0.78	Upper	5H-5, 95	44.03	48.82	6H-3, 45	45.45	49.56	6H-1, 40	42.8	49.45	5H-4, 65	43.15	49.59	5H-4, 85	43.35	49.61
		Lower	5H-7, 15	45.46	50.30	6H-3, 90	45.9	50.01	6H-1, 115	43.55	50.20	5H-4, 85	43.35	49.79	5H-4, 110	43.6	49.86
C1r.1n (t) Jaramillo	0.99	Upper	7H-1, 130	57.40	65.31	7H-5, 60	58.1	65.35	7H-6, 55	57.92	65.25						
		Lower	7H-2, 115	58.75	66.66	7H-5, 135	58.85	66.1	7H-7, 55	59.42	66.75						
C1r.1n (b) Jaramillo	1.07	Upper				8H-3, 105	65.05	71.86	8H-1, 105	62.45	71.69	7H-3, 20	63.20	72.04	7H-5, 15	63.15	71.88
		Lower				8H-4, 30	65.8	72.61	8H-2, 25	63.15	72.39	7H-3, 50	63.50	72.34	7H-5, 65	63.65	72.38
(t) Cobb Mountain	1.19	Upper				9H-3, 110	74.6	83.36	9H-2, 85	73.25	83.39	8H-3, 110	73.60	83.41	8H-6, 20	74.20	84.40
		Lower				9H-4, 45	75.45	84.21	9H-3, 30	74.2	84.34	8H-4, 25	74.25	84.06	8H-6, 115	75.15	85.35
(b) Cobb Mountain	1.215	Upper				9H-4, 115	76.15	84.91	9H-3, 115	75.05	85.19	8H-4, 85	74.85	84.66			
		Lower				9H-4, 145	76.45	85.21	9H-4, 15	75.55	85.69	8H-4, 120	75.20	85.01			
C2n (t) Olduvai	1.77	Upper										13H-2, 30	117.80	132.93	13H-4, 50	118.03	133.27
		Lower										13H-2, 130	118.80	133.93	13H-4, 140	118.93	134.17
C2n (b) Olduvai	1.95	Upper				15H-3, 5	130.55	146.71	15H-2, 140	130.8	146.74	14H-3, 110	129.48	146.51	14H-5, 125	129.75	146.16
		Lower				15H-3, 75	131.25	147.41	15H-3, 60	131.5	147.44	14H-4, 30	130.18	147.21	14H-7, 10	131.6	148.01
C2r.1n (t) Reunion	2.115	Upper	16H-3, 20	144.8	160.7	16H-3, 125	141.25	160.75	16H-4, 85	142.75	160.15				16H-1, 90	142.4	160.55
		Lower	16H-3, 90	145.50	161.40	16H-4, 45	141.94	161.44	16H-4, 145	143.55	160.75				16H-2, 15	143.15	161.30
C2r.1n (b) Reunion	2.153	Upper	16H-4, 95	147.05	162.95	16H-4, 145	142.94	162.44	16H-5, 85	144.25	161.65	16H-1, 50	143.85	162.48	16H-2, 130	144.3	162.45
		Lower	16H-5, 20	147.8	163.7	16H-5, 50	143.49	162.99	16H-5, 115	144.55	161.95	16H-1, 80	144.30	162.78	16H-3, 15	144.65	162.80
C2An.1n (t) Gauss/ Matuyama	2.581	Upper						19H-6, 25	173.65	193.42				19H-2, 105	172.55	194.24	
		Lower						19H-7, 35	177.60	198.18				19H-5, 70	176.70	198.39	
C2An.1n (b)	3.04	Upper						23H-6, 10	211.5	234.79				23H-3, 115	212.15	234.34	
		Lower						23H-7, 45	212.85	236.14				23H-4, 130	213.8	235.99	
C2An.2n (t)	3.11	Upper						24H-4, 50	218.4	242.51				24H-1, 75	218.25	243.68	
		Lower						24H-5, 15	219.55	243.66				24H-2, 85	219.85	245.28	
C2An.2n (b)	3.22	Upper						25H-6, 5	230.45	254.56							
		Lower						25H-6, 95	231.35	255.46							
C2An.3n (t)	3.33	Upper						26H-5, 40	238.8	262.91							
		Lower						26H-5, 100	240.3	264.41							

Note: (b) = bottom, (t) = top.

Table T27. Age interpretation, Site U1308.

Polarity chron interpretation	Age (Ma)	Depth	
		(mcd)	± (m)
C1n (b) Matuyama/Brunhes	0.78	49.8	0.4
C1r.1n (t) Jaramillo	0.99	65.7	0.4
C1r.1n (b) Jaramillo	1.07	72.0	0.7
Cobb Mountain	1.20	84.5	±1.0
C2n (t) Olduvai	1.77	133.5	0.7
C2n (b) Olduvai	1.95	147	1.0
C2r.1n Reunion	2.113	161.2	±1.2
C2An.1n (t) Gauss/Matuyama	2.581	196	2.5
C2An.1n (b)	3.04	235.5	1.1
C2An.2n (t)	3.11	243.5	1.5
C2An.2n (b)	3.22	255	0.5
C2An.3n (t)	3.33	263.7	0.7

Table T28. Shipboard composite and corrected composite depths, Holes U1308A, U1308B, U1308C, U1308D, U1308E, and U1308F. (Continued on next page.)

Core	Top depth (mbsf)	Offset (m)	Top depth		Core	Top depth (mbsf)	Offset (m)	Top depth	
			(mcd)	(cmcd)				(mcd)	(cmcd)
303-U1308A-					9H	70.5	8.76	79.26	74.07
1H	0.0	0.46	0.46	0.43	10H	80.0	10.56	90.56	84.64
2H	8.6	0.98	9.58	8.95	11H	89.5	11.84	101.34	94.71
3H	18.1	1.42	19.52	18.24	12H	99.0	12.59	111.59	104.29
4H	27.6	3.94	31.54	29.48	13H	108.5	14.77	123.27	115.21
5H	37.1	4.84	41.94	39.20	14H	118.0	15.27	133.27	124.55
6H	46.6	6.09	52.69	49.24	15H	127.5	16.16	143.66	134.26
7H	56.1	7.91	64.01	59.82	16H	137.0	19.50	156.50	146.26
8H	65.6	7.68	73.28	68.49	17H	146.5	19.93	166.43	155.54
9H	75.1	9.06	84.16	78.65	18H	156.0	20.91	176.91	165.34
10H	84.6	9.22	93.82	87.68	19H	165.5	22.24	187.74	175.46
11H	94.1	8.39	102.49	95.79	21H	184.5	22.24	206.74	193.21
12H	103.6	9.91	113.51	106.08	22H	194.0	22.24	216.24	202.09
13H	113.1	11.08	124.18	116.06	303-U1308C-				
14H	122.6	12.40	135.00	126.17	1H	0.0	0.00	0.00	0.00
15H	132.1	13.46	145.56	136.04	2H	4.4	1.89	6.29	5.88
16H	141.6	15.90	157.50	147.20	3H	13.9	3.70	17.60	16.45
17H	151.1	17.42	168.52	157.50	4H	23.4	5.93	29.33	27.41
18H	160.6	17.42	178.02	166.37	5H	32.9	4.68	37.58	35.12
19H	170.1	13.63	183.73	171.71	6H	42.4	6.65	49.05	45.84
20H	179.6	13.63	193.23	180.59	7H	51.9	7.33	59.23	55.36
21H	189.1	15.15	204.25	190.89	8H	61.4	9.24	70.64	66.02
22H	198.6	14.65	213.25	199.30	9H	70.9	10.14	81.04	75.74
23H	208.1	15.17	223.27	208.66	10H	80.4	10.21	90.61	84.68
24H	217.6	15.17	232.77	217.54	11H	89.9	11.69	101.59	94.94
25H	227.1	15.17	242.27	226.42	12H	99.4	12.79	112.19	104.85
26H	236.6	15.17	251.77	235.30	13H	108.9	14.41	123.31	115.24
28H	255.6	15.17	270.77	253.06	14H	118.4	15.16	133.56	124.82
29H	265.1	15.17	280.27	261.93	15H	127.9	15.94	143.84	134.43
30H	274.6	15.17	289.77	270.81	16H	137.4	17.40	154.80	144.67
31H	284.1	15.17	299.27	279.69	17H	146.9	16.53	163.43	152.74
32H	293.6	15.17	308.77	288.57	18H	156.4	18.27	174.67	163.24
33H	303.1	15.17	318.27	297.45	19H	165.9	19.77	185.67	173.52
34H	312.6	15.17	327.77	306.33	20H	175.4	20.58	195.98	183.16
35H	322.1	15.17	337.27	315.21	21H	184.9	21.86	206.76	193.23
36H	331.6	15.17	346.77	324.08	22H	194.4	22.87	217.27	203.06
303-U1308B-					23H	203.9	23.29	227.19	212.33
1H	0.0	0.35	0.35	0.33	24H	213.4	24.11	237.51	221.97
2H	4.0	1.20	5.20	4.86	25H	222.9	24.11	247.01	230.85
3H	13.5	1.66	15.16	14.17	26H	232.4	24.11	256.51	239.73
4H	23.0	3.16	26.16	24.45	27H	241.9	24.11	266.01	248.61
5H	32.5	4.59	37.09	34.66	28H	251.4	24.11	275.51	257.49
6H	42.0	4.11	46.11	43.09	29H	260.9	24.11	285.01	266.36
7H	51.5	7.25	58.75	54.91	30H	270.4	24.11	294.51	275.24
8H	61.0	6.81	67.81	63.37					

Table T28 (continued).

Core	Top depth (mbsf)	Offset (m)	Top depth	
			(mcd)	(cmcd)
303-U1308D-				
1H	0.0	1.07	1.07	1.00
303-U1308E-				
1H	0.0	1.32	1.32	1.23
2H	9.5	2.18	11.68	10.92
3H	19.0	4.64	23.64	22.09
4H	28.5	5.60	34.10	31.87
5H	38.0	6.44	44.44	41.53
6H	47.5	7.11	54.61	51.04
7H	60.0	8.84	68.84	64.34
8H	69.5	9.81	79.31	74.12
9H	79.0	5.47	84.47	78.94
10H	84.0	9.63	93.63	87.50
11H	97.0	10.34	107.34	100.32
12H	106.5	13.07	119.57	111.75
13H	116.0	15.13	131.13	122.55
14H	125.5	17.03	142.53	133.21
15H	134.0	18.48	152.48	142.50
16H	143.5	18.48	161.98	151.38
17H	153.0	19.36	172.36	161.08
18H	162.5	20.62	183.12	171.14
19H	172.0	19.08	191.08	178.58
20H	181.5	19.44	200.94	187.79
21H	191.0	19.92	210.92	197.12
303-U1308F-				
1H	0.0	4.84	4.84	4.52
2H	9.5	3.68	13.18	12.32
3H	19.0	4.04	23.04	21.53
4H	28.5	4.32	32.82	30.67
5H	38.0	6.26	44.26	41.36
6H	47.5	6.44	53.94	50.41
7H	57.0	8.73	65.73	61.43
8H	66.5	10.20	76.70	71.68
9H	76.0	11.70	87.70	81.96
10H	85.5	13.10	98.60	92.15
11H	94.0	14.91	108.91	101.79
12H	103.5	14.51	118.01	110.29
13H	113.0	15.24	128.24	119.85
14H	122.5	16.41	138.91	129.82
15H	132.0	17.34	149.34	139.57
16H	141.5	18.15	159.65	149.21
17H	151.0	19.83	170.83	159.65
18H	160.5	22.02	182.52	170.58
19H	170.0	21.69	191.69	179.15
20H	179.5	21.49	200.99	187.84
21H	189.0	22.31	211.31	197.49
22H	198.5	22.94	221.44	206.95
23H	208.0	22.19	230.19	215.13
24H	217.5	25.43	242.93	227.04

Table T29. Sampling splice tie points, Site U1308.

Hole, core, section, interval (cm)	Depth			Hole, core, section, interval (cm)	Depth	
	(mbsf)	(mcd)			(mbsf)	(mcd)
1308C-1H-2, 149.8	3.00	3.00	Tie to	1308E-1H-2, 17.7	1.68	3.00
1308E-1H-6, 33.9	7.84	9.16	Tie to	1308B-2H-3, 95.8	7.96	9.16
1308B-2H-6, 72.0	12.22	13.42	Tie to	1308E-2H-2, 21.2	11.24	13.42
1308E-2H-6, 142.5	18.42	20.60	Tie to	1308C-3H-2, 150.5	16.90	20.60
1308C-3H-7, 10.8	22.16	25.86	Tie to	1308E-3H-2, 71.8	21.22	25.86
1308E-3H-4, 89.9	24.40	29.04	Tie to	1308B-4H-2, 135.0	25.88	29.04
1308B-4H-6, 21.6	30.72	33.88	Tie to	1308A-4H-2, 83.9	29.94	33.88
1308A-4H-5, 141.6	35.02	38.95	Tie to	1308C-5H-1, 136.4	34.27	38.95
1308C-5H-5, 69.1	39.59	44.27	Tie to	1308A-5H-2, 83.0	39.43	44.27
1308A-5H-6, 75.6	45.34	50.18	Tie to	1308C-6H-1, 113.0	43.53	50.18
1308C-6H-5, 134.3	49.71	56.36	Tie to	1308F-6H-2, 149.0	49.92	56.36
1308F-6H-6, 123.8	55.67	62.11	Tie to	1308B-7H-3, 33.3	54.86	62.11
1308B-7H-6, 67.8	59.68	66.93	Tie to	1308A-7H-2, 142.4	59.02	66.93
1308A-7H-3, 142.1	60.52	68.43	Tie to	1308F-7H-2, 119.6	59.70	68.43
1308F-7H-5, 136.6	64.37	73.10	Tie to	1308C-8H-2, 93.2	63.86	73.10
1308C-8H-5, 65.4	68.05	77.29	Tie to	1308A-8H-3, 100.7	69.61	77.29
1308A-8H-6, 74.0	73.84	81.52	Tie to	1308B-9H-2, 75.5	72.76	81.52
1308B-9H-5, 76.8	77.27	86.03	Tie to	1308E-9H-2, 3.9	80.56	86.03
1308E-9H-5, 28.5	85.29	90.75	Tie to	1308F-9H-3, 5.1	79.05	90.75
1308F-9H-6, 119.1	84.69	96.39	Tie to	1308A-10H-2, 107.0	87.17	96.39
1308A-10H-6, 98.7	93.09	102.30	Tie to	1308B-11H-1, 96.0	90.46	102.30
1308B-11H-6, 78.7	97.79	109.63	Tie to	1308F-11H-1, 72.0	94.72	109.63
1308F-11H-6, 64.4	102.14	117.06	Tie to	1308A-12H-3, 54.1	107.14	117.06
1308A-12H-6, 59.3	111.69	121.61	Tie to	1308E-12H-2, 51.7	108.54	121.61
1308E-12H-6, 2.7	114.03	127.10	Tie to	1308C-13H-3, 79.2	112.69	127.10
1308C-13H-6, 61.2	117.01	131.42	Tie to	1308F-13H-3, 14.1	116.18	131.42
1308F-13H-6, 73.8	121.27	136.51	Tie to	1308B-14H-3, 23.5	121.24	136.51
1308B-14H-5, 117.8	125.20	140.47	Tie to	1308F-14H-2, 5.6	124.06	140.47
1308F-14H-7, 7.3	131.57	147.98	Tie to	1308C-15H-3, 111.8	132.04	147.98
1308C-15H-6, 45.6	135.86	151.80	Tie to	1308F-15H-2, 95.4	134.46	151.80
1308F-15H-7, 35.6	141.36	158.70	Tie to	1308B-16H-2, 69.1	139.20	158.70
1308B-16H-6, 20.4	144.69	164.19	Tie to	1308F-16H-4, 3.7	146.04	164.19
1308F-16H-6, 53.6	149.54	167.69	Tie to	1308B-17H-1, 126.0	147.76	167.69
1308B-17H-5, 136.2	153.86	173.79	Tie to	1308E-17H-2, 12.9	154.43	173.79
1308E-17H-6, 5.9	160.36	179.72	Tie to	1308B-18H-2, 130.8	158.81	179.72
1308B-18H-7, 9.1	165.09	186.00	Tie to	1308F-18H-3, 47.5	163.98	186.00
1308F-18H-5, 35.2	166.85	188.87	Tie to	1308A-19H-4, 64.2	175.24	188.87
1308A-19H-6, 141.5	179.01	192.65	Tie to	1308F-19H-1, 96.0	170.96	192.65
1308F-19H-5, 129.7	177.30	198.98	Tie to	1308C-20H-2, 150.1	178.40	198.98
1308C-20H-6, 36.6	183.30	203.88	Tie to	1308F-20H-2, 135.6	182.39	203.88
1308F-20H-6, 111.8	188.12	209.61	Tie to	1308C-21H-2, 133.0	187.75	209.61
1308C-21H-5, 130.1	192.20	214.06	Tie to	1308E-21H-3, 12.6	194.14	214.06
1308E-21H-6, 100.2	199.50	219.42	Tie to	1308C-22H-2, 65.2	196.55	219.42
1308C-22H-6, 35.2	202.27	225.14	Tie to	1308F-22H-3, 69.2	202.20	225.14
1308F-22H-5, 119.4	205.69	228.63	Tie to	1308C-23H-1, 141.6	205.34	228.63
1308C-23H-6, 12.7	211.53	234.82	Tie to	1308F-23H-4, 11.8	212.63	234.82
1308F-23H-6, 114.8	216.65	238.84	Tie to	1308C-24H-1, 130.0	214.73	238.84
1308C-24H-7, 62.7	223.03	247.14				

Table T30. Depth ranges and sedimentation rates, Site U1308.

Depth interval (mcd)	Sedimentation rate (cm/k.y.)
0–49.8	6.4
49.8–65.7	7.6
65.7–72.0	7.9
72.0–84.5	9.6
84.5–133.5	8.6
133.5–147.0	7.5
147.0–161.2	7.9
161.2–196.0	7.7
196.0–235.5	8.6
235.5–243.5	11.4
243.5–255.0	10.5
255.0–263.7	7.9

Table T31. Headspace hydrocarbon gases, Hole U1308A.

Core, section, interval (cm)	Depth		C <sub>1</sub> (ppmv)	C <sub>2</sub> (ppmv)
	(mbsf)	(mcd)		
303-U1308A-				
1H-2, 0–5	1.50	1.50	1.9	0
2H-2, 0–5	10.10	11.08	2.2	0
3H-2, 0–5	19.60	21.02	2.8	0
4H-2, 0–5	29.10	33.04	2.9	0
5H-2, 0–5	38.60	43.44	3.5	0
6H-2, 0–5	48.10	54.19	3.7	0
7H-2, 0–5	57.60	65.51	3.3	0
8H-2, 0–5	67.10	74.78	3.7	0
9H-2, 0–5	76.60	85.66	3.4	0
10H-2, 0–5	86.10	95.32	4.0	0
11H-2, 0–5	95.60	103.99	3.9	0
12H-2, 0–5	105.10	115.01	3.8	0
13H-2, 0–5	114.60	125.68	3.6	0
14H-2, 0–5	124.10	136.50	4.0	0
15H-2, 0–5	133.60	147.06	3.4	0
16H-2, 0–5	143.10	159.00	2.7	0
17H-2, 0–5	152.60	170.02	3.2	0
18H-3, 0–5	163.60	181.02	2.5	0
19H-2, 0–5	171.60	185.23	2.7	0
20H-2, 0–5	180.94	194.57	2.1	0
21H-3, 0–5	192.10	207.25	2.4	0
22H-2, 0–5	200.10	214.75	2.2	0
23H-2, 0–5	209.60	224.77	2.1	0
24H-2, 0–5	219.10	234.27	2.2	0
25H-2, 0–5	228.60	243.77	2.1	0
26H-2, 0–5	238.10	253.27	2.0	0
28H-2, 0–5	257.10	272.27	2.5	0
29H-2, 0–5	266.60	281.77	2.2	0
30H-2, 0–5	276.10	291.27	2.3	0
31H-2, 0–5	285.60	300.77	2.0	0
32H-2, 0–5	295.10	310.27	2.0	0
33H-2, 0–5	304.60	319.77	2.0	0
34H-2, 0–5	314.10	329.27	2.1	0
35H-2, 0–5	323.60	338.77	2.1	0
36H-2, 0–5	333.10	348.27	2.3	0



Table T32. Bulk sedimentary carbon and nitrogen, Hole U1308A.

Core, section, interval (cm)	Depth		Carbon (wt%)				Nitrogen (wt%)	Organic C/N
	(mbsf)	(mcd)	Inorganic	CaCO <sub>3</sub>	Total	Organic		
303-U1308A-								
1H-1, 138-139	1.38	1.38	2.81	23.41	2.79	0.00	0.06	—
1H-6, 3-4	7.53	7.53	9.94	82.80	10.38	0.44	0.02	22.0
2H-1, 138-139	9.98	10.96	7.37	61.39	7.78	0.41	0.03	16.0
2H-6, 3-4	16.13	17.11	9.22	76.80	9.62	0.40	0.02	18.0
3H-1, 138-139	19.48	20.90	1.45	12.08	1.51	0.06	0.05	1.3
3H-6, 3-4	25.63	27.05	3.45	28.74	3.54	0.09	0.04	2.4
4H-1, 138-139	28.98	32.92	10.48	87.30	10.87	0.39	0.01	29.0
4H-6, 3-4	35.13	39.07	6.25	52.06	6.57	0.32	0.03	11.0
5H-1, 144-145	38.54	43.38	8.73	72.72	9.09	0.36	0.02	21.0
6H-1, 144-145	48.04	54.13	8.20	68.31	8.46	0.26	0.02	14.0
6H-6, 1-2	54.11	60.20	8.32	69.31	8.70	0.38	0.02	19.0
7H-4, 1-2	60.61	68.52	8.80	73.30	9.18	0.38	0.02	20.0
8H-1, 147-148	67.07	74.75	7.06	58.81	7.43	0.37	0.03	15.0
8H-6, 0-1	73.10	80.78	6.42	53.48	6.51	0.09	0.09	1.0
9H-6, 0-1	82.60	91.66	1.86	15.49	2.24	0.38	0.07	5.7
10H-1, 144-145	86.04	95.26	4.51	37.57	5.01	0.50	0.06	7.8
10H-6, 1-2	92.11	101.33	9.14	76.14	9.52	0.38	0.02	21.0
11H-2, 3-4	95.63	104.02	10.85	90.38	9.76	0.00	0.02	—
11H-6, 3-4	101.63	110.02	7.68	63.97	7.80	0.12	0.02	4.8
12H-1, 138-139	104.98	114.89	6.37	53.06	6.88	0.51	0.04	14.0
12H-6, 3-4	111.13	121.04	9.95	82.88	10.48	0.53	0.02	32.0
13H-1, 138-139	114.48	125.56	6.13	51.06	6.48	0.35	0.03	11.0
13H-6, 3-4	120.58	131.66	7.60	63.31	7.89	0.29	0.02	12.0
14H-1, 138-139	123.98	136.38	8.60	71.64	8.99	0.39	0.02	21.0
14H-6, 3-4	130.13	142.53	7.61	63.39	8.05	0.44	0.03	17.0
15H-6, 3-4	139.63	153.09	7.79	64.89	8.11	0.32	0.02	13.0
16H-1, 138-139	142.98	158.88	5.02	41.82	5.32	0.30	0.03	10.0
16H-6, 3-4	149.13	165.03	3.67	30.57	4.24	0.57	0.05	12.0
17H-1, 138-139	152.48	169.90	7.11	59.23	7.69	0.58	0.03	17.0
17H-6, 3-4	158.63	176.05	7.69	64.06	8.36	0.67	0.02	30.0
18H-6, 0-1	168.10	185.52	7.61	63.39	8.06	0.45	0.03	17.0
19H-1, 144-145	171.54	185.17	8.96	74.64	9.35	0.39	0.02	21.0
19H-6, 0-1	177.60	191.23	9.40	78.30	9.40	0.00	0.02	—
20H-6, 148-149	188.42	202.05	8.70	72.47	9.18	0.48	0.02	26.0
21H-2, 144-145	192.04	207.19	8.14	67.81	9.65	1.51	0.03	56.0
21H-6, 0-1	196.60	211.75	9.45	78.72	9.82	0.37	0.02	20.0
22H-2, 0-1	200.10	214.75	8.77	73.05	9.18	0.41	0.02	20.0
23H-2, 3-4	209.63	224.80	9.67	80.55	10.09	0.42	0.02	22.0
23H-6, 3-4	215.63	230.80	8.40	69.97	8.78	0.38	0.03	15.0
24H-1, 143-144	219.03	234.20	8.67	72.22	9.13	0.46	0.02	19.0
24H-6, 3-4	225.13	240.30	9.54	79.47	9.97	0.43	0.02	25.0
28H-1, 113-114	256.73	271.90	11.09	92.38	11.54	0.45	0.07	6.5
28H-6, 18-19	263.28	278.45	11.20	93.30	11.47	0.27	0.09	3.2
29H-1, 143-144	266.53	281.70	11.21	93.38	11.52	0.31	0.07	4.5
29H-6, 3-4	272.63	287.80	11.04	91.96	11.47	0.43	0.09	4.7
30H-1, 143-144	276.03	291.20	11.04	91.96	11.44	0.40	0.08	5.1
31H-1, 143-144	285.53	300.70	10.85	90.38	10.76	0.00	0.01	0.0
31H-6, 3-4	291.63	306.80	11.01	91.71	11.41	0.40	0.09	4.3
32H-3, 7-8	296.67	311.84	11.31	94.21	11.55	0.24	0.07	3.2
33H-1, 145-146	304.55	319.72	10.94	91.13	11.06	0.12	0.13	1.0
33H-6, 1-2	310.61	325.78	11.31	94.21	11.35	0.04	0.08	0.5
34H-6, 0-1	320.10	335.27	10.81	90.05	10.98	0.17	0.11	1.6
34H-6, 144-145	321.54	336.71	10.54	87.80	10.56	0.02	0.00	—
35H-1, 149-150	323.59	338.76	10.91	90.88	10.94	0.03	0.00	—
35H-6, 0-1	329.60	344.77	10.17	84.72	10.20	0.03	0.00	—
36H-1, 149-150	333.09	348.26	10.29	85.72	10.39	0.10	0.00	—
36H-6, 1-2	339.11	354.28	10.91	90.88	10.98	0.07	0.00	—

Note: — = no organic carbon.



Table T33. Interstitial water geochemistry, Hole U1308A.

Core, section, interval (cm)	Depth		Anions (mM)		pH	Alkalinity (mM)	Salinity (g/kg)	Major cations (mM)				Minor and trace constituents (μM)							Sr/Ca (μM/mM)	
	(mbsf)	(mcd)	SO <sub>4</sub> <sup>2-</sup>	Cl <sup>-</sup>				Na <sup>+</sup>	K <sup>+</sup>	Mg <sup>2+</sup>	Ca <sup>2+</sup>	NH <sub>4</sub> <sup>+</sup>	B	Ba <sup>2+</sup>	Fe <sup>2+</sup>	Li <sup>+</sup>	Mn <sup>2+</sup>	H <sub>4</sub> SiO <sub>4</sub>		Sr <sup>2+</sup>
303-U1308A-																				
1H-1, 145-150	1.45	1.45	28.4	562	7.08	2.95	36	486	11.5	51.7	10.6	24	460	0.1	0.7	21.6	65.7	397	91	9
2H-1, 145-150	10.05	11.03	25.5	565	7.04	4.26	36	482	11.5	53.1	9.9	162	459	0.2	27.1	18.0	54.1	532	112	11
3H-1, 145-150	19.55	20.97	24.4	562	7.31	5.18	36	485	11.8	50.1	9.6	269	457	0.2	21.9	18.5	32.8	576	134	14
4H-1, 145-150	29.05	32.99	21.7	568	7.00	5.36	35	491	11.1	48.8	8.5	354	451	0.2	11.5	19.5	23.4	589	160	19
5H-1, 145-150	38.55	43.39	19.5	567	7.03	5.49	36	491	11.1	47.1	7.9	422	441	0.0	29.4	16.2	27.3	499	176	22
6H-1, 145-150	48.05	54.14	17.7	567	7.02	5.67	36	492	11.0	45.4	7.3	497	442	0.1	26.6	20.8	22.2	611	225	31
7H-1, 145-150	57.55	65.46	17.1	565	7.10	6.11	35	491	11.2	44.5	7.3	613	426	0.1	20.6	20.6	16.5	693	271	37
10H-1, 145-150	86.05	95.27	14.8	567	7.10	6.22	35	494	11.0	41.6	7.0	733	434	0.2	13.9	22.7	13.0	759	401	58
13H-1, 145-150	114.55	125.63	12.3	565	7.10	5.75	35	495	10.8	38.2	6.8	831	425	0.2	28.6	23.7	7.6	716	570	83
16H-1, 145-150	143.05	158.95	12.1	565	6.99	5.79	35	497	10.5	35.9	7.9	902	455	0.4	21.8	24.8	5.4	832	783	100
19H-1, 145-150	171.55	185.18	11.2	565	6.94	5.99	36	498	10.9	33.4	8.6	992	443	0.5	14.0	30.6	10.4	965	945	110
22H-1, 145-150	200.05	214.70	11.8	566	6.94	5.69	35	500	10.4	32.3	9.8	982	455	0.3	30.2	46.4	8.7	954	1124	115
25H-1, 145-150	228.55	243.72	10.6	566	6.86	5.32	35	499	10.4	30.0	11.4	981	457	0.4	16.1	87.2	2.9	1061	1278	112
28H-1, 145-150	257.05	272.22	10.2	565	6.66	6.19	35	498	9.9	28.7	13.0	968	497	0.6	4.7	167.8	1.5	1215	1395	107
31H-1, 145-150	285.55	300.72	9.9	566	6.67	6.57	36	500	9.3	26.4	14.9	985	536	0.5	11.8	258.9	1.9	1119	1514	101
34H-1, 145-150	314.05	329.22	9.0	563	6.75	6.19	35	497	8.6	24.4	16.4	1029	549	0.5	28.9	322.3	1.9	729	1592	97